The 511 keV emission from positron annihilation in the Galaxy

N. Prantzos

CNRS, UMR7095, UMPC and Institut d'Astrophysique de Paris, F-75014, Paris, France

C. Boehm

LAPP, 9 Chemin de Bellevue, BP 110 F-74941 Annecy-le-Vieux, France

A. M. Bykov

A. F. Ioffe Institute of Physics and Technology, Russian Academy of Sciences, 194021, St. Petersburg, Russia

R. Diehl

Max Planck Institut für Extraterrestrische Physik, D-85741 Garching, Germany

K. Ferrière

Laboratoire d'Astrophysique de Toulouse-Tarbes, Université de Toulouse, CNRS, 14 avenue Edouard Belin, F-31400 Toulouse, France

N. Guessoum

American University of Sharjah, College of Arts & Sciences/Physics Department, P.O. Box 26666, Sharjah, United Arab Emirates

P. Jean and J. Knoedlseder

CESR, Université de Toulouse, CNRS, 9, Avenue du Colonel Roche, Boîte Postal 4346, F-31028 Toulouse Cedex 4, France

A. Marcowith

L.U.P.M., Université Montpellier II, CNRS, Place Eugène Bataillon, F-34095 Montpellier, France

I. V. Moskalenko

Hansen Experimental Physics Laboratory and Kavli Institute for Particle Astrophysics and Cosmology, Stanford University, Stanford, California 94305, USA

A. Strong

Max Planck Institut für Extraterrestrische Physik, D-85741, Garching, Germany

G. Weidenspointner

Max Planck Institut fur Extraterrestrische Physik, Garching, D-85741 Germany, and MPI Halbleiterlabor, Otto-Hahn-Ring 6, D-81739 Muenchen, Germany

(Received 10 February 2010; published 29 September 2011)

The first γ-ray line originating from outside the Solar System that was ever detected is the 511 keV emission from positron annihilation in the Galaxy. Despite 30 years of intense theoretical and observational investigation, the main sources of positrons have not been identified up to now. Observations in the 1990s with OSSE/CGRO (Oriented Scintillation Spectrometer Experiment on GRO satellite/Compton Gamma Ray Observatory) showed that the emission is strongly concentrated toward the Galactic bulge. In the 2000s, the spectrometer SPI aboard the European Space Agency's (ESA) International Gamma Ray Astrophysics Laboratory (INTEGRAL) allowed scientists to measure that emission across the entire Galaxy, revealing that the bulge-to-disk luminosity ratio is larger than observed at any other wavelength. This mapping prompted a number of novel explanations, including rather ''exotic'' ones (e.g., dark matter annihilation). However, conventional astrophysical sources, such as type Ia supernovae, microquasars, or x-ray binaries, are still plausible candidates for a large fraction of the observed total 511 keV emission of the bulge. A closer study of the subject reveals new layers of complexity, since positrons may propagate far away from their

production sites, making it difficult to infer the underlying source distribution from the observed map of 511 keV emission. However, in contrast to the rather well-understood propagation of high-energy (>GeV) particles of Galactic cosmic rays, understanding the propagation of low-energy (~MeV) positrons in the turbulent, magnetized interstellar medium still remains a formidable challenge. The spectral and imaging properties of the observed 511 keV emission are reviewed and candidate positron sources and models of positron propagation in the Galaxy are critically discussed.

DOI: 10.1103/RevModPhys.83.1001 PACS numbers: 26.20.−f

CONTENTS

I. INTRODUCTION

The existence of a particle with equal mass but opposite charge to that of the electron was predicted by Dirac (1931), who named it the "antielectron." Unaware of Dirac's prediction, Anderson (1932) found the first experimental hints for such a particle in cloud-chamber photographs of cosmic rays (CRs), and he called it the *positron*. His finding was confirmed the following year by Blackett and Occhialini (1933), who identified it with Dirac's antielectron. One year later, Klemperer and Chadwick (1934) detected the characteristic γ-ray line at 511 keV resulting from e^--e^+ annihilation, a convincing proof that positrons are indeed electron's antiparticles. That same year, the Croatian physicist Mohorovicic (1934) predicted the existence of a bound system composed of an electron and a positron (analogous to the hydrogen atom, but with the proton replaced by a positron), which he called "electrum." This state was experimentally found by Deutsch (1951) at MIT and became known as *positronium*.

For about 30 years after their discovery, all detected positrons were of terrestrial origin. Those detected by Anderson (1932) and Blackett and Occhialini (1933) were created by cosmic-ray interactions with molecules in Earth's atmosphere. Joliot and Curie (1934) identified another positron producing process, β^+ radioactivity of artificially created unstable nuclei. The first positrons of extraterrestrial origin were reported by de Shong *et al.* (1964), who loaded a spark chamber on a stratospheric balloon to detect positrons within the cosmic rays. Ginzburg (1956) had already suggested that high-energy p-p interactions in cosmic rays would produce pions π^+, which would decay to positrons (via μ decays) . The production rate of those pions was evaluated by Pollack and Fazio (1963) who

predicted a γ-ray flux from the Galaxy at 511 keV of $\sim 10^{-3}$ cm^{-2} s^{-1}.

The properties of e^--e^+ annihilation were explored in the 1940s. Direct e^--e^+ annihilation produces a single γ-ray line at 511 keV, while the annihilation of positronium produces a composite spectrum with a lower-energy continuum and a 511 keV line (Ore and Powell, 1949 and Sec. II.A). Stecker (1969) was the first to point out that in the conditions of the interstellar medium, most positrons would annihilate after positronium formation; this would reduce the 511 keV flux from cosmic rays to values lower than those evaluated by Pollack and Fazio (1963).

The 511 keV emission of e^+ annihilation was first detected from the general direction of the Galactic center (GC) in the early 1970s, by balloon-borne instruments of low-energy resolution (Johnson *et al.*, 1972). It was unambiguously identified a few years later with high-resolution Ge detectors (Leventhal *et al.*, 1978). It is the first and most intense γ-ray line originating from outside the Solar System that was ever detected. Its flux on Earth ($\sim 10^{-3}$ cm^{-2} s^{-1}), combined with the distance to the Galactic center (~ 8 kpc[1]), implies the annihilation of $\sim 2 \times 10^{43}$ e^+ s^{-1} (Sec. II.B.3), releasing a power of $\sim 10^{37}$ erg s^{-1} or $\sim 10^4 L_\odot$ in γ rays. Assuming a steady state, i.e., equality between production and annihilation rates of positrons, one should then look for a source (or sources) able to provide $\sim 2 \times 10^{43}$ e^+ s^{-1}. If the activity of that site were maintained to the same level during the $\sim 10^{10}$ yr of the Galaxy's lifetime, a total amount of positrons equivalent to $\sim 3 M_\odot$ would have been annihilated.

A few years earlier, the Sun had already become the first astrophysical laboratory for the study of positron annihilation (Crannell *et al.*, 1976). The solar annihilation γ-ray line had been detected with a simple NaI instrument aboard the OSO-7 satellite (Chupp *et al.*, 1975). The solar maximum mission (SMM), designed for solar flare observations and launched in 1980, featured a γ-ray spectrometer with exceptional stability. Based on detailed measurements with the SMM, positrons in solar flares were found to originate from flare-accelerated particles when they hit the upper photosphere. Nuclear interactions of flare-accelerated protons and ions with atomic nuclei of the photosphere produce radioactive nuclei and pions that decay by emission of positrons, which annihilate locally (Ramaty *et al.*, 1983; Murphy, Skibo *et al.*, 2005).

Imaging the Galaxy in annihilation γ rays was considered to be the exclusive way to identify the cosmic e^+ sources (assuming that the spatial morphology of the γ-ray emission reflects the spatial distribution of the sources, i.e., that positrons annihilate close to their production sites). Because of the difficulties of imaging in the MeV region, progress was extremely slow in that field: only in the 1990s were the first constraints on the spatial distribution of the 511 keV emission in the inner Galaxy obtained by the OSSE instrument aboard the Compton Gamma Ray Observatory (CGRO, Cheng *et al.*, 1997; Purcell *et al.*, 1997). The most reliable imaging of the 511 keV emission was obtained by the SPI instrument aboard ESA's INTEGRAL Gamma Ray Observatory: The emission is strongly concentrated in the inner Galaxy (the bulge, Knödlseder *et al.*, 2005) and a weaker emission is detected from the Galactic disk (Weidenspointner *et al.*, 2008a), unlike the situation at any other wavelength.

Several candidate sources of positrons have been proposed over the years: radioactivity from β^+ decay of unstable nuclei produced in stellar explosions, high-energy interactions occurring in cosmic rays or near compact objects (such as pulsars and x-ray binaries), or the supermassive black hole in the Galactic center, etc. For a long time, radioactivity from ^{56}Co produced in thermonuclear supernovae (SNIa) appeared as the most promising candidate, provided that just a few per cent of the released positrons could escape the supernova remnant and annihilate in the interstellar medium. However, none of the candidate sources has a spatial pattern resembling that of the detected γ-ray emission. In particular, the release of the first year of SPI data, revealing the bulge but not yet the disk, prompted a series of "exotic" explanations involving dark matter (DM) particles, superconducting cosmic strings, etc. The confirmation of disk emission a few years later caused a loss of interest in such explanations, but they have not been completely eliminated so far.

The spectral analysis of the 511 keV emission had already established in the late 1970s that most of the positrons annihilate after positronium formation (Bussard *et al.*, 1979). This result constitutes an important diagnostic tool for the physical properties of the annihilation medium, as analyzed by Guessoum *et al.* (1991). Only recently, in the 2000s, was it realized that the spectral analysis may also provide important hints on the e^+ source(s). In particular, positrons appear to annihilate at low energies, while in most candidate sources they are produced at relativistic energies; during the long period of their slowing down, positrons may travel far away from their sources, making the detected γ-ray emission useless as a tracer of their production sites. Unfortunately, propagation of low-energy positrons in the turbulent, magnetized interstellar plasma of the Galaxy is poorly understood at present.

In this paper we present a synthetic view of the various facets of this complex issue, concerning the production, propagation, and annihilation of positrons in the Galaxy, in relation to the characteristic signature of that annihilation, namely, the 511 keV emission. The paper is structured as follows.

In Sec. II we first present a historical account of observations of the 511 keV emission, which illustrates the difficulties of the γ-ray line astronomy in the MeV range. We also provide a summary of the latest SPI/INTEGRAL data analysis, of relevant observations at other wavelengths, and of the constraints imposed on the e^+ sources.

Section III provides astrophysical background material concerning the stellar and supernova populations of the Milky Way (MW), as well as the properties of the various phases of the interstellar medium (ISM) and of the Galactic magnetic fields in which positrons propagate. This material can be skipped at a first reading by astronomers, but it contains important and updated information, which is used in all other sections.

In Sec. IV we discuss the physical processes and candidate sources of positron production (radioactivity from stars and supernovae, high-energy processes in cosmic rays, compact objects, and the central supermassive black hole, dark matter, other "exotica," etc.) and, in some cases, we present new estimates of their e^+ yields. We discuss the properties of

[1] 1 pc (parsec) = 3.26 light years = 3.09×10^{18} cm.

those sources, in light of the observational constraints presented in Sec. II.

Section V summarizes the various physical processes of slowing down and annihilation of e^+, taking into account the properties of the ISM, as well as the corresponding γ-ray spectral signature. The spectral analysis of the SPI data is then used to constrain the energy of the emitted positrons (thus eliminating some of the candidate sources) and the properties of the annihilation medium. The results of this analysis offer some hints for e^+ propagation away from the sources.

The intricacies of low-energy positron propagation are discussed in some depth in Sec. VI, in light of recent work. The implications of e^+ propagation for the 511 keV emission are also discussed. This is not a mature topic yet, and our scanty knowledge of the plasma properties in the inner Galaxy prevents any definitive conclusions. A synthetic summary of the subject and directions for future research are presented in the last section.

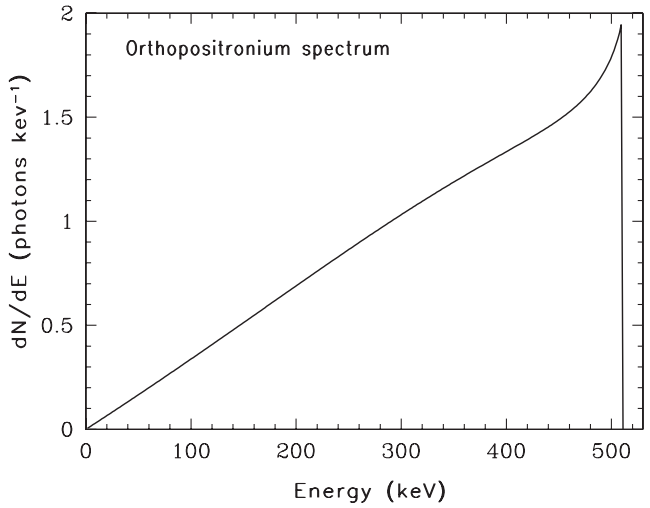

FIG. 1. Spectrum of ortho-positronium annihilation with the three-photon continuum. From Ore and Powell, 1949.

II. OBSERVATIONS

Gamma-ray observations in the MeV domain (from ~100 keV up to a few MeV) provide access to Galactic positrons through three main windows:

(i) emission from e^+ annihilation at subrelativistic energies, with its prominent 511 keV line and the associated three-photon continuum from positronium annihilation;
(ii) continuum emission at energies $E > 0.5$ MeV from energetic positrons propagating through interstellar space and annihilating "in flight";
(iii) emission of characteristic γ-ray lines from radioactive nuclei, such as ^{26}Al and ^{44}Ti, which also produce positrons by β^+ decay.

In this section, we describe the relevant observations and the constraints that they impose on our understanding of Galactic positrons (see also Diehl and Leising, 2009). We start with a brief description of the radiative signatures of positron annihilation.

A. Radiative signatures of positron annihilation

The annihilation of a positron with an electron releases a total (rest-mass) energy of 1022 keV in the form of two or more photons. Direct annihilation of an e^--e^+ pair at rest produces two photons of 511 keV each. The situation is more complex in the case of positronium (Ps). The ground state of positronium has two total spin states, depending on the relative orientations of the spins of the electron and the positron. The singlet state has antiparallel spins, total spin $S = 0$, is denoted as $^1S_0$ and is known as *para-positronium* (p-Ps). The triplet state has parallel spins, total spin $S = 1$, is denoted as $^3S_1$ and is known as *ortho-positronium* (o-Ps). From the $(2S + 1)$ spin degeneracy, it follows that Ps will be formed $1/4$ of the time in the p-Ps state and $3/4$ of the time in the o-Ps state.[2]

Spin and momentum conservation constrain the release of annihilation energy in the form of photons. Para-positronium annihilation releases two photons of 511 keV each in opposite directions (as in the case of direct e^--e^+ annihilation). Ortho-positronium annihilation requires a final state with more than two photons from spin conservation; momentum conservation distributes the total energy of 1022 keV among three photons[3] producing a continuum of energies up to 511 keV (Fig. 1). The corresponding lifetimes before annihilation (in vacuum) are 1.2×10^{-10} s for p-Ps and 1.4×10^{-7} s for o-Ps.

If a fraction $f_{\rm Ps}$ of the positrons annihilates via positronium formation, then the three-photon γ-ray continuum of ortho-positronium will have an integrated intensity of

$$I_{3\gamma} \propto \tfrac{3}{4} 3 f_{\rm Ps}. \tag{1}$$

The remaining fraction $1 - f_{\rm Ps}$ will annihilate directly to two photons of 511 keV each, to which should be added the two-photon contribution of the para-positronium state; thus, the two-photon (511 eV line) intensity will be

$$I_{2\gamma} \propto 2(1 - f_{\rm Ps}) + \tfrac{1}{4} 2 f_{\rm Ps} = 2 - 1.5 f_{\rm Ps}. \tag{2}$$

By measuring the intensities of the 511 keV line and of the Ps continuum one can then derive the positronium fraction

$$f_{\rm Ps} = \frac{8 I_{3\gamma}/I_{2\gamma}}{9 + 6 I_{3\gamma}/I_{2\gamma}}, \tag{3}$$

[2]The energy difference between the two spin states ("hyperfine splitting") is 8.4×10^{-4} eV. Transitions between these states, similar to the spin-flip transition in hydrogen, which produces the astrophysically important 21 cm line, are unimportant due to the short Ps lifetimes (see text).

[3]Annihilation into a larger number of photons (an even number for para-positronium, an odd number for ortho-positronium) is possible, but the corresponding branching ratios are negligible (~10^{-6} for four photons in the case of para-positronium or five photons in the case of ortho-positronium). Even lower are the branching ratios for annihilation into neutrino-antineutrino pairs. Finally, a single-photon annihilation is also possible, provided momentum conservation is obtained through positronium being bound to another particle, such as a dust grain. None of those cases is important in astrophysical settings.

which offers a valuable diagnostic of the physical conditions of the ISM where positrons annihilate (see the discussion in Sec. V.E).

The state of Ps can be formally treated as that of the hydrogen atom. The corresponding Schrödinger equations are identical, with the reduced mass being half of the electron mass in the case of Ps. Because of that, the frequencies of the deexcitation spectral lines are roughly half those of the H atom (Canter *et al.*, 1975). Radiative recombination of o-Ps could, under certain circumstances, be observed in the near infrared by next generation instruments (see Ellis and Bland-Hawthorn, 2009).

B. Observations of ~MeV emission from e^+ annihilation

1. Early balloon and satellite observations

The first evidence for Galactic 511 keV emission was obtained in the early 1970s, through a series of balloon flights by teams from Rice University. Johnson *et al.* (1972) announced the first detection of a celestial γ-ray line originating from outside the Solar System. Using a sodium iodine (NaI) scintillation detector they observed a spectral excess with a flux of 1.8×10^{-3} photons $\mathrm{cm}^{-2}\,\mathrm{s}^{-1}$ at an energy of 473 ± 30 keV during a balloon flight in 1970. A second balloon flight of the same team in 1971 confirmed this signal (Johnson and Haymes, 1973). Although they mentioned e^+ annihilation as a possible origin of the observed feature, the significant offset between the observed (473 keV) and expected (511 keV) line centroids led them to conclude that the feature was, perhaps, due to radioactive decay of unknown origin.

Leventhal (1973) proposed an interesting alternative explanation that could reconcile the observations with a positron origin of the feature. As e^+ annihilation in the interstellar medium occurs mainly via positronium, a superposition of a narrow line at 511 keV and a continuum emission below 511 keV is expected (Fig. 1). Because of the poor spectral resolution of the NaI detector and the low signal-to-noise ratio of these balloon flights, these two contributions could not be disentangled and were reported as a single emission peak at an energy of ~490 keV, in reasonable agreement with the observations.

It took 5 years before a group from Bell-Sandia (Leventhal *et al.*, 1978) confirmed this conjecture. With their high-resolution balloon-borne germanium (Ge) detector they could separate the line and continuum components of the emission. Leventhal *et al.* (1978) located the narrow component [full width at half maximum (FWHM) = 3.2 keV] at an energy of 510.7 ± 0.5 keV, consistent with the expectations for e^+ annihilation at rest. The observed line flux of $(1.2 \pm 0.2) \times 10^{-3}$ photons $\mathrm{cm}^{-2}\,\mathrm{s}^{-1}$ was below the value reported by Johnson *et al.* (1972), as expected if the earlier measurements were a superposition of two components. Leventhal *et al.* (1978) also detected the positronium continuum component, and the comparison of line and continuum intensities implied that 92% of the annihilations occurred after the formation of a positronium atom.

Subsequent observations of the Galactic center by different balloon-borne instruments in the 1970s found a surprising variability of the 511 keV line flux (Haymes *et al.*, 1975; Leventhal *et al.*, 1980; Albernhe *et al.*, 1981; Gardner *et al.*, 1982). But Albernhe *et al.* (1981) recognized that the flux measured by the various balloon experiments increased with increasing size of the detector's field of view, which could mean that the annihilation emission was extended along the Galactic plane. Riegler *et al.* (1981) proposed a different scenario, based on analysis of their HEAO-3 satellite data. These data showed a decline by almost a factor of 3 of the 511 keV flux between the fall of 1979 and the spring of 1980, suggesting that positron annihilation was variable in time. From the $\Delta t \sim 6$ months interval between the observations they inferred a maximum size of $\Delta r \sim c\Delta t \sim 0.3$ pc of the annihilation site, which implies gas densities for the annihilation medium of 10^4–10^6 cm^{-3}. These extreme conditions suggest that the positrons were produced by a compact source such as a massive black hole within 4° of the Galactic center (Lingenfelter *et al.*, 1981).

While balloon-borne experiments seemed to establish the variability of the 511 keV emission (Leventhal *et al.*, 1982; Paciesas *et al.*, 1982; Leventhal *et al.*, 1986), contemporaneous observations by the SMM satellite did not confirm such a trend. SMM carried a NaI detector with a large field of view (130°) and provided the first long-term monitoring of the inner Galaxy (1980–1987). The variability of the 511 keV emission was constrained to be less than 30% (Share *et al.*, 1988; Share *et al.*, 1990). The apparent disagreement between the balloon and SMM observations could still be understood by assuming an extended distribution of 511 keV emission along the Galactic plane; however, in order to reconcile the observations with a time-variable source one had to adopt rather complex scenarios. For example, Lingenfelter and Ramaty (1989) suggested the combination of a steady, extended 511 keV emission along the Galactic plane and a compact variable source at the Galactic center (assumed to be active from 1974 through 1979) in order to explain all data available at that time. Such a scenario could not be ruled out, since no imaging of the 511 keV emission had been achieved and the morphology and spatial extent of the positron annihilation emission were essentially unconstrained.

The hypothesis of a time-variable central Galactic positron source was revitalized in the early 1990s by the observation of transient γ-ray line features with the SIGMA telescope. The French coded mask imager SIGMA was launched in 1989 on board the soviet GRANAT satellite. It was the first imaging γ-ray instrument, with an angular resolution of 15 arc min and it used NaI detectors covering the energy range 35–1300 keV. In October 1991, an unusual spectrum was observed from 1E 1740.7-2942, during an outbreak of this hard x-ray source which lasted ~17 h (Bouchet *et al.*, 1991; Sunyaev *et al.*, 1991). Superimposed on a candidate typical black hole continuum spectrum, there appeared a strong (flux $F \sim 10^{-2}$ photons $\mathrm{cm}^{-2}\,\mathrm{s}^{-1}$) and broad (FWHM ~200 keV) emission line centered at about 440 keV. If interpreted as a broadened and redshifted annihilation line, this observation seemed to make 1E 1740.7-2942 the long-sought compact and variable source of positrons. Follow-up observations led to the classification of 1E 1740.7-2942 as the first microquasar (Mirabel *et al.*, 1992): a binary system involving a compact object (neutron star or black hole, see Sec. IV.B.3) accreting material from its companion and emitting part of the accreted energy in the form of jets. It was therefore

proposed that 1E 1740.7-2942 would occasionally emit jets of positrons (produced in e^--e^+ pairs), some of which would annihilate in the inner edge of the accretion disk as presumably observed by SIGMA; the remaining positrons would eventually lose their energy and give rise to a time-variable narrow 511 keV line emission. Different SIGMA teams also reported narrow and/or broad γ-ray lines near 511 keV, lasting for a day or so, from the transient x-ray source "Nova Muscae" (Goldwurm *et al.*, 1992; Sunyaev *et al.*, 1992) and the Crab nebula (Gilfanov *et al.*, 1994). Another transient γ-ray line source was discovered from archival HEAO 1 data by Briggs *et al.* (1995).

However, the line feature seen by SIGMA was not seen in simultaneous observations of 1E 1740.7-2942 performed with the OSSE (Jung *et al.*, 1995) and BATSE (Smith *et al.*, 1996a) instruments aboard the NASA CGRO, launched in 1991. Besides, BATSE data did not confirm the transient event seen by SIGMA from the Crab nebula (Smith *et al.*, 1996a). Moreover, a search on 6 years of BATSE data did not reveal any transient line feature from any direction of the sky (Smith *et al.*, 1996b; Cheng *et al.*, 1998). Similarly, 9 years of SMM data did not show any transient event from the Galactic center direction (Harris *et al.*, 1994a) or the Crab nebula (Harris *et al.*, 1994b). A reanalysis of HEAO 3 data then revealed that the drop in 511 keV flux reported earlier by Riegler *et al.* (1981) was not significant (Mahoney *et al.*, 1994). Thus, the idea of a steady 511 keV Galactic emission was gradually established.

The contradictory results obtained during the 1980s and early 1990s provide a dramatic illustration of the difficulties affecting the analysis of γ-ray line data. In this domain, astrophysical signals rarely exceed the instrumental background by more than a few percent and any systematic uncertainty in the treatment of the background immediately disturbs the analysis. In particular, the time variability of the instrumental background (due to changing radiation environments along the orbital trajectory, or due to solar activity) can easily fake time-variable signals. In addition, hard x-ray sources often exhibit highly variable continuum emission components that may further affect the data analysis and require their proper modeling; this concerns, in particular, the densely populated regions toward the Galactic center, which were not spatially resolved by older instruments.

2. Early mapping of the spatial distribution of e^+ annihilation

Before the launch of CGRO in 1991 with its OSSE collimated ($11.4° \times 3.8°$) spectrometer, the spatial distribution of 511 keV line emission was only poorly constrained. Hypotheses on a possible extent of the emission were mainly based on theoretical expectations (Kozlovsky *et al.*, 1987), on the different fluxes received by detectors with different fields of view (Albernhe *et al.*, 1981; Dunphy *et al.*, 1983), and on a marginal detection of the 511 keV line near $\sim 25°$ Galactic longitude with the balloon-borne GRIS telescope (Leventhal *et al.*, 1989; Gehrels *et al.*, 1991). Nine years of OSSE observations drastically improved this situation.

OSSE data could clearly exclude a single point source as the origin of observed 511 keV line emission (Purcell *et al.*, 1994). The data were best understood in terms of an extended source consisting of a symmetrical bulge (centered on the Galactic center) and emission from the Galactic plane. Cheng *et al.* (1997) and Purcell *et al.* (1997) established the first 511 keV line emission map of the central Galactic ridge (Fig. 2). Beyond the aforementioned components, there was hint of a third component located at Galactic coordinates of longitude $l \sim -2°$ and latitude $b \sim 12°$, dubbed the positive latitude enhancement (PLE). However, the intensity and morphology of this feature were only weakly constrained by the data (Milne *et al.*, 2001b), and the nonuniform exposure of the sky may have biased the sky maps (Von Ballmoos *et al.*, 2003). Kinzer *et al.* (1996), Milne *et al.* (1998), and Kinzer *et al.* (2001) studied the spatial distribution of the continuum emission from positronium annihilation and concluded that it closely follows the distribution of the 511 keV line. However, no PLE was visible in the continuum emission image (Milne *et al.*, 2001a).

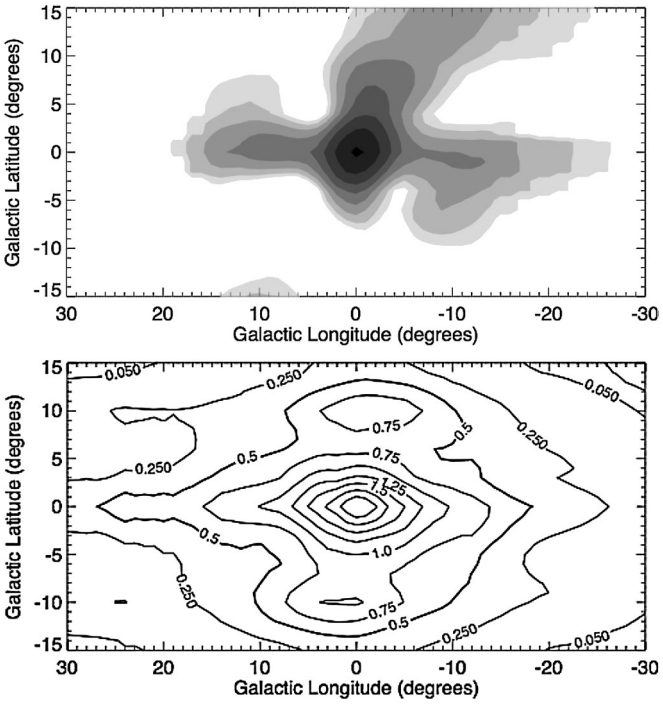

FIG. 2. OSSE 511 keV line map of the Galactic center region (top panel) and corresponding exposure map (bottom panel). From Purcell *et al.*, 1997.

At this point one should mention that images in the hard x-ray and soft γ-ray domains are obtained through complex nonlinear iterative deconvolution techniques, and they generally represent only a family of solutions, which explains the observed data within the given statistical and convergence constraints. The reader should be aware of this particularly important point when inspecting all images in this paper. For instance, other OSSE images of the Galactic 511 keV line emission are presented by Milne *et al.* (2001a, 2002).

Several models have been proposed to describe the spatial distribution of the annihilation emission observed by OSSE (Prantzos, 1993; Purcell *et al.*, 1994; Kinzer *et al.*, 1996; Purcell *et al.*, 1997; Kinzer *et al.*, 2001; Milne *et al.*, 2001b). They all had in common a two-component emission from a spheroid located in the inner Galaxy and from the extended Galactic disk (see Sec. III.A for a detailed discussion of the Galaxy's morphology). However, both morphology and

relative intensity of these two components were only poorly constrained by the data; depending on the adopted model, the spheroidal component was claimed to be dominant or subdominant, i.e., the Galactic spheroidal-to-disk flux ratio was constrained only in the broad interval $F_{\rm spher}/F_{\rm disk} \sim 0.2$–$3.3$. The uncertainty on the total Galactic 511 keV line flux was also rather large, spanning the range $(1–3) \times 10^{-3}$ photons cm^{-2} s^{-1}.

Despite the considerable progress achieved by OSSE observations, the origin of Galactic positrons remained unclear. The data did not constrain the morphology of the 511 keV emission enough to clarify the underlying source population. Yet, the strong concentration of the 511 keV emission toward the Galactic bulge led several authors to suggest that the β^+ decay of radioactive ^{56}Co, produced by Galactic SNIa, should be the dominant Galactic positron source (Kinzer *et al.*, 1996, 2001; Milne *et al.*, 2002). The emission from the Galactic disk was generally attributed to radioactive β^+ decays of ^{26}Al, ^{56}Co, and ^{44}Ti produced by a variety of stellar sources (Purcell *et al.*, 1994; Kinzer *et al.*, 1996; Purcell *et al.*, 1997). In fact, ^{26}Al had already been detected from the inner region of the Galaxy through its characteristic γ-ray line at 1809 keV in the 1979/1980 HEAO-C data (Mahoney *et al.*, 1982), and its contribution to Galactic-disk e^+ production was established (see Secs. II.B.2 and IV.A.2).

3. Imaging with INTEGRAL and SPI

With the launch of ESA's INTEGRAL observatory (Winkler *et al.*, 2003) in 2002 for a multiyear mission, a new opportunity became available for the study of Galactic e^+ annihilation. The SPI imaging spectrometer (Vedrenne *et al.*, 2003) combined for the first time imaging with high-resolution spectroscopy. The spatial resolution of 3° (FWHM) of SPI, though inferior to telescopes optimized for slightly lower energies (SIGMA, IBIS), is superior to that of OSSE; its energy coverage and sensitivity around the annihilation line and its large field of view allow an improved study of the 511 keV emission morphology. The spectral resolution of ~2.1 keV (FWHM, at 0.5 MeV) is comparable to that of other Ge detectors employed on balloons or the HEAO 3 satellite, allowing for a spatially resolved fine spectroscopy of the signal (including the underlying continuum emission).

The first 511 keV line and positronium continuum all-sky maps were presented by Knödlseder *et al.* (2005) and Weidenspointner *et al.* (2006), respectively, based on approximately 1 year of SPI data (Fig. 3). The two maps are compatible with each other (within their uncertainties), suggesting that the positronium fraction does not vary over the sky. The images illustrate the remarkable predominance of the spheroidal component. In contrast to OSSE data, which suggested a relatively strong disk component, the Galactic disk seemed to be completely absent in the first-year SPI images. Model fitting indicated only a marginal signal from the Galactic disk, corresponding to a bulge-to-disk flux ratio >1 (see Knödlseder *et al.*, 2005). This strong predominance of the Galactic bulge, unseen in any other wavelength, stimulated "unconventional" models involving dark matter (see Sec. IV.C). However, Prantzos (2006) pointed out that the data could not exclude the presence of disk emission of a larger latitudinal extent (resulting from positrons propagating far away from their sources), which could be rather luminous and still undetectable by SPI, because of its low surface brightness.

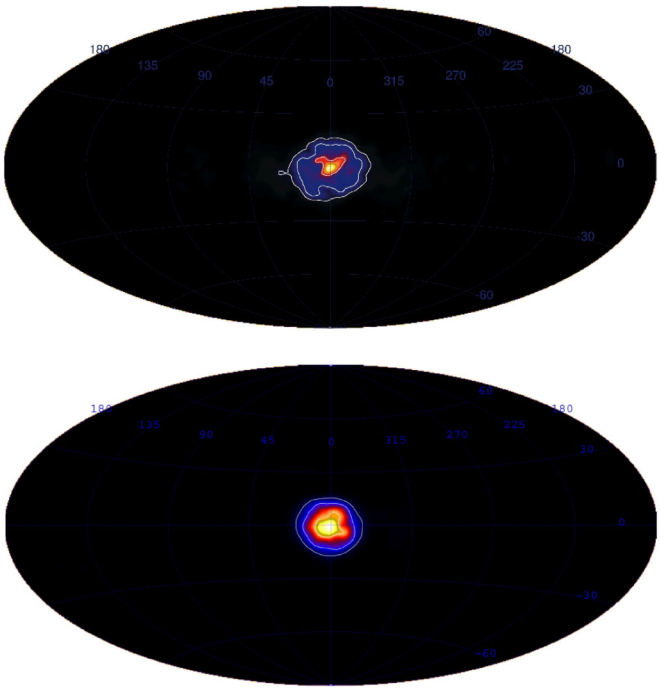

FIG. 3 (color online). 511 keV line map (top panel) and positronium continuum map (bottom panel) derived from 1 year of INTEGRAL/SPI data. From Knödlseder *et al.*, 2005 and Weidenspointner *et al.*, 2006, respectively.

After accumulating 5 years of INTEGRAL/SPI data the 511 keV line emission all-sky image revealed also fainter emission extending along the Galactic plane (Fig. 4). With a much improved exposure with respect to the first year (in particular, along the Galactic plane), 511 keV emission from the Galactic disk is now clearly detected (Weidenspointner *et al.*, 2008a). However, the detailed quantitative characterization of components of 511 keV emission requires parametrizing these in the form of (necessarily idealized) spatial emission models fitted to the data. No unique description emerges at present, since both the spheroid and the disk may have faint extensions contributing substantially to their total γ-ray emissivities. It turns out that the bulge emission is best described by combining a narrow and a broad Gaussian, with

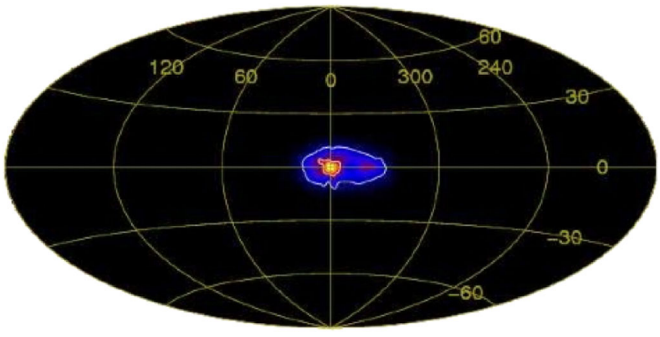

FIG. 4 (color online). 511 keV line map derived from 5 years of INTEGRAL/SPI data. From Weidenspointner *et al.*, 2008a.

TABLE I. Two model fits of the Galactic 511 keV emission (from Weidenspointner *et al.*, 2008b): fluxes, photon emissivities, and e^+ annihilation rates (computed for a positronium fraction of $f_{ps} = 0.967$, see Sec. II.B.4). Note that "thin" and "thick" disks do not have the same meaning as in Sec. III.

	F_{511} (10^{-4} cm^{-2} s^{-1})	L_{511} (10^{42} s^{-1})	$\dot{N}_{e^+}$ (10^{42} s^{-1})
Bulge + thick disk			
Narrow bulge	$2.7^{+0.9}_{-0.4}$	$2.3^{+0.8}_{-0.7}$	$4.1^{+1.5}_{-1.2}$
Broad bulge	$4.8^{+0.7}_{-0.4}$	$4.1^{+0.6}_{-0.4}$	$7.4^{+1.0}_{-0.8}$
Thick disk	$9.4^{+1.8}_{-1.4}$	$4.5^{+0.8}_{-0.7}$	$8.1^{+1.5}_{-1.4}$
Total	17.1	10.9	19.6
Bulge-to-disk ratio	0.8	1.4	1.4
Halo + thin disk			
Halo	$21.4^{+1.1}_{-1.2}$	$17.4^{+0.9}_{-1.1}$	$31.3^{+2.2}_{-2.6}$
Disk	$7.3^{+2.6}_{-1.9}$	$2.9^{+0.6}_{-0.6}$	$5.2^{+1.1}_{-1.1}$
Total	28.7	20.3	36.5
Halo-to-disk ratio	2.9	6	6

widths (FWHM, projected onto the sky) of 3° and 11°, respectively. Another, more extended component is needed to fit the data, a rather thick disk of vertical extent 7° (FWHM projected on the sky). The model implies a total e^+ annihilation rate of $2 \times 10^{43} e^+$ s^{-1} and a spheroid-to-disk ratio of 1.4 (Table I). It should be noted, however, that alternative models, involving extended components of low surface brightness (thus far undetected by SPI) are also possible. One such alternative (Weidenspointner *et al.*, 2008b) involves a centrally condensed but very extended halo and a thinner disk (projected vertical extent of 4°), with a spheroid-to-disk ratio of 6 (Table I).

With more SPI data, it was possible to proceed to more detailed constraints on the morphology of the disk emission. The flux in the disk component remains concentrated to longitudes $|l| < 50°$; no significant 511 keV line emission has been detected from beyond this interval so far. The accumulated SPI data yield a flux from negative longitudes of the Galactic disk that is twice as large as the flux from an equivalent region at positive longitudes. The significance of this asymmetry is still rather low, about $\sim 4\sigma$. Indications for such an asymmetry were already noticed in the OSSE data (M. Leising, private communication). It should be noted, however, that a different analysis of the same SPI data finds no evidence for a disk asymmetry (Bouchet *et al.*, 2008, 2010), although it cannot exclude it, either. Clearly, clarifying the asymmetric or symmetric nature of the disk profile should be a major aim of the 511 keV studies in the years to come.[4]

4. Spectroscopy with INTEGRAL and SPI

Before INTEGRAL, the spectral shape of the positron annihilation emission was only poorly constrained by observations. All high-resolution observations suggested a modest line broadening of FWHM $\sim$ 2 keV (Leventhal *et al.*, 1993; Smith *et al.*, 1993; Mahoney *et al.*, 1994; Harris *et al.*, 1998). The excellent spectral resolution of SPI allows one for the first time to study the spectrum of this emission in detail and for different regions.

[4]INTEGRAL will continue operations until 2014, at least.

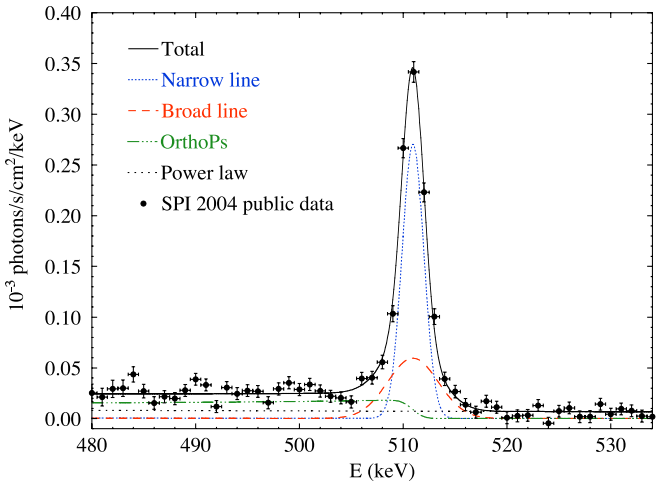

FIG. 5 (color online). Fit of the spectrum of the annihilation emission measured by SPI with narrow and broad Gaussian lines and an ortho-positronium continuum. The power-law accounts for the Galactic diffuse continuum emission. From Jean *et al.*, 2006.

Spectral results for the Galactic spheroidal emission were presented by Churazov *et al.* (2005) and Jean *et al.* (2009), based on the first year of SPI data. The line displays no spectral shift, i.e., it has an energy $E = 511 \pm 0.08$ keV (Churazov *et al.*, 2005) and it is composed of two spectral components (assumed to be represented by Gaussians): a narrow line with a FWHM $= 1.3 \pm 0.4$ keV and a broad component with a FWHM $= 5.4 \pm 1.2$ keV (Fig. 5). The width of the broad line is in agreement with the broadening expected from positronium annihilation via charge exchange with hydrogen atoms (see Sec. V.B.2). The narrow line component contains $\sim 2/3$ of the total annihilation line flux while the broad one makes up the remaining $\sim 1/3$ of the flux. Table II summarizes the results of the spectral analysis of the Galactic 511 keV emission after the first year of SPI data.

SPI also clearly detected the ortho-positronium continuum with an intensity that corresponds to a positronium fraction of $f_{Ps} = 97\% \pm 2\%$ [Jean *et al.*, 2006; see Eq. (3)]. This value is in good agreement with earlier measurements obtained by OSSE ($97\% \pm 3\%$, Kinzer *et al.*, 1996) and Transient Gamma-Ray Spectrometer (TGRS) ($94\% \pm 4\%$, Harris *et al.*, 1998).

The shape of the annihilation line and the relative intensity of the ortho-positronium continuum are closely related to the

TABLE II. Results of spectral analysis of Galactic 511 keV emission from the region within 8° from the Galactic center. I_n, Γ_n, I_b, and Γ_b are the flux and width (FWHM) of the narrow and broad lines, respectively, $I_{3\gamma}$ is the flux of the orthopositronium continuum, and A_c is the amplitude of the Galactic continuum at 511 keV. The first set of error bars refers to 1σ statistical errors and the second set to systematic errors (from Jean *et al.*, 2006).

Parameters	Measured values
I_n (10^{-3} s^{-1} cm^{-2})	$0.72 \pm 0.12 \pm 0.02$
Γ_n (keV)	$1.32 \pm 0.35 \pm 0.05$
I_b (10^{-3} s^{-1} cm^{-2})	$0.35 \pm 0.11 \pm 0.02$
Γ_b (keV)	$5.36 \pm 1.22 \pm 0.06$
$I_{3\gamma}$ (10^{-3} s^{-1} cm^{-2})	$4.23 \pm 0.32 \pm 0.03$
A_c (10^{-6} s^{-1} cm^{-2} keV^{-1})	$7.17 \pm 0.80 \pm 0.06$

physical conditions such as temperature, ionization stage, and chemical abundances of the interstellar medium in which positrons annihilate. These conditions, obtained from the analysis of the measured spectrum, are presented and discussed in Sec. V.E. Important complementary information on the energies of the annihilating positrons is obtained from the analysis of the observed continuum emission at somewhat higher energies (above 511 keV and into the MeV region), as discussed in the next section and Sec. V.B.

C. Relevant observations at MeV energies

1. The MeV continuum

Positrons are typically emitted at relativistic energies, in some cases even far above 1 MeV (Sec. IV). They behave essentially like relativistic electrons of cosmic rays, by producing bremsstrahlung and inverse-Compton emission while slowing down to the thermal energies (eV) of the interstellar medium, where they eventually annihilate. But positrons may also annihilate in flight while still having relativistic energies, giving rise to a unique γ-ray continuum signature at energies above 511 keV (as the center-of-mass energy is transferred to annihilation photons; see Sec. V). The shape and amplitude of this γ-ray emission depend on the injection spectrum of positrons and the corresponding total annihilation rate. For positrons injected at low energies (of the order of ~MeV, such as those released by radioactivity), the amplitude of the in-flight annihilation continuum above 1 MeV is quite small, while for sources injecting positrons at much higher energy (such as cosmic-ray positrons from pion decay), the annihilation γ-ray spectrum would extend up to GeV energies and include a considerable γ-ray flux. The high-energy γ-ray continuum above 1 MeV therefore constrains the energy and the annihilation rate of relativistic positrons, when all other sources of such high-energy emission are properly accounted for.

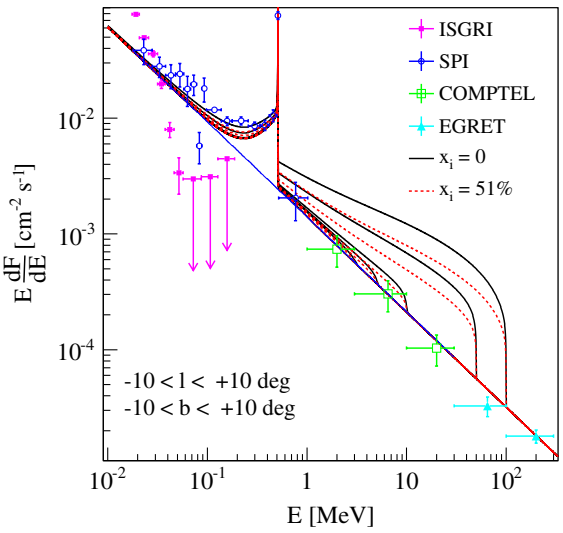

FIG. 6 (color online). Spectrum of the inner galaxy as measured by various instruments, compared to various theoretical estimates made under the assumption that positrons are injected at high energy: The four pairs of curves result from positrons injected at 100, 30, 10, and 3 MeV (from top to bottom) and correspond to positrons propagating in neutral (solid lines) or 50% ionized (dotted lines) media. This constrains the injected positron energy (or, equivalently, the mass of decaying and/or annihilating dark matter particles) to a few MeV. From Sizun *et al.*, 2006.

Diffuse Galactic continuum emission has been well measured at least in the inner part of the Galactic disk (longitudes $-30° < l < 30°$) in the hard-x-ray through γ-ray regime by INTEGRAL, OSSE, COMPTEL, and EGRET (Strong *et al.*, 1994; Kinzer *et al.*, 1999; Bouchet *et al.*, 2008). The spectrum of the underlying continuum emission in the 511 keV region is best represented as a power law with index 1.55 (Bouchet *et al.*, 2008) and is mostly due to emission from cosmic-ray electrons and positrons (Sec. IV.B.2). The corresponding emission processes are modeled in detail in, e.g., the GALPROP code (Strong *et al.*, 2007), which includes 3D distributions of interstellar gas and photon fields, as well as all relevant interaction cross sections and constraints from near-Earth observations of cosmic-ray fluxes and spectra. This model reproduces well the entire range of γ-ray observations, from keV to GeV energies; however, tantalizing hints of residual emission exist in the MeV region, when comparison is made to COMPTEL measurements[5]: The data points appear to lie on the high side of model predictions. In view of the possible systematic uncertainties of such measurements, but also of the parameters of the GALPROP code and the possible contributions of unresolved x-ray binaries, some room is still left for a contribution of in-flight e^+ annihilation to the MeV continuum.

The physics of the in-flight annihilation of positrons will be analyzed in Sec. V. Here we simply note that the corresponding constraints on the injection energy of positrons were pointed out many years ago by Agaronyan and Atoyan (1981). They showed that the positrons that are responsible for the Galactic 511 keV line cannot be produced in a steady state by the decay of the π^+ created in proton-proton collisions or else the in-flight annihilation emission should have been detected. A similar argument was used by Beacom and Yüksel (2006) and Sizun *et al.* (2006) to constrain the mass of the dark matter particle which could be the source of positrons in the Galactic spheroid (see Sec. IV.C). If such particles produce positrons (in their decay or annihilation) at a rate which corresponds to the observed 511 keV emission, then their mass should be less than a few MeV; otherwise the kinetic energy of the created positrons would have been sufficiently high to produce a measurable γ-ray continuum emission in the 1–30 MeV range (Fig. 6). The same argument allows one to constrain the initial kinetic energy of positrons and thus to eliminate several classes of candidate sources, such as, pulsars, millisecond pulsars, magnetars, cosmic rays, etc., as major positron producers (see Sec. IV.D).

[5]The CGRO/COMPTEL data points have an uncertainty of up to a factor of 2 due to the difficulty of producing sky maps with a Compton telescope with high background. The most reliable COMPTEL values come from a maximum-entropy imaging analysis and are model independent, but the zero level is uncertain and contributes to the systematic error. The enormous gap in sensitivity between the current Fermi mission (>30 MeV) and the 1–30 MeV range (sensitivity factor ~100) highlights the urgent need for new experiments in the MeV range.

2. Gamma rays and positrons from radioactive ^{26}Al

^{26}Al is a long-lived (half-life $\tau_{1/2} = 7.4 \times 10^5$ yr) radioactive isotope. It decays by emitting a positron, while the deexcitation of daughter nucleus ^{26}Mg emits a characteristic γ-ray line at 1808.63 keV. Based on predictions of nucleosynthesis calculations in the 1970s, Arnett (1977) and Ramaty and Lingenfelter (1977) suggested that its γ-ray emission should be detectable by forthcoming space instruments. The detection of the 1809 keV line from the inner Galaxy with the HEAO-C germanium spectrometer (Mahoney *et al.*, 1982) came as a surprise (Clayton, 1984) because of its unexpectedly high flux ($\sim 4 \times 10^{-4}$ cm^{-2} s^{-1}). Being the first radioactivity ever detected through its γ-ray line signature, it provided direct proof of ongoing nucleosynthesis in our Galaxy (see the review by Prantzos and Diehl, 1996).

Several balloon experiments, and, in particular, the gamma-ray spectrometer (GRS) aboard the SMM, rapidly confirmed the HEAO-C finding (Share *et al.*, 1985). Early experiments had large fields of view (130° for SMM, 42° for HEAO-C) with no or modest imaging capabilities. The first map of Galactic 1.8 MeV emission was obtained with the COMPTEL instrument aboard CGRO (Diehl *et al.*, 1995), which had a spatial resolution of 3.8° (FWHM) within a field of view of 30°. The sky map derived from the 9-year survey of COMPTEL is shown in Fig. 7. Unlike the 511 keV maps of Figs. 3 and 4, the ^{26}Al emission is concentrated along the Galactic plane (brightest within the inner Galactic radian) and is irregular, with emission maxima aligned with spiral-arm tangents. The Cygnus region stands out as a significant and bright emission region. The "patchy" nature of the ^{26}Al γ-ray emission indicates that massive stars are the most important contributors to Galactic ^{26}Al, as suggested at a time when the morphology of ^{26}Al emission was unknown (Prantzos, 1991 and Sec. IV.A.2). It is consistent with the (statistically significant) similarity to the Galactic free-emission map, which reflects electron radiation from HII regions ionized from the same massive stars that eventually release ^{26}Al (Knödlseder, 1999).

The total flux of ^{26}Al γ rays depends slightly on the measuring instrument. In terms of statistical precision, the SMM result of $4.0 \pm 0.4 \times 10^{-4}$ photons cm^{-2} s^{-1} rad^{-1} has been considered the canonical value. Imaging instruments, however, have consistently reported lower flux values of $2.6 \pm 0.8 \times 10^{-4}$ photons cm^{-2} s^{-1} rad^{-1} (COMPTEL) and $3.1 \pm 0.4 \times 10^{-4}$ photons cm^{-2} s^{-1} rad^{-1} (SPI), respectively. The latest SPI value is compatible with the full range of measured values by other instruments (within statistical uncertainties), and we adopt it here. The detected flux translates into a decay rate of ^{26}Al which depends slightly on the adopted 3D distribution of ^{26}Al in the Galaxy (Diehl *et al.*, 2006). The most recent analysis of SPI data results in a rate of $\dot{N}_{26} = 4.3 \times 10^{42}$ s^{-1} or $2.7 M_\odot$/Myr (Wang *et al.*, 2009). Assuming a steady state, i.e., equality between production and decay rates, this is also the present production rate of ^{26}Al in the Galaxy; recent models of massive star nucleosynthesis can readily explain such a production rate (Diehl *et al.*, 2006 and Sec. IV.A.2).

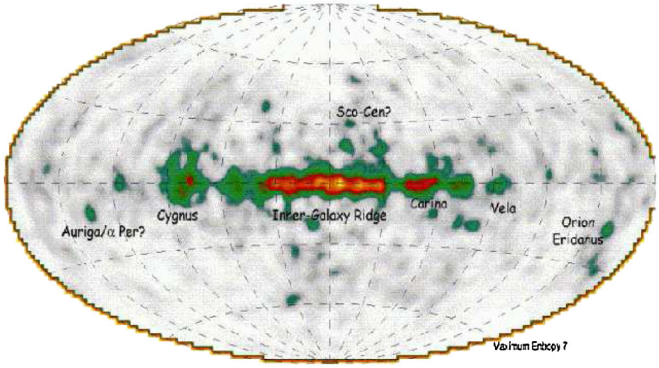

FIG. 7 (color online). Map of Galactic ^{26}Al γ-ray emission after 9-year observations with COMPTEL/CGRO. From Plüschke *et al.*, 2001.

Being predominantly a β^+ emitter (with a branching ratio of $f_{e^+,26} = 82\%$; see Table VII), ^{26}Al is itself a source of positrons. The corresponding Galactic e^+ production rate is $\dot{N}_{e^+,26} = f_{e^+,26} \dot{N}_{26} \sim 3.5 \times 10^{42}$ s^{-1}. This constitutes a significant contribution to the total Galactic e^+ production rate (see Sec. II.B.3 and Table I): 17% of the total e^+ annihilation rate and almost one-half of the (thick) disk in the double bulge + thick disk model, or 10% of the total and 70% of the thin disk in the halo + thin disk model. We shall see in Sec. IV that positrons from other β^+-decaying nuclei can readily explain the remaining disk emissivity, while the bulge emissivity remains hard to explain.

D. Summary of observational constraints

The results of the analysis of Galactic γ-ray emissions in the MeV range can be summarized as follows:

(1) Intensity: The total rate of positron annihilation observed in γ rays is at least $L_{e^+} = 2 \times 10^{43}$ s^{-1}, depending on the adopted source configuration. Most of it comes from the bulge (unless there is important emission from an extended, low-surface-brightness, disk).

(2) Morphology: The bulge-to-disk ratio of e^+ annihilation rates is $B/D \sim 1.4$; however, substantially different ratios cannot be excluded if there is important emission of low surface brightness (currently undetectable by SPI) either from the disk or the spheroid. About one-half of the disk emission can be explained by the observed radioactivity of ^{26}Al (provided its positrons annihilate in the disk). There are hints for an asymmetric disk emission with flux ratio $F(l<0°)/F(l>0°) \sim 1.8$, which has yet to be confirmed.

(3) Spectroscopy: The ratio of the 511 keV line to the $E <$ 511 keV continuum suggests a positronium fraction of $97\% \pm 2\%$ and constrains the physical conditions in the annihilation region. The observed continuum at ~MeV energies can only partly be explained with standard inverse-Compton emission from cosmic-ray electrons. A contribution from unresolved compact sources is also probable, while a (small) contribution from high-energy (>MeV) positrons annihilating in flight cannot be excluded.

These are the key observational constraints that should be satisfied by the source(s) and annihilation site(s) of Galactic positrons. We shall reassess them in light of theoretical analysis at the end of Secs. IV and V.

III. THE GALAXY

The expected spatial distribution and intensity of the positron annihilation emission obviously depends on the corresponding distribution of the potential e^+ sources, as well as on the properties of the ISM in which positrons first slow down and then annihilate. One may distinguish two types of e^+ sources, depending on whether their lifetimes (τ_S) are shorter or longer than the lifetime of positrons in the ISM (τ_{e^+}). Calculation of the total e^+ production rate requires in the former case ($\tau_S < \tau_{e^+}$) an estimate of (i) the Galactic birthrate R_S of the sources and (ii) the individual e^+ yields n_{e^+} (i.e., the average amount of positrons released by each source). In the latter case ($\tau_S > \tau_{e^+}$), the total number of such sources in the Galaxy, N_S, is required, as well as the individual e^+ production rate $\dot{n}_{e^+}$ of each source. In the former class belong supernovae or novae and the corresponding positron production rate is $\dot{N}_{e^+} = R_S n_{e^+}$; in the latter class belong, e.g., low-mass x-ray binaries (XRBs) or millisecond pulsars, and the corresponding positron production rate is $\dot{N}_{e^+} = N_S \dot{n}_{e^+}$.

The Galactic distribution of any kind of stellar source of positrons is somewhat related to the distribution of stars in the Milky Way. Similarly, the birthrate of any kind of positron source is somewhat related to the Galactic star formation rate. In this section we present a summary of current knowledge about the stellar populations of the Milky Way and their spatial distribution and we discuss the birthrates of stars and supernovae. Since the slowing down and annihilation of positrons depend on the properties of the ISM, we present a brief overview of the ISM in the bulge and the disk of the Milky Way. Positron propagation depends also on the properties of the Galactic magnetic field, which are reviewed in Sec. III.D. Finally, the main properties of the Milky Way's dark matter halo are presented in Sec. III.E.

A. Stellar populations

The Milky Way is a typical spiral galaxy, with a total baryonic mass of $\sim 5 \times 10^{10} M_\odot$, of which more than 80% is in the form of stars. Stars are found in three main components: the central bulge, the disk, and the halo, while the gas is found essentially in the plane of the disk. Because of its low mass, estimated to $4 \times 10^8 M_\odot$, i.e., less than 1% of the total (Bell *et al.*, 2008), the Galactic halo plays no significant role in the positron production. The bulge contains $\sim 1/3$ of the total mass and an old stellar population (age >10 Gyr). The dominant component of the Milky Way is the so-called *thin disk*, a rotationally supported structure composed of stars of all ages (0–10 Gyr). A non-negligible, contribution is brought by the *thick disk*, an old (>10 Gyr) and kinematically distinct entity identified by Gilmore and Reid (1983).

To a first approximation, and by analogy with external galaxies, the bulge of the Milky Way can be considered as spherical, with a density profile either exponentially decreasing with radius r or of Einasto type $\rho(r) \propto \exp(-Ar^\alpha)$. Measurements in the near infrared, concerning either integrated starlight observations or star counts, revealed that the bulge is not spherical, but elongated. Recent models suggest a triaxial ellipsoid, but its exact shape is difficult to determine (López-Corredoira *et al.*, 2005; Rattenbury *et al.*, 2007) because of the presence of a Galactic bar. The mass of the bulge lies in the range $(1–2) \times 10^{10} M_\odot$ (Dwek *et al.*, 1995; Robin *et al.*, 2003). By comparing color-magnitude diagrams of stars in the bulge and in metal-rich globular clusters, Zoccali *et al.* (2003) found that the populations of the two systems are coeval, with an age of ~ 10 Gyr.

The innermost regions of the bulge, within a few hundred pc, are dominated by a distinct, disklike component, called the nuclear bulge, which contains about 10% of the bulge stellar population ($\sim 1.5 \times 10^9 M_\odot$) within a flattened region of radius 230 ± 20 pc and scale height 45 ± 5 pc (Launhardt *et al.*, 2002). It is dominated by three massive stellar clusters (Nuclear Stellar Cluster in the innermost 5 pc, Arches, and Quintuplex), which have a mass distribution substantially flatter than the classical Salpeter IMF (Figer, 2008).[6] Finally, in the center of the Milky Way, at the position of the SgrA* source, lies the supermassive Galactic black hole (SMBH) with a total mass of $\sim 4 \times 10^6 M_\odot$ (Gillessen *et al.*, 2009).

The Sun is located in the thin disk of the Milky Way, at a distance of $R_\odot \sim 8$ kpc from the Galactic center; a recent evaluation, based on Cepheids, gives $R_\odot = 7.94 \pm 0.37(\text{stat}) \pm 0.26(\text{syst})$ kpc (Groenewegen *et al.*, 2008, and references therein). Furthermore, the Sun is not located exactly on the plane, but at a distance from it $z_\odot \sim 25$ pc, as evaluated from the recent analysis of the Sloan Digital Sky Survey (SDSS) data (Jurić *et al.*, 2008).

In studies of the Milky Way the solar neighborhood plays a pivotal role, since local properties can, in general, be measured with greater accuracy than global ones. The total baryonic surface density of the solar cylinder[7] is estimated to $\Sigma_T = 48.8 M_\odot\ \text{pc}^{-2}$ (Flynn *et al.* (2006), with $\sim 13 M_\odot \text{pc}^{-2}$ belonging to the gas (see Sec. III.B). This falls on the lower end of the dynamical mass surface density estimates (from kinematics of stars perpendicularly to the plane) which amount to $\Sigma_D = (50–62) M_\odot\ \text{pc}^{-2}$ (Holmberg and Flynn, 2004) or $57–66 M_\odot\ \text{pc}^{-2}$ (Bienaymé *et al.*, 2006). Thus, the values for the baryon content of the solar cylinder, summarized in Table III, should be considered rather as lower limits (Flynn *et al.*, 2006): The total stellar surface density could be as high as $40 M_\odot\ \text{pc}^{-2}$.

The density profiles of the stellar thin and thick disks can be satisfactorily fitted with exponential functions, both in the radial direction and perpendicularly to the Galactic plane. The recent SDSS data analysis of star counts, with no *a priori* assumptions as to the functional form of the density profiles finds exponential disks with scale lengths as displayed in Table III [from Jurić *et al.* (2008)]. The thin and thick disks cannot extend all the way to the Galactic center, since dynamical arguments constrain the spatial coexistence of such

[6]Stars are born with a mass distribution called initial mass function (IMF). Observed IMFs of young stellar clusters in the Milky Way and other galaxies have similar IMFs, with the upper part ($M > 1 M_\odot$) described by a power law $dN/dM \propto M^{-(1+X)}$, where X is the slope of the IMF; in most cases, $X = 1.35$ [as determined by Salpeter (1955)], for the local IMF.

[7]The solar cylinder is defined as a cylinder of radius 500 pc centered on the Sun's position and extending perpendicularly to the Galactic plane up to several kpc.

TABLE III. Properties of the stellar populations of the thin and thick disks.[a]

			Thin	Thick
Mass density	$\rho_{0,\odot}$	$(M_\odot\,\mathrm{pc}^{-3})$	4.5×10^{-2}	5.3×10^{-3}
Surface density	$\Sigma_\odot$	$(M_\odot\,\mathrm{pc}^{-2})$	28.5	7
Scale height	$H_\odot$	(pc)	300	900
Scale length	L	(pc)	2600	3600
Star mass	M_D	$(10^{10}M_\odot)$	2.3	0.53
$\langle\mathrm{Age}\rangle_\odot$	$\langle A\rangle_\odot$	(Gyr)	5	10
$\langle\mathrm{Metallicity}\rangle_\odot$	$\langle[\mathrm{Fe/H}]\rangle_\odot$	(dex)	−0.1	−0.7

[a]The indice ⊙ here denotes quantities measured at galactocentric distance $R_\odot = 8$ kpc. Average quantities are given within $\langle\,\rangle$.

TABLE IV. Physical properties (typical temperatures, hydrogen densities, and ionization fractions) of the different ISM phases in the Galactic disk.

Phase	T (K)	n_H (cm^{-3})	x_ion
Molecular (MM)	10–20	10^2–10^6	$\lesssim 10^{-4}$
Cold neutral (CNM)	20–100	20–100	4×10^{-4}–10^{-3}
Warm neutral (WNM)	10^3–10^4	0.2–2	0.007–0.05
Warm ionized (WIM)	∼8000	0.1–0.3	0.6–0.9
Hot ionized (HIM)	$\sim10^6$	0.003–0.01	1

rotationally supported structures with the pressure-supported bulge. The exact shape of the ''central hole'' of the disks is poorly known [see, e.g., Freudenreich (1998) and Robin *et al.* (2003), for parametrizations], but for most practical purposes (i.e., estimates of the total disk mass) the hole can be considered as truly void of stars for disk radius $R < 2$ kpc.

The data presented in this section (as summarized in Table III) allow one to estimate the total mass of the thin and thick disks as $M_{D,\mathrm{thin}} = 2.3\times10^{10}M_\odot$ and $M_{D,\mathrm{thick}} = 0.5\times10^{10}M_\odot$, respectively, in the galactocentric distance range of 2–15 kpc. Overall, the disk of the MW is twice as massive as the bulge.

B. Interstellar matter

Interstellar matter is primarily composed of hydrogen, but it also contains helium (≃ 9% by number or 28% by mass) and heavier elements, called ''metals'' (≃ 0.12% by number or 1.5% by mass in the solar neighborhood). All the hydrogen, all the helium, and approximately half the metals exist in the form of gas; the other half of the metals is locked up in small solid grains of dust. Interstellar dust manifests itself through its selective absorption of starlight (leading to extinction, reddening, and polarization of starlight) and through its thermal infrared emission. Dust grains cover a whole range of radii, from $a_\mathrm{min} \lesssim 100$ Å to $a_\mathrm{max} \gtrsim 0.25$ μm, as implied from the overall shape of extinction curves which can be reproduced with a power-law distribution in radius, $N(a)da \propto a^{-3.5}da$ (Mathis *et al.*, 1977; Kim, *et al.*, 1994; Boulanger *et al.*, 2000). Overall, gas and dust appear to be spatially well correlated (Boulanger and Perault, 1988; Boulanger *et al.*, 1996).

Interstellar gas can be found in molecular, atomic (cold or warm) and ionized (warm or hot) forms. The physical properties of the different gas components in the Galactic disk were reviewed by Ferrière (2001) and are summarized in Table IV. The gas properties in the Galactic bulge are less well established, but on the whole, all gas components appear to be hotter and denser in the bulge than in the disk (Ferrière *et al.*, 2007).

Spatially, the molecular gas is confined to discrete clouds, which are roundish, gravitationally bound, and organized hierarchically from large complexes (size ∼20–80 pc, mass $\sim10^5$–$2\times10^6M_\odot$) down to small clumps (size $\lesssim 0.5$ pc, mass $\lesssim 10^3M_\odot$) (Goldsmith, 1987). The cold atomic gas is confined to more diffuse clouds, which often appear sheetlike or filamentary, cover a wide range of sizes (from a few pc up to ∼2 kpc), and have random motions with typical velocities of a few km s^{-1} (Kulkarni and Heiles, 1987). The warm and hot components are more widespread and they form the intercloud medium.

The different gas components also differ by their spatial distributions at large scales. The observational situation was reviewed by Ferrière (2001) for the Galactic disk and by Ferrière *et al.* (2007) for the Galactic bulge. Figure 8 gives the radial variation of the azimuthally averaged surface densities of H_2, H I, H II, and the total gas (accounting for a 28% contribution from He), while Fig. 9 gives the vertical variation of their respective space-averaged volume densities averaged along the solar circle (at $R = R_\odot$). The total interstellar masses of the three gas components in the Galactic disk are uncertain and their sum in the Galactic disk, i.e., between 2 and 20 kpc, is probably comprised between $\sim0.9\times10^{10}M_\odot$ and $\sim1.5\times10^{10}M_\odot$.

Since most of the transport and annihilation of positrons takes place in the Galactic bulge, its gas distribution deserves a more detailed description. In the bulge, the interstellar gas is roughly equally divided between the neutral (molecular + atomic) and ionized components, and the neutral component is ∼90% molecular. The molecular gas tends to concentrate in the so-called central molecular zone (CMZ) (Morris and Serabyn, 1996), a thin sheet parallel to the Galactic plane, which, in the plane of the sky, extends out to $R \sim 250$ pc at longitudes $l > 0°$ and $R \sim 150$ pc at $l < 0°$ and has a FWHM thickness ∼30 pc. Projected onto the Galactic plane, the CMZ appears as a 500×200 pc ellipse inclined (clockwise) by ∼70° to the line of sight (Sawada *et al.*, 2004). Outside the CMZ, the molecular gas is contained in a significantly tilted disk (Liszt and Burton, 1978; Burton and Liszt, 1992), extending in the plane of the sky out to $R \sim 1.3$ kpc on each side of the GC and having a FWHM thickness ∼70 pc. According to Liszt and Burton (1980), the tilted disk has the shape of a 3.2×1.0 kpc ellipse, which is tilted (counterclockwise) by ∼13.5 out of the Galactic plane and inclined (near side down) by ∼70° to the plane of the sky. The tilted disk is also believed to feature an elliptical hole in the middle, just large enough to enclose the CMZ. The spatial distribution of the atomic gas is arguably similar to that of the molecular gas [Burton and Liszt (1992), but see also Combes (1991) for another point of view], with this difference that the atomic layer is about 3 times thicker than the molecular layer, both in the CMZ and in the tilted disk. The ionized gas, for its part, is not confined to either the CMZ or the tilted disk; it appears to fill the entire bulge and to connect with the ionized gas present in the disk.

The dramatic density and temperature contrasts between the different ISM phases as well as the supersonic random

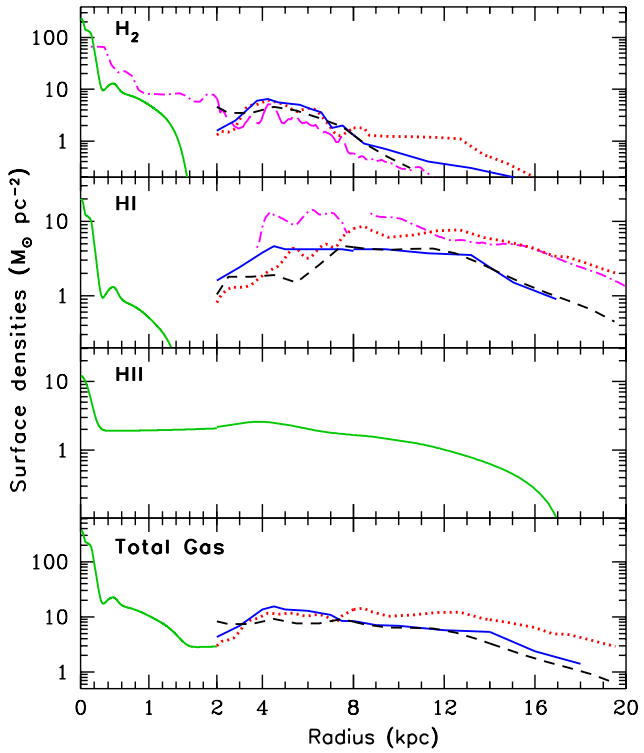

FIG. 8 (color online). Azimuthally averaged surface densities of interstellar atomic, molecular, and ionized hydrogen as functions of the Galactic radius. The total gas (bottom panel) includes a 40% contribution by helium. Notice the change of scale at $R = 2$ kpc. For $R < 2$ kpc (bulge) data are derived by Ferrière *et al.* (2007), based on a compilation of earlier works: Sawada *et al.* (2004) for the molecular gas in the central molecular zone, Liszt and Burton (1980) for the neutral gas in the tilted disk, and Cordes and Lazio (2002) for the ionized gas. In all panels, disk data ($R > 2$ kpc) are from Dame (1993) (solid lines); Olling and Merrifield (2001) (dotted lines); Nakanishi and Sofue (2006) for H I, and Nakanishi and Sofue (2003) for H_2, respectively (dashed lines); and Kalberla and Dedes (2008) for H I and Pohl *et al.* (2008) for H_2, respectively (dot-dashed lines). The curve in the H II panel is from the NE2001 free-electron density model of Cordes and Lazio (2002) (for simplicity, we identified the H density with the free-electron density, i.e., we neglected the contribution of free electrons originating from He in the HIM).

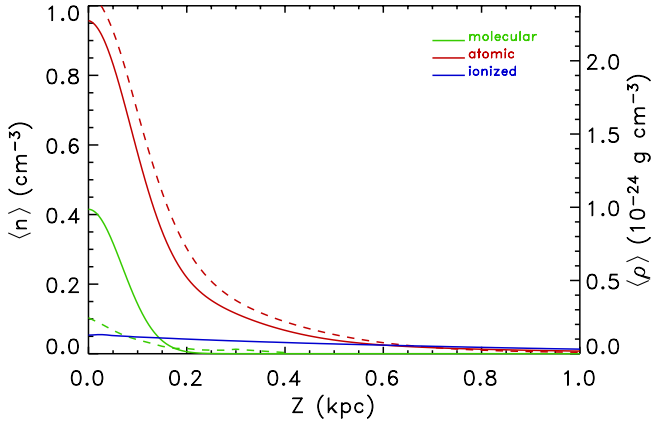

FIG. 9 (color online). Space-averaged volume densities of interstellar H_2, H I, and H II, averaged along the solar circle ($R = R_\odot$), as functions of distance from the Galactic plane Z. Data: H_2 from Bronfman *et al.* (1988), rescaled to $X_{CO} = 2.3 \times 10^{20}$ cm^{-2} K^{-1} km^{-1} s, as in Olling and Merrifield (2001); H I from Dickey and Lockman (1990), scaled up by a factor of 1.58 such as to match the H I surface density of Olling and Merrifield (2001). All other curves are from the same sources as in Fig. 8.

motions observed in all of them bear witness to a highly turbulent state. The powerful winds and terminal supernova explosions of the most massive stars are mainly responsible for this turbulence. Interstellar turbulence manifests itself over a huge range of spatial scales, from $\lesssim 10^{10}$ up to $\gtrsim 10^{20}$ cm; throughout this range, the power spectrum of the free-electron density in the local ISM is consistent with a Kolmogorov-like power law (Armstrong *et al.*, 1995).

C. Star formation and supernova rates

Determination of absolute values of star formation rates (SFRs, in $M_\odot$ yr^{-1}) constitutes one of the most challenging tasks in modern astrophysics (Kennicutt, 1998). In the case of the Milky Way, methods based on counts of various short-lived objects [with lifetimes less than a few Myr, such as pulsars, supernovae (SN) remnants, or OB associations] are used. Those methods establish, in fact, the *relative* star formation rate across the Galactic disk. Surface density profiles of various stellar tracers appear in Fig. 10. For the calibration of the SFR profile one needs to know either the total SFR of the MW disk or the local one in the solar neighborhood. A "ballpark" estimate of the former value is obtained by noting that the late spectral type (Sbc) of the MW suggests a slow formation at a relatively steady rate ⟨SFR⟩ over the past $\Delta T \sim 10$ Gyr, leading to $\langle \mathrm{SFR} \rangle = M_{D,\mathrm{thin}}/\Delta T \sim 2.3 M_\odot\,\mathrm{yr}^{-1}$. Most empirical estimates of the present-day total Galactic SFR, based on the aforementioned tracers (and *assumptions* on the IMF) produce values within a factor of 2 of the ⟨SFR⟩ [see, e.g., McKee and Williams (1997) and Robitaille and Whitney (2010), and references therein].

In the context of Galactic positrons, special attention should be paid to the star formation activity in the central regions of the bulge. The massive star population of the three major star clusters inside the nuclear bulge clearly indicates important recent star formation, obviously fed from the gas of the CMZ. Deep field observations of late-type stars with the Near Infrared Camera and Multi-Object Spectrometer/Hubble Space Telescope (Figer *et al.*, 2004) and with the Spectrograph for INtegral Field Observations in the Near Infrared/Very Large Telescope (Maness *et al.*, 2007) suggest that the star forming activity in that region has proceeded at a relatively steady rate, of the order of a few $10^{-2} M_\odot$/yr, over the past ~10 Gyr.

From the theoretical point of view, SNs are now classified mainly as *thermonuclear* supernovae (the explosion energy being due to the thermonuclear disruption of a white dwarf accreting matter in a binary system) or *core collapse* supernovae (CCSN, where the energy originates from the gravitational collapse of the iron core of a massive star that has exhausted all its nuclear fuel). Thermonuclear supernovae are identified with SNIa (lacking hydrogen in their spectra) and are observed in all types of galaxies: old ellipticals with no current star formation, but also young, star-forming, spiral,

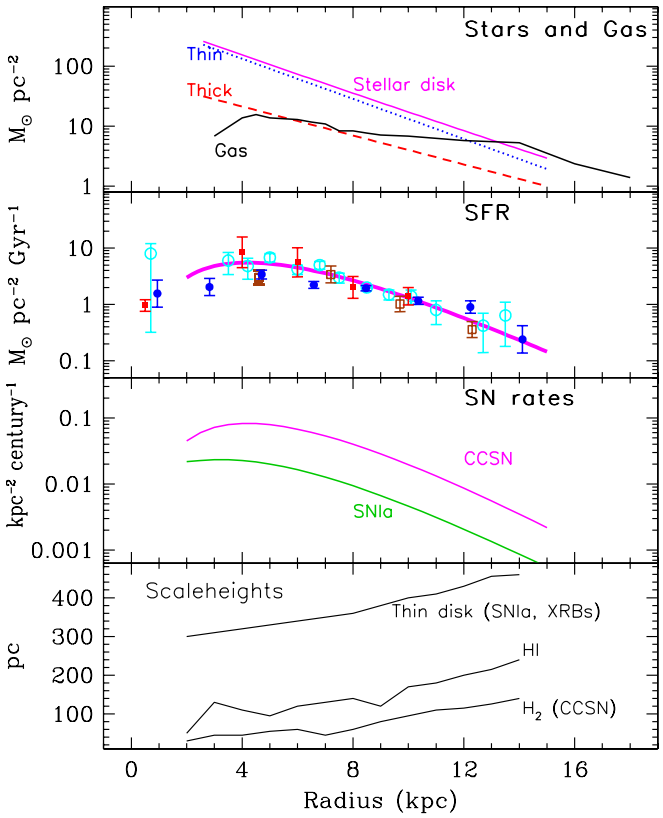

FIG. 10 (color online). Surface densities of stars + gas, SFR, SN rates, and scale heights of gas and stars as a function of galactocentric distance. The star profiles are from the data of Table II and the gas profile is the one of Dame (1993) (bottom panel of Fig. 6). Data for SFR are from Lyne *et al.* (1985) (open cicles); Case and Bhattacharya (1998) (filled circles); McKee and Williams (1997) (open squares); Guibert *et al.* (1978) (filled squares). The solid curve is an approximate fit, normalized to 2 $M_\odot$ yr^{-1} for the whole Galaxy. The same curve is used for the CCSN rate profile (third panel), normalized to 2 CCSN/century; the SNIa rate profile is calculated by Eq. (4) and normalized to 0.5 SNIa/century (Table V).

and irregular galaxies. All other supernova types (SNII, SNIb, SNIc) are exclusively observed in the star-forming regions of spirals (i.e., inside spiral arms) and irregulars[8].

No supernovae have been observed in the Galaxy in the past four centuries, and the handful of so-called "historical supernovae" offers a very biased estimate of the Galactic SN frequency (Tammann *et al.*, 1994). All methods used to determine the Galactic SN rate which are based exclusively on Galactic data suffer from various systematic uncertainties and converge to a value of $R_{\rm CCSN}$ equal to a few per century (Diehl *et al.*, 2006, and references therein). The most accurate way to evaluate the Galactic SN rate is, probably, through statistics of SN rates in external galaxies. The work of Mannucci *et al.* (2005), corrected for various observational biases, offers a valuable database for such an estimate and can be used, along with the stellar masses of the various Galactic components (Sec. III.A), to derive the Galactic rate of the main SN types (Table V).

The spatial distribution of core collapse SN in the MW should obviously follow that of the SFR (Fig. 10). Such an azimuthally averaged surface density masks the fact that CCSNs are exclusively concentrated inside spiral arms. The scale height of core collapse SN should be comparable to the scale height of the molecular gas, i.e., less than 100 pc, and little varying with galactocentric distance. More difficult is the evaluation of the radial profile of SNIa, since the progenitor white dwarfs may originate from stars of a wide variety of stellar masses ($(1–8)M_\odot$) and corresponding lifetimes (10–0.05 Gyr). Various models have been developed in order to calculate the SNIa rate [see, e.g., Greggio (2005)]. A useful empirical approach is the one adopted by Scannapieco and Bildsten (2005), where the SNIa rate is calculated as the sum of two terms: one depending on the stellar mass M_* and one on the SFR of the system, i.e.,

$$\frac{R_{\rm SNIa}}{\rm century} = A\frac{M_*}{10^{10}M_\odot} + B\frac{\rm SFR}{M_\odot\ {\rm yr}^{-1}} \tag{4}$$

with parameters A and B empirically determined (Scannapieco and Bildsten, 2005; Sullivan *et al.*, 2006). The parametrized SNIa profile in the Milky Way disk appears in the third panel of Fig. 10. Taking into account the nature of the SNIa progenitors, it is expected that the distribution of SNIa vertically to the disk plane will follow the corresponding distribution of the thin disk, i.e., with a scale height of 300 pc (an insignificant contribution from the thick disk is also expected).

D. Interstellar magnetic fields

The magnetic field strength B in cold, dense regions of interstellar space can be inferred from the Zeeman splitting of the 21 cm line of H I (in atomic clouds) and centimeter lines of OH and other molecules (in molecular clouds). In practice, it is the line-of-sight component of the magnetic field $B_\parallel$ that is measured. With appropriate statistical corrections for projection effects, it is found that in atomic clouds, B is typically a few microgauss, with a slight tendency to increase with increasing density (Troland and Heiles, 1986; Heiles and Troland, 2005), while in molecular clouds, B increases approximately as the square root of density, from $\sim$10 to $\sim$3000 μG (Crutcher, 1999, 2007).

The interstellar magnetic field **B** in the ionized medium is generally probed with Faraday rotation measures of Galactic pulsars and extragalactic radio sources. Here, too, the quantity that is actually measured is $B_\parallel$. Faraday rotation studies provided the following interesting pieces of information:

(1) **B** has a uniform (or regular) component $\mathbf{B}_u$, and a random (or turbulent) component $\mathbf{B}_r$. Near the Sun, $B_u \simeq 1.5$ μG and $B_r \sim 5$ μG (Rand and Kulkarni, 1989). Away from the Sun, B_u increases toward the GC, to $\gtrsim 3$ μG at $R = 3$ kpc (Han *et al.*, 2006), i.e., with an exponential scale length $\lesssim 7.2$ kpc. In addition, B_u decreases away from the midplane, albeit at a very uncertain rate; for reference, the exponential scale height inferred from the rotation measures of extragalactic sources is $\sim$1.4 kpc (Inoue and Tabara, 1981).

[8]The degree of mass loss suffered by the massive star prior to the explosion determines the appearance of the core collapse supernova as SNII (little H lost), SNIb (all H and little He lost), or SNIc (all H and most He lost).

TABLE V. Supernova rates in the Milky Way. SNuM: = 1 SN per $10^{10} M_\odot$ per century.

	Stellar mass[a] $10^{10} M_\odot$	Spectral type	SNIa Specific rate[b] SNuM	SNIa Rate century^{-1}	Core collapse SN Specific rate[b] SNuM	Core collapse SN Rate century^{-1}
Bulge	1.4	E0	0.044	0.062	—	—
Nuclear bulge	0.15	Sbc/d − Irr[c]	0.17–0.77	0.025–0.115	0.86–2.24	0.13–0.33
Thin disk	2.3	Sbc	0.17	0.4	0.86	2
Thick disk	0.5	E0	0.044	0.022	—	
Total bulge	1.5			0.087–0.18		0.13–0.33
Total disk	2.8			0.42		2
Total Milky Way	4.3			0.5–0.6		2.13–2.33
Bulge-to-disk ratio	<0.5			0.21–0.43		0.06–0.15

[a]See Sec. III.A for references.
[b]Mannucci *et al.* (2005).
[c]Very uncertain, in view of uncertainties in star formation efficiency and slope of IMF (see text).

(2) In the Galactic disk, $\mathbf{B}_u$ is nearly horizontal and generally dominated by its azimuthal component. It is now widely accepted that $\mathbf{B}_u$ reverses several times with decreasing radius, but the number and radial locations of the reversals are still highly controversial (Rand and Lyne, 1994; Han *et al.*, 1999; Vallée, 2005; Han *et al.*, 2006; Brown *et al.*, 2007). These reversals have often been interpreted as evidence that $\mathbf{B}_u$ is bisymmetric (azimuthal wave number $m = 1$), while an axisymmetric ($m = 0$) field would be expected from dynamo theory. In reality, Men *et al.* (2008) showed that neither the axisymmetric nor the bisymmetric picture is consistent with the existing pulsar rotation measures, and they concluded that $\mathbf{B}_u$ must have a more complex pattern.

(3) In the Galactic halo, $\mathbf{B}_u$ could have a significant vertical component. For the local halo, Taylor *et al.* (2009) obtained $(B_u)_Z \sim -0.14$ μG above the midplane ($Z > 0$) and $(B_u)_Z \sim +0.30$ μG below the midplane ($Z < 0$), whereas Mao *et al.* (2010) obtained $(B_u)_Z \sim 0.00$ μG toward the Galactic North Pole and $(B_u)_Z \sim +0.31$ μG toward the Galactic South Pole. In contrast to the situation in the Galactic disk, the azimuthal component of $\mathbf{B}_u$ shows no sign of reversal with decreasing radius.

(4) At low latitudes (basically, in the disk), $\mathbf{B}_u$ appears to be roughly symmetric in Z (Rand and Lyne, 1994; Frick *et al.*, 2001), while at high latitudes (in the halo), $\mathbf{B}_u$ appears to be roughly antisymmetric and/or symmetric in Z inside and/or outside the solar circle (Han *et al.*, 1997, 1999). Finding $\mathbf{B}_u$ to be symmetric in the disk and antisymmetric in the inner halo is consistent with the predictions of dynamo theory and with the results of Galactic dynamo calculations [see, e.g., Moss and Sokoloff (2008) and Ruzmaikin *et al.* (1988)]. However, there is no reason to believe that $\mathbf{B}_u$ is simply a pure quadrupole (in the disk) and a pure dipole (in the inner halo), sheared out in the azimuthal direction by the Galactic differential rotation. In this respect, one should emphasize that the picture of an azimuthally sheared pure dipole, originally proposed by Han (2002) and often used in the cosmic-ray propagation community [see, e.g., Alvarez-Muñiz *et al.* (2002) and Prouza and Šmída (2003)], is supported neither by numerical simulations of Galactic dynamos nor by observations of external edge-on galaxies, which generally reveal X-shaped field patterns (Beck, 2008).

A more global method to map out the spatial distribution of $\mathbf{B}$ rests on the observed Galactic synchrotron emission. Relying on the synchrotron map of Beuermann *et al.* (1985) and assuming equipartition between magnetic fields and cosmic rays, Ferrière (1998) found that the total magnetic field has a local value $\simeq 5.1$ μG, a radial scale length $\simeq 12$ kpc, and a local vertical scale height $\simeq 4.5$ kpc. Besides, synchrotron polarimetry indicates that the local ratio of ordered (regular + anisotropic random) to total fields is $\simeq 0.6$ (Beck, 2001), implying an ordered field $\simeq 3$ μG near the Sun.

In the vicinity of the GC, the interstellar magnetic field has completely different properties from those prevailing in the Galactic disk. In that region, systems of nonthermal radio filaments were discovered, which run nearly perpendicular to the Galactic plane and pass through it with little or no distortion (Yusef-Zadeh *et al.*, 1984; Liszt, 1985). The morphology of the filaments strongly suggests that they follow magnetic field lines, and radio polarization measurements (assuming synchrotron emission) confirm that the magnetic field in the filaments is oriented along their long axis (Tsuboi *et al.*, 1985; Reich, 1994). From this, it was naturally concluded that the interstellar magnetic field near the GC is approximately vertical, at least close to the midplane. Farther from the midplane, the filaments tend to lean somewhat outward, consistent with the interstellar magnetic field having an overall poloidal geometry (Morris, 1990).

The radio filaments have equipartition or minimum-energy field strengths ~50–200 μG (Anantharamaiah *et al.*, 1991; LaRosa *et al.*, 2004, and references therein). On the other hand, the fact that the filaments remain nearly straight all along their length suggests that their magnetic pressure is stronger than the ram pressure of the ambient interstellar clouds, or, equivalently, that their field strength is $B \gtrsim 1$ mG (Yusef-Zadeh and Morris, 1987).

Low-frequency radio observations of diffuse nonthermal (supposedly synchrotron) emission from a $6° \times 2°$ region centered on the GC imply that the diffuse ISM near the GC has a minimum-energy field strength $\gtrsim 6$ μG—possibly up to ~80 μG if the cosmic-ray proton-to-electron energy ratio is as high as 100 and the filling factor of the synchrotron-emitting gas is as low as 0.01 (LaRosa *et al.*, 2005). A more reliable estimation of the general field strength in the GC region emerges from the recent analysis of Crocker *et al.* (2010), which combines radio and γ-ray data and comes to the conclusion that $B \gtrsim 50$ μG.

Far-infrared and submillimeter polarization studies of dust thermal emission from the GC region indicate that the magnetic field inside GC molecular clouds is roughly parallel to the Galactic plane (Novak *et al.*, 2003). More precisely, the field direction appears to depend on the molecular gas density, being nearly parallel to the plane in high-density regions and nearly perpendicular to it in low-density regions (Chuss *et al.*, 2003). Near-infrared polarization studies of starlight absorption by dust also find the magnetic field inside GC molecular clouds to be roughly horizontal, although without any obvious correlation between field direction and gas density (Nishiyama *et al.*, 2009).

Zeeman splitting measurements yielded mixed results. In the circumnuclear disk, the innermost molecular region with radius $\lesssim 7$ pc, Killeen *et al.* (1992) and Plante *et al.* (1995) derived line-of-sight magnetic fields $|B_{\|}| \simeq 2$ mG and $|B_{\|}| \simeq 0.6$–4.7 mG, respectively. Farther from the GC, Crutcher *et al.* (1996) measured values of $|B_{\|}|$ ranging between $\simeq 0.1$ and 0.8 mG toward the main and north cores of Sgr B2. In contrast, Uchida and Guesten (1995) reported only nondetections, with 3σ upper limits to $|B_{\|}| \sim 0.1$–1 mG, toward 13 selected positions within a few degrees of the GC (including Sgr B2).

Faraday rotation measures also yielded somewhat disparate results. The disparity lies not so much in the absolute value of $B_{\|}$, which is generally estimated at a few μG [see, e.g., Gray *et al.* (1991), Tsuboi *et al.* (1985), and Yusef-Zadeh and Morris (1987)], but more in the (l, b) dependence of its sign. Novak *et al.* (2003), who collected all the available rotation measures toward synchrotron sources within 1° of the GC, found that $B_{\|}$ reverses sign both across the rotation axis and across the midplane. A different pattern was uncovered by Roy *et al.* (2005), who derived the rotation measures of 60 background extragalactic sources through the region ($|l| < 6°$, $|b| < 2°$) and obtained mostly positive values, with no evidence for a sign reversal either with l or with b.

The properties of the turbulent magnetic field are not well established. Rand and Kulkarni (1989) provided a first rough estimate for the typical spatial scale of magnetic fluctuations, ~55 pc, although they recognized that the turbulent field cannot be characterized by a single scale. Later, Minter and Spangler (1996) presented a careful derivation of the power spectrum of magnetic fluctuations over the spatial range ~(0.01–100) pc; they obtained a Kolmogorov spectrum below ~4 pc and a flatter spectrum consistent with 2D turbulence above this scale. In a complementary study, Han *et al.* (2004) examined magnetic fluctuations at larger scales, ranging from ~0.5 to 15 kpc; at these scales, they found a nearly flat magnetic spectrum, with a 1D power-law index ~ -0.37 (Fig. 11).

The properties, poorly understood at present, of the turbulent Galactic magnetic field as well as its overall configuration, are extremely important for understanding positron propagation in the Milky Way (Sec. VI).

E. The dark matter halo

A large body of observational data on the extragalactic Universe suggests that its mass is dominated by nonbaryonic dark matter. In the presently widely accepted "standard" cosmological model (ΛCDM, for cold dark matter with cosmological constant Λ) dark matter accounts for a fraction $\Omega_{\rm DM} \sim 24\%$ of the overall matter and energy budget of the Universe, baryons for ~4%, and dark energy, or cosmological constant, for the remaining ~72% (Bartelmann, 2010).

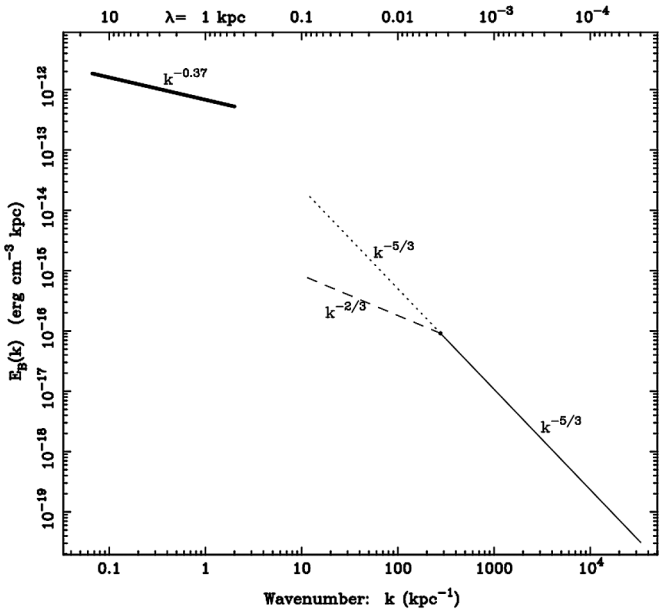

FIG. 11. Composite magnetic energy spectrum in our Galaxy. The thick solid line is the large-scale spectrum. The thin solid and dashed or dotted lines give the Kolmogorov and two-dimensional turbulence spectra, respectively, inferred from the Minter and Spangler (1996) study. The two-dimensional turbulence spectrum is uncertain; it probably lies between the dashed [$E_B(k) \propto k^{-2/3}$] and dotted [$E_B(k) \propto k^{-5/3}$] lines. From Han *et al.*, 2004.

The presence of dark matter in spiral galaxies is deduced from the fact that their rotation curves beyond a radius of ~3 scale lengths do not fall off as rapidly as expected from their baryonic content. In the case of the Milky Way, the rotation curve is poorly determined beyond the Sun's location ($R_\odot = 8$ kpc). It is then assumed, rather than directly inferred from observations, that the MW is found inside a dark matter halo with a density profile $\rho_{\rm DM}(r)$ similar to those found in numerical simulations of structure formation in a ΛCDM universe [see, e.g., Navarro *et al.* (1997)]. In the absence of baryons such simulations predict approximately universal density profiles $\rho_{\rm DM}(r) \propto r^{-k}$, with k being itself a positive function of radius r: $k(r) \propto r^s$ ("Einasto profile"). Because of finite numerical resolution, values of k cannot yet be reliably determined in the inner halo. Some simulations find $k = 1.5$ in the inner galaxy (Moore *et al.*, 1999), but the analysis of one of the largest simulations so far (Navarro *et al.*, 2010) suggests that $k = 0.9 \pm 0.1$, i.e., a value compatible with the value of $k = 1$ in the classical Navarro-Frenck-White (NFW) profile (Navarro *et al.*, 1997). For values of $k \geq 1$ mass diverges as $r \to 0$ (*cuspy* profiles). Including interactions of dark matter with baryons (Blumenthal *et al.*, 1986) or with a central black hole (Gondolo and Silk, 1999) generically tend to enhance the cusp [see, e.g., Sellwood and McGaugh (2005)].

The shape of the dark matter density profile in the inner Galaxy is obviously crucial for the corresponding profile of the putative positrons released from dark matter decay,

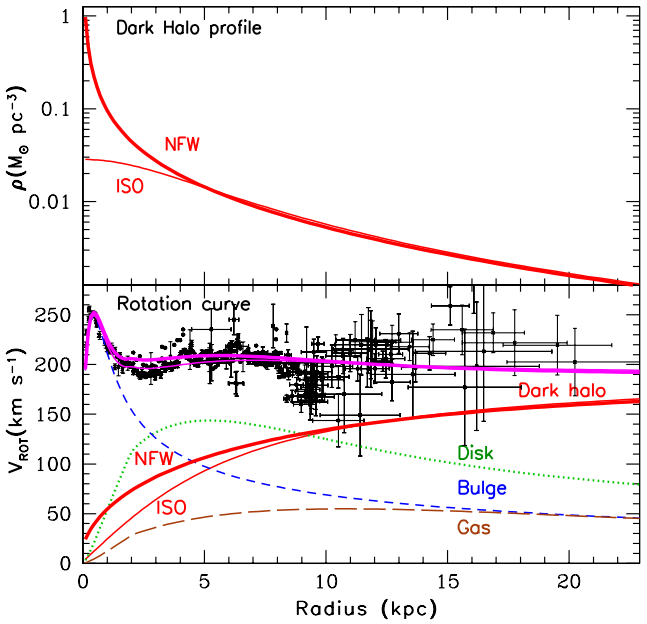

FIG. 12 (color online). Dark matter density profile (top panel) and rotational velocity (bottom panel) of the Milky Way; the various components (bulge, stellar disk, gas, and dark halo) contributing to the latter are also indicated. In both panels thick and thin solid curves correspond to NFW and isothermal ("ISO") dark halo profiles, respectively. Data points are from Sofue *et al.*, 2008.

annihilation, or deexcitation (see Sec. IV.C). Since dark matter is subdominant in the inner Galaxy (see Fig. 12), observations of the rotation curve cannot help to determine its density profile. Analyzing observations of the optical depth of the inner Galaxy to microlensing events (which are affected only by the baryonic mater), Binney and Evans (2001) found $k \sim 0.3$. On the other hand, rotation curves of dwarf galaxies (which are dominated by dark matter) systematically suggest flat profiles (Gentile *et al.*, 2007; Spano *et al.*, 2008) with $k \sim 0$, such as those obtained in the case of cored isothermal dark halo [see also Merritt (2010)]. A useful parametrization of the density profiles is

$$\rho(r) = \frac{\rho_0(r_0)}{(r/r_0)^{\gamma}[1 + (r/r_0)^{\alpha}]^{(\beta-\gamma)/\alpha}}, \tag{5}$$

where ρ_0 and r_0 are, respectively, the characteristic mass and energy density and radius of the halo and α, β, and γ are parameters with values (found, either from simulations or from observations), reported in Table VI.

The shape of the dark halo profile may deviate from spherical symmetry. A triaxial shape arises naturally from the fact that gravitational collapse of the halo starts first (and proceeds more rapidly) in one direction. However, other processes may subsequently erase it (e.g., gas cooling, Kazantzidis *et al.*, 2004). Various observations in the Milky Way have been interpreted as suggesting a spherical (Martinez-Delgado *et al.*, 2004), oblate (Martinez-Delgado *et al.*, 2004), or prolate (Helmi, 2004) dark halo, but in any case, deviations from spherical symmetry appear to be small.

TABLE VI. Models for the Milky Way dark halo profile.

DM profile:	ISO	BE	NFW	M99
α	2	1	1	1.5
β	2	3	3	3
γ	0	0.3	1	1.5
r_0 (kpc)	5	10	20	30
ρ_0 ($M_\odot$ pc^{-3})	5.0×10^{-2}	7.0×10^{-2}	1.0×10^{-2}	1.7×10^{-3}
ρ_0 (GeV cm^{-3})	1.89	2.65	0.38	0.065

Structure formation in the ΛCDM model leads to a hierarchy of dark halos embedded within the main halo of a galaxy. Since smaller galaxies are more dark matter dominated than larger ones, the strongest signal from dark matter annihilation may not arise from the main halo, but from satellite galaxies. This important issue has been extensively studied recently. Analyzing one of the largest "Milky Way size" simulations so far, Springel *et al.* (2008) found that the most intense emission is expected to arise from the main halo. We discuss this point further in Sec. IV.D.3.

IV. POSITRON PRODUCTION: PROCESSES AND SOURCES

A. Radioactivity from stellar nucleosynthesis

1. Radioactivity

Positrons are emitted by the β^+ decay of unstable nuclei which turns a proton into a neutron, provided the mass difference between parent and daughter nucleus is $\Delta M > m_e c^2$ (where m_e is the electron's mass and c is the light velocity). β^+ decay of unstable nuclei produced in stellar explosions was one of the earliest candidates proposed to explain the Galactic 511 keV emission (Clayton, 1973).

Astrophysically important e^+ emitters are produced in proton-rich environments, either hydrostatically (e.g., in massive star cores) or explosively (in novae or SN explosions); in both cases, proton captures occur on shorter time scales than the corresponding lifetimes of β^+-decaying nuclei along the nucleosynthesis path. Important e^+ emitters are also found in the Fe-peak region and are produced in the so-called nuclear statistical equilibrium (NSE) regime, at temperatures $T > 4 \times 10^9$ K. In the short time scale of the explosion ($\tau \sim 1$ s in SNIa and in the inner layers of CCSN) weak interactions can hardly operate and material is nuclearly processed under the effect of strong interactions alone, moving in the neutron versus proton ($N - Z$) plane along a $N/Z \sim$ const trajectory. The original stellar material is essentially composed either of ^{28}Si ($N = Z = 14$) in the case of CCSN or of ^{12}C ($N = Z = 6$) and ^{16}O ($N = Z = 8$) in the case of the white dwarf progenitors of SNIa; this $N/Z \sim 1$ ratio is mostly preserved during the explosion. Since the last stable nucleus with $N = Z$ is ^{40}Ca ($N = Z = 20$), NSE reactions produce mostly unstable Fe-peak nuclei, which later decay back to the nuclear stability valley by electron captures (EC) or e^+ emission. This is typically the case of the most abundant Fe-peak nucleus ^{56}Fe ($Z = 26$, $N = 30$), which is produced as ^{56}Ni ($Z = N = 28$) through the decay chain $^{56}\text{Ni} \rightarrow {}^{56}\text{Co} \rightarrow {}^{56}\text{Fe}$; the first decay proceeds by EC and the second one by both EC and e^+ emission, with branching ratios of 81% and 19%, respectively (Nadyozhin, 1994).

Other important astrophysical e^+ emitters are displayed in Table VII, along with various relevant data. An important feature of β^+ decay is that positrons are released with

TABLE VII. Astrophysically important positron-emitting radioactivities.

Nuclide	Decay chain	Decay mode and e^+ BR[a]	Lifetime	Associated γ-ray line energy in keV (BR[a])	End point e^+ energy (keV)	Mean e^+ energy (keV)	Sources
^{56}Ni	$^{56}\text{Ni} \rightarrow {}^{56}\text{Co}^*$	EC[b]	6.073 d	158 (0.99), 812 (0.86)			SNIa
	$^{56}\text{Co} \rightarrow {}^{56}\text{Fe}^*$	e^+ (0.19)	77.2 d	2598 (0.17), 1771 (0.15)	1458.9	610	
^{22}Na	$^{22}\text{Na} \rightarrow {}^{22}\text{Ne}^*$	e^+ (0.90)	2.61 y	1275 (1)	1820.2	215.9	Novae
^{44}Ti	$^{44}\text{Ti} \rightarrow {}^{44}\text{Sc}^*$	EC[b]	59.0 y	68 (0.94), 78 (0.96)			Supernovae
	$^{44}\text{Sc} \rightarrow {}^{44}\text{Ca}^*$	e^+ (0.94)	3.97 h	1157 (1)	1474.2	632.	
^{26}Al	$^{26}\text{Al} \rightarrow {}^{26}\text{Mg}^*$	e^+ (0.82)	7.4×10^5 y	1809 (1)	1117.35	543.3	Massive stars

[a]BR: branching ratio (in parentheses).
[b]EC: electron capture.

energies in the MeV range, i.e., they naturally satisfy the constraint imposed by the continuum observations of the inner Galaxy in that energy range (see Sec. II.B.1).

Contrary to all other e^+ sources presented in this section, it is well established that stellar radioactivities contribute at a non-negligible level to the e^+ production rate, because of the observed presence of ^{26}Al in the disk (see Sec. II.B.2). The uncertainties related to their overall contribution stem from two factors:

(i) In the case of short-lived radioactivities (i.e., with lifetimes short compared to the characteristic time scales of SN expansion), positrons are released in high-density environments and in magnetic fields of unknown configuration. Those conditions render difficult the evaluation of the fraction of e^+ escaping to environments of sufficiently low density for their annihilation photons to be detectable. This is the case of ^{56}Co in SNIa.

(ii) In some cases of long-lived radioactivities, the corresponding stellar yields and/or the frequencies of the nucleosynthesis sites are quite uncertain. Indirect methods should then be used to evaluate their contribution to the Galactic e^+ production. This is the case of ^{44}Ti.

2. Massive stars: ^{26}Al and ^{44}Ti

The observed irregularities in the ^{26}Al γ-ray emission along the plane of the Galaxy as shown in the COMPTEL map (Diehl *et al.*, 1995) suggest that massive stars are the dominant source, as these are the only candidate ^{26}Al sources clustered along spiral arms [see Prantzos and Diehl (1996), and Sec. II.B]. ^{26}Al is produced in such stars both hydrostatically (during H burning) and explosively (in the C-Ne-O) layers; it is ejected by the Wolf-Rayet stellar winds in the former case and by the supernova explosion in the latter. Limongi and Chieffi (2006) found that in their $Z = Z_\odot$ models explosive nucleosynthesis is always dominant; however, models with rotation and at $Z > Z_\odot$ (appropriate for the inner Galaxy) may modify this conclusion somewhat. Stellar nucleosynthesis models find typical yields of $\sim 10^{-4} M_\odot$ of ^{26}Al per star, which combined with the derived CCSN frequency in the Galaxy (Table V) results in a production rate comparable to the observed one of $\sim 2.7 M_\odot$/Myr; thus, the nucleosynthesis of ^{26}Al is considered to be rather well understood quantitatively (within a factor of 2). Independently of theoretical considerations, however, the observed Galactic decay rate of ^{26}Al corresponds to a production rate of $\dot{N}_{e+,26} \sim 4 \times 10^{42}$ s^{-1} in the Galactic disk.

^{44}Ti is produced in the innermost layers of the supernova, in the "α-rich freeze-out" regime of NSE (Meyer, 1993, Thielemann, *et al.*, 1996). Its yields are much more uncertain than the ones of ^{26}Al because of uncertainties either in the nuclear reaction rates [which affect its yields by a factor of 2 (The *et al.*, 2006; Magkotsios *et al.*, 2008)] or, most importantly, in the explosion mechanism itself (Woosley and Weaver, 1995; Timmes *et al.*, 1996). Moreover, asphericity effects (due, e.g., to rotation) appear to be critical, leading to the production of substantially higher ^{44}Ti yields (and ^{44}Ti/^{56}Ni ratios) than in the case of spherically symmetric models (Nagataki *et al.*, 1998).

Observations offer little help in this case. ^{44}Ti has been directly detected in the Cassiopeia A (CasA) SN remnant, through its γ-ray lines, both with COMPTEL/CGRO (Iyudin *et al.*, 1994) and with SPI/INTEGRAL (Renaud *et al.*, 2006). Its presence is also indirectly derived in SN1987A, the closest observed supernova in the past four centuries, since it is required to explain the late light curve (Motizuki and Kumagai, 2004). In both cases the derived ^{44}Ti yield is $Y_{44} \sim 2 \times 10^{-4} M_\odot$, substantially larger than predictions of spherically symmetric models, but comparable to predictions of aspherical models. Asphericity is also favored for CasA and SN1987A on the basis of other observables (Prantzos, 2004, and references therein). Does this mean that typical sources of ^{44}Ti are aspherical and have the aforementioned yield?

CasA is found at a distance of $\sim$3 kpc from the Earth in the outer Galaxy (outside the active star forming regions of the inner Galaxy) and its age is estimated to be 300 yrs (much larger than the ^{44}Ti lifetime). That a supernova with such properties is the only one detected so far through its ^{44}Ti lines, despite the sensitivity of COMPTEL/CGRO and SPI/INTEGRAL Galactic surveys, appears to be statistically improbable (The, *et al.*, 2006; Renaud *et al.*, 2006). It may imply that typical ^{44}Ti sources are rare, i.e., with frequencies much lower than the CCSN frequencies of Table V, and, consequently, much larger yields. Sub-Chandrasekhar mass SNIa (i.e., thermonuclear SN induced by surface He detonation, see Sec. IV.D) are potential candidates, since they produce 10–20 times more ^{44}Ti than a typical massive star explosion (Woosley and Weaver, 1994); but, provided that such objects exist and have the required yields, their frequencies are totally unknown.

In those conditions, the only way to evaluate the Galactic ^{44}Ti production rate is through a nucleosynthesis argument, based on (i) the solar $(^{44}\text{Ca}/^{56}\text{Fe})_\odot = 1.2 \times 10^{-3}$ ratio (Lodders, 2003), i.e., the ratio of the stable products of ^{44}Ti

and ^{56}Ni decays, and (ii) the knowledge of the current production rate of ^{56}Fe, based on disk SN frequencies of Table V and on presumably well-known typical yields of ^{56}Fe: $Y_{56}^{\mathrm{SNIa}} \sim 0.7 M_{\odot}$ (see Sec. IV.A.4) and $Y_{56}^{\mathrm{CCSN}} \sim 0.07 M_{\odot}$ (from the observed light curve of SN1987A, Arnett *et al.*, 1989). The production rate of ^{44}Ti is then

$$\dot{M}_{44} = \left(\frac{^{44}\mathrm{Ca}}{^{56}\mathrm{Fe}}\right)_{\odot} (R_{\mathrm{SNIa}} Y_{56}^{\mathrm{SNIa}} + R_{\mathrm{CCSN}} Y_{56}^{\mathrm{CCSN}}), \tag{6}$$

and the corresponding e^+ production rate is $\dot{N}_{e^+,44} \sim 3 \times 10^{42} e^+ \mathrm{s}^{-1}$, i.e., comparable to that of ^{26}Al. Thus, the two long-lived radioactivities together may account for most, if not all, of the disk production rate of positrons, as revealed by the SPI/INTEGRAL analysis. The same analysis, applied to the bulge (and assuming the bulge ^{44}Ca/^{56}Fe ratio to be solar) leads to a e^+ production rate 3 times smaller, i.e., an insignificant fraction of the obervationally required rate for that region.

3. Hypernovae and γ-ray bursts

Hypernovae are very energetic supernova explosions, with typical observed kinetic energies $>10^{52}$ ergs (i.e., about 10 times larger than normal supernovae) and ejected ^{56}Ni masses of $\sim 0.5 M_{\odot}$ [see, e.g., Nomoto *et al.* (2010)]. Their properties are usually interpreted in terms of aspherical explosions of rotating massive stars (with mass $>30 M_{\odot}$). The rotating Fe core implodes to a black hole, around which the surrounding material forms a short-lived (~ 0.1 s) accretion disk. The gravitational energy of accretion is partially transferred (by some still unclear mechanism) to two jets along the rotation axis, which launch the supernova explosion. Heavy nuclei (among which ^{56}Ni) are formed in the hot basis of the jet and ejected in the ISM. This model was originally proposed to account for the phenomenon of γ-ray bursts (GRB), the most powerful electromagnetic beacons in the Universe, releasing $\sim 10^{51}$ erg in short flashes of γ rays beamed along the jet direction [the ''collapsar'' model of Woosley (1993)]. Observed metallicities of GRB host galaxies are typically a few times lower than solar (Savaglio *et al.*, 2009); such low metallicities prevent substantial losses of mass and angular momentum and allow for a rapid rotation of the core at the moment of the explosion, a crucial ingredient of the collapsar model.

Hypernovae and GRBs have been suggested as potential sources of the Galactic positrons, produced either from the ^{56}Ni decay (Nomoto *et al.*, 2001; Cassé *et al.*, 2004) or from pair creation, as photons backscattered from the ionized medium ahead of the jet interact with the GRB γ-ray photons (Parizot *et al.*, 2005; Bertone *et al.*, 2006). Because of the complex (and still very uncertain) nature of those objects, the corresponding positron yield is virtually unknown. In light of the observational (and theoretically motivated) constraint of low metallicity for the progenitor stars, the existence of such objects in the metal-rich bulge (see Sec. III.A) should be excluded. Besides, a small bulge-to-disk ratio would be logically expected in that case, contrary to observations.

4. Thermonuclear supernovae (SNIa)

SNIa display a remarkable uniformity in their properties, such as the peak luminosity, which is attributed to the power input of $\sim 0.7 M_{\odot}$ of radioactive ^{56}Ni (Arnett, 1982).[9] There is general agreement that SNIa result from the thermonuclear disruption of a white dwarf, explosively igniting its carbon. The thermonuclear flame may propagate either subsonically (deflagration) or supersonically (detonation) inside the white dwarf; Mazzali *et al.* (2007) showed that the SNIa variety can be understood within a single, combined model, involving both deflagration and detonation. There are two main scenarios for the precursors of SNIa: the single degenerate (SD) model, in which accretion is made from a main sequence or red giant companion (Whelan and Iben, 1973); and the double degenerate model, which involves the merging of two white dwarfs in a close binary system (Webbink, 1984; Iben and Tutukov, 1984). Parthasarathy *et al.* (2007) discussed all available observational evidence and found that the SD channel is by far the dominant one [see Gilfanov and Bogdán (2010) for a different view].

Most studies of SNIa were made in the framework of the SD scenario and, up to the late 1990s with 1D models. Detailed 1D models exploring the various possibilities (and the corresponding parameter space) have been developed over the years. Perhaps the most successful 1D model developed so far is the so-called W7 model (Nomoto *et al.*, 1984), the physics of which has been updated by Iwamoto *et al.* (1999); it is a deflagration model producing in its inner layers $\sim 0.7 M_{\odot}$ of ^{56}Ni and negligible amounts of other positron emitters. A more accurate description of reality is pursued by the upcoming generation of multidimensional models (Travaglio *et al.*, 2004; Bravo and García-Senz, 2006; Schmidt and Niemeyer, 2006; Röpke *et al.*, 2007; Röpke and Niemeyer, 2007). Preliminary results show interesting features for the stratification of radioactivities, in particular, the presence of substantial ^{56}Ni amounts within outer, high velocity, layers (Fig. 13).

The fate of the β^+-decay products (γ rays and positrons) in the expanding SNIa ejecta has been extensively studied in 1D (Gómez-Gomar *et al.*, 1998; Milne *et al.*, 2004), and more recently, in 3D models (Isern *et al.*, 2007; Sim and Mazzali, 2008). Generically, before peak luminosity, the SNIa envelope is opaque, and both the energy of the explosion and of β^+ decay are deposited in and diffuse outward through the ejecta. After the peak of the bolometric light curve (~ 20 days after the explosion), the luminosity evolves from radioactive energy deposits and increasing energy leakage in a way following (surprisingly closely, given the interplay of these processes) the decay rate of ^{56}Co. About 6 months later, the ejecta are completely transparent to

[9] In fact, the ^{56}Ni mass may vary by a factor of ~ 10, as shown by Stritzinger *et al.* (2006), who found values in the range of 0.1–0.9 $M_{\odot}$ for a sample of 17 well-observed SNIa. However, observations indicate that the shape of the SNIa light curves is associated with the ^{56}Ni mass (with brighter SNIa fading more slowly) and after a correction is made to that effect (Phillips, 1993), SNIa can indeed be used as ''standard candles'' for the determination of cosmological distances [see Leibundgut (2001) for a review].

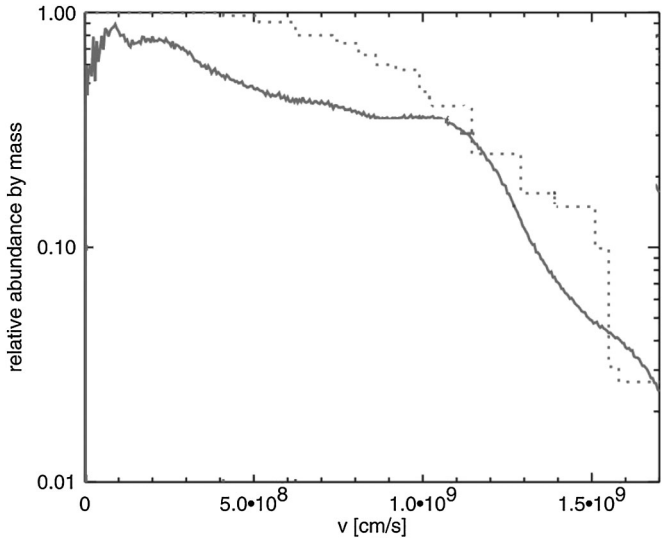

FIG. 13. Mass fraction of ^{56}Ni as a function of ejecta velocity after a SNIa explosion. The space-averaged profile of the 3D mode [solid curve from Röpke *et al.* (2007)] is compared to observational data (dotted curve). Both theory and observations find non-negligible amounts of ^{56}Ni in the outer (high-velocity) ejecta. From Röpke *et al.*, 2007.

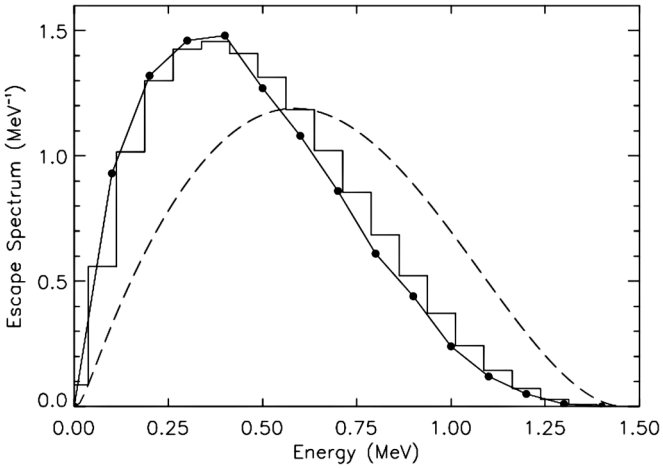

FIG. 14. Distribution of emitted positron kinetic energies as estimated by Segre (1977) (dashed curve) compared to the spectrum of escaping positrons from W7, as estimated by Chan and Lingenfelter (1993) (solid curve) and Milne *et al.* (1993) (solid histogram). The slowing of the positrons leads to the mean energy shifting from 632 to 494 keV. From Milne *et al.*, 1999.

γ rays and the SNIa luminosity results almost exclusively from energy deposited by positrons from ongoing radioactive decays. If positrons are trapped (escape) a flattening (steepening) of the light curve results. How many positrons ultimately escape to the ISM depends on the distribution of the parent radioactivities within the supernova, the evolution of its density, temperature, and ionization profiles and, most importantly for the late phases, on the unknown configuration of its magnetic field. Progenitor white dwarfs have field strengths of 10^5–10^9 G. Chan and Lingenfelter (1993) found that, in the case of radially combed magnetic fields and fully mixed ejecta, a substantial fraction of ^{56}Co positrons ($>10\%$) may escape. Building on the same ideas, Milne *et al.* (1999) compared SNIa models to observations of late light curves of a dozen SNIa (mostly in B and V bands) and concluded that, typically, a few per cent of positrons finally escape the ejecta; the average positronic yield of a SNIa is $n_{e^+}(\mathrm{SNIa}) \sim 8 \times 10^{52}$ (corresponding to an escape fraction of $f_{\mathrm{esc}} \sim 0.03$). They also found that the mean energy of escaping positrons is ~0.5 MeV (Fig. 14).

The corresponding Galactic positron yield is then estimated as

$$\dot{N}_{e+,\mathrm{SNIa}} = n_{e^+}(\mathrm{SNIa}) R_{\mathrm{SNIa}} \sim 1.6 \times 10^{43}\ \mathrm{s}^{-1}, \qquad (7)$$

where R_{SNIa} is the SNIa frequency in Table V. The total e^+ yield is comparable to the observed Galactic one, but the bulge-to-disk positron emissivity ratio is $B/D \sim 0.4$, considerably less than derived from observations.

This simplified picture may not apply to SNIa in general, though. Bolometric observations (including the near IR) of the late light curves of SN 2000cx (a rather peculiar at early times SNIa) and of SN2001el and SN2003hv (two typical SNIa), interpreted in the framework of 1D models, suggest that no positrons escape (Sollerman *et al.*, 2004; Stritzinger and Sollerman, 2007; Leloudas *et al.*, 2009); in that case, despite their large β^+-decay yields, the SNIa would be insignificant e^+ producers.

However, 3D effects may considerably alter the stratification of radioactivities inside the SNIa (Blinnikov *et al.*, 2006), allowing for substantial amounts of ^{56}Ni to be mixed out to the surface (Fig. 13) and for the released positrons to escape at early times (i.e., when the light curve is dominated by γ rays, and not yet e^+ deposition) without being noticed. Studying the very early optical spectra of six SNIa, Tanaka *et al.* (2008) found indeed indications for asphericity and substantial amounts of ^{56}Ni present in the high velocity ejecta ($v \sim 10\,000$–$15\,000$ km/s). Positrons produced by the subsequent decay of ^{56}Co may escape the ejecta if the magnetic field of the supernova is radially combed. Observations indicate that this may be the dominant configuration of magnetic fields in young SN remnants [see, e.g., Milne *et al.* (1993), and Kothes and Reich (2001)], although the origin of such a configuration is not yet clearly understood (Jun and Norman, 1996; Schure *et al.*, 2008). On the other hand, the late light curve of SNIa may also be (at least partially) powered by internal conversion and Auger electrons released from the decay of ^{57}Co (Seitenzahl *et al.*, 2009), thus allowing for some ^{56}Co positrons to escape. Thus, the issue of the positron yield of SNIa is not settled yet: n_{e+} may well be as high as envisioned by Milne *et al.* (1999) (albeit for different reasons), but also much lower.

When the SN becomes sufficiently diluted, the annihilation γ-ray photons may be directly observed. Kalemci *et al.* (2006) found no such signal in observations with SPI/INTEGRAL of the SN remnant SN1006. They exclude then SNIa as major e^+ producers in the Galaxy under the assumption that the e^+ lifetime is $\tau_{e^+} < 10^5$ yr. However, even the low-energy positrons of β^+ decay may live much longer before annihilation and then escape the SN remnant, especially in the case of a radially combed magnetic field.

5. Novae

Novae result from explosive H burning on the surfaces of white dwarfs in binary systems. Accretion of material from the companion star increases the density, pressure, and temperature at the base of the white dwarf envelope, up to the point where hydrogen ignites in degenerate conditions and burns explosively at peak temperatures of several 10^8 K. The ejected mass is $\sim 10^{-4} M_\odot$ and is substantially enriched with the material of the white dwarf, leading to CO or to ONe novae [see, e.g., Hernanz (2005) for a review].

Major positron producers are ^{13}N and ^{18}F (produced in the hot-CNO cycle) and, in the case of ONe novae, ^{22}Na (produced in the hot-NeNa cycle). The short lifetimes of ^{13}N and ^{18}F ($\tau = 862$ s and 158 min, respectively) make it unlikely for a substantial escape of their positrons from the nova ejecta. Positrons from ^{22}Na decay certainly escape and recent calculations suggest that up to $10^{-8} M_\odot$ of this nucleus may be produced in ONe novae (Hernanz and José, 2006), releasing up to $n_{e^+,\mathrm{nova}} = 10^{48} e^+$.

The novae frequency in the Galaxy is estimated to be $R_{\mathrm{nova}} \sim 35\ \mathrm{yr}^{-1}$ (Shafter, 1997; Darnley *et al.*, 2006). About 1/3 of those may originate from ONe white dwarfs (Gil-Pons *et al.*, 2003), leading to a Galactic e^+ production rate of $\dot{N}_{e+,\mathrm{Novae}} = R_{\mathrm{nova}} n_{e^+,\mathrm{nova}} \sim 1.5 \times 10^{41}\ \mathrm{s}^{-1}$, i.e., smaller by 2 orders of magnitude than the observed rate in the bulge or in the disk. It should be noted that ONe novae appear mostly close to the Galactic plane (della Valle and Livio, 1998).

B. High-energy processes in cosmic rays and compact objects

1. High-energy processes

a. Inelastic p-p collisions

Relativistic protons and heavier nuclei are present in many astrophysical environments in the Galaxy. Their inelastic interactions with interstellar gas produce secondary particles including numerous neutral and charged pions and kaons $pp \rightarrow \pi + X$, $pp \rightarrow K + X$. In turn, decay of positively charged mesons produces secondary positrons. The dominant channel is pion decay $\pi^+ \rightarrow \mu^+ \nu_\mu$, $\mu^+ \rightarrow \tilde{\nu}_\mu \nu_e e^+$, though a non-negligible contribution comes from the charged kaon decays. The two main kaon decay modes contributing to the secondary $e^\pm$ spectrum are $K^\pm \rightarrow \mu \nu_\mu$ (63.5%) and $K^\pm \rightarrow \pi^0 \pi^\pm$ (21.2%). The processes as the source of secondary cosmic-ray positrons and diffuse γ-ray emission have been thoroughly studied [see, e.g., Strong *et al.* (2007), and references therein]. A review of the experimental data for pion production in proton-proton collisions and relevant cross-section parametrizations <50 GeV were presented by Blattnig *et al.* (2000). New parametrizations of neutral and charged pion cross sections which provide an accurate description of the experimental data in a wide energy range from the pion production threshold up to 10^5 TeV are discussed by Kelner *et al.* (2006), and Kamae *et al.* (2006, 2007).

The energy spectra of positrons from the decay of π^+ mesons produced in collisions of isotropic monoenergetic protons with protons at rest are shown in Fig. 15; they typically present a maximum at $E \sim 30$–40 MeV.

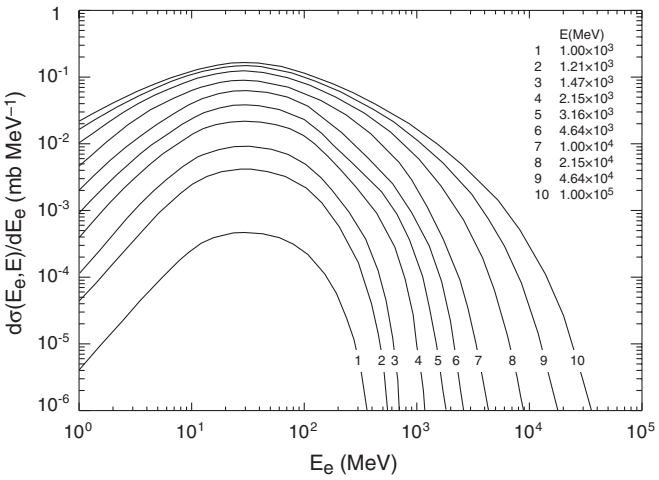

FIG. 15. The energy spectra of positrons from the decay of π^+ produced in collisions of isotropic monoenergetic protons with protons at rest for various proton kinetic energies (from bottom to top): 0.316, 0.383, 0.464, 0.562, 0.681, 1.0, 1.78, 3.16, 10.0, and 100.0 GeV. From Murphy *et al.*, 1987, updated by R. Murphy.

b. γ-γ pair production

Positrons can also be produced in photon-photon interactions when the product of their energies is $>2m_e^2c^4/(1-\cos\theta)$, where θ is the angle between the photon directions. The total unpolarized cross section for the creation of $e^\pm$ by two photons $\gamma\gamma \rightarrow e^+e^-$ can be expressed as a function of a dimensionless velocity β of the produced particles in the center-of-mass frame:

$$\sigma_{\gamma\gamma} = \frac{3\sigma_T}{16}(1-\beta^2)\left[(3-\beta^2)\ln\frac{1+\beta}{1-\beta} - 2\beta(2-\beta^2)\right], \tag{8}$$

where $\sigma_T \approx 6.65 \times 10^{-25}\ \mathrm{cm}^2$ is the Thomson scattering cross section (Breit and Wheeler, 1934; Greiner, 2003).

In Fig. 16 the cross section is presented as a function of the Lorentz factor of created positron in the center-of-mass frame. The positron production due to photon-photon collisions is suppressed at the threshold and reaches a maximum at $\beta \approx 0.7$.

The production of a e^+e^- pair by a single photon is possible in magnetic fields $B \gtrsim 10^{12}$ G observed in highly magnetized objects such as pulsars and magnetars (Klepikov, 1954; Daugherty and Harding, 1983). This occurs with significant probability when the photon energy is $\simeq 3/(B_{12}\sin\theta)$ MeV, where B_{12} is the external magnetic field strength in units 10^{12} G and θ is the angle between the photon direction and the magnetic field.

2. Galactic cosmic rays (GCR)

The majority of positrons in CR are believed to be secondaries produced by interactions of relativistic particles with interstellar gas; however, recent measurements of positron fraction in cosmic rays $e^+/(e^- + e^+)$ by PAMELA (Adriani *et al.*, 2009) indicate that there may be another component at high energies. If produced by CR interactions, the positron fraction is expected to decrease with energy (Moskalenko and Strong, 1998), while the PAMELA data show it rises above

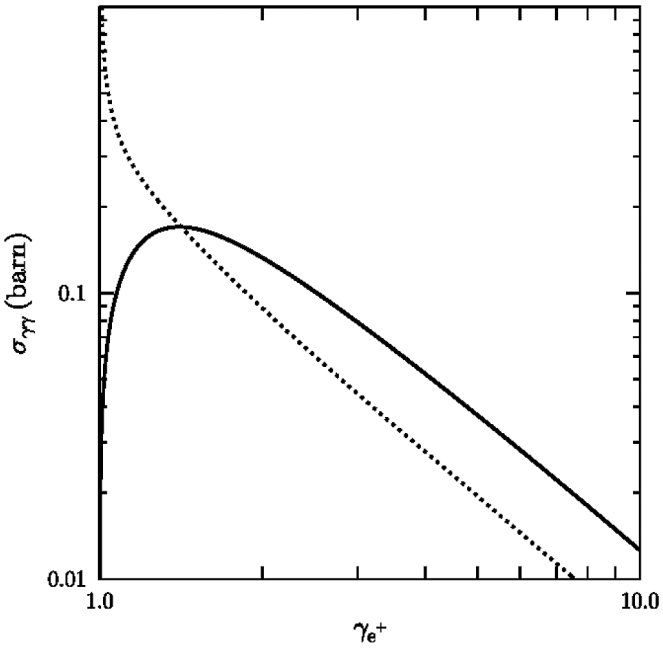

FIG. 16. The total cross section of $\gamma+\gamma\rightarrow e^+ + e^-$ reaction as a function of the Lorentz factor of created positron in the center-of-mass frame (solid curve). The total cross section σ_a for two-photon pair annihilation reaction $e^+ + e^- \rightarrow \gamma + \gamma$ (unpolarized) is indicated as a dotted curve.

~10 GeV. The origin of this additional component is intensively debated. The ideas proposed can be roughly divided into two broad classes: conventional sources, such as supernova remnant or nearby pulsars [see, e.g., Blasi (2009), and references therein] and exotic sources such as weakly interacting massive particle (WIMP) annihilation or decay [see, e.g., Arvanitaki *et al.* (2009), and references therein]. The predicted behavior of the positron fraction at energies higher than currently measured (~ 100 GeV) depends on the model and can be used to distinguish between different possibilities.

In this section we discuss positrons produced by conventional CR interactions with interstellar gas. The most important factors are the energetics of cosmic rays and their diffusion in the interstellar medium; for more details, see, Strong *et al.* (2007).

The major CR sources are believed to be supernovae (SN) and their remnants (SNRs) with some fraction coming from pulsars, compact objects in close binary systems, and stellar winds. Recent observations of x-ray and γ-ray emission from SNRs (Pannuti *et al.*, 2003; Aharonian *et al.*, 2006) reveal the presence of energetic electrons, thus testifying to efficient acceleration processes near these objects. The total power of Galactic CR sources needed to sustain the observed CR density is estimated at $\sim 10^{41}$ erg s^{-1} which corresponds to approximately 10^{50} erg per SN, if the SN rate in the Galaxy is 1 every 30 years (Table V). This value is ~10% of the corresponding total kinetic power of the SN ejecta, an efficiency which is in agreement with the predictions of diffusive shock acceleration theory (Blandford and Eichler, 1987; Jones and Ellison, 1991). After injection into the ISM, cosmic rays remain contained in the gaseous disk for ~15 Myr and in the Galaxy for ~100 Myr before escaping into intergalactic space (Berezinskii *et al.*, 1990). Note that the latter value is much larger than estimates based on the so-called leaky-box model (Yanasak *et al.*, 2001); see Strong *et al.* (2007) for a full discussion of this point.

Propagation of cosmic rays in the ISM is usually modeled as diffusion, where the energetic particles scatter on irregularities (fluctuations) of the turbulent Galactic magnetic field (see Sec. III.D). The diffusion equation may include stochastic reacceleration in the ISM, convection by the Galactic wind, continuous and catastrophic energy losses, nuclei fragmentation, radioactive decay, and production of secondary particles and isotopes [for a recent review of cosmic-ray transport, see Strong *et al.* (2007)]. Isotopes of light elements (Li, Be, B) in cosmic rays are almost all secondaries produced in spallations of heavier (CNO) nuclei during CR propagation. If the diffusion is fast (slow), the secondary nuclei are present, after propagation, in small (large) amounts; therefore, the relative abundances of secondary and primary nuclei can be used to determine the propagation parameters.[10] The derived propagation parameters (time scale of CR confinement, diffusion coefficient, etc.) are model dependent and can vary significantly [see, e.g., Ptuskin *et al.* (2006)].

The production spectra of secondary particles are determined by the kinematics of the collision and depend on the ambient spectrum of cosmic rays while their propagation is governed by the same propagation equation as for other cosmic-ray species. The production rate of secondary positrons slightly depends on the assumed propagation model and is about $(1–2)\times 10^{42}$ s^{-1} (Porter *et al.*, 2008), i.e., ~5%–10% of the Galactic e^+ annihilation rate. A cosmic-ray origin of the positrons annihilating at the Galactic center can still be reconciled with the production rate if cosmic-ray intensities are significantly higher than in the past (see Sec. IV.B.5 for an analogous situation for the Galactic supermassive black hole).

Heliospheric influence (modulation) changes the spectra of cosmic-ray particles below ~10–20 GeV/nucleon as they propagate from the boundaries of the Solar System toward the orbits of the inner planets (Parker, 1965; Gleeson and Axford, 1968). The heliospheric modulation is a combination of effects of convection by the solar wind, diffusion, adiabatic cooling, drifts, and diffusive acceleration [see, e.g., Potgieter (1998)]. Although the e^+ fraction inside the heliosphere is small (~0.1), the e^+ flux in the ISM below ~1 GeV is estimated to be comparable to CR electron flux at the same energies (Strong *et al.*, 2004).

Direct information about the CR fluxes and spectra in distant locations is provided by the Galactic diffuse γ rays. Continuum diffuse emission is expected in the hard x-ray and γ-ray regime from the physical processes of positron annihilation (through formation of positronium), inverse-Compton scattering and bremsstrahlung from CR electrons and positrons, and via decay of neutral pions produced by interactions

[10]The stable secondary-to-primary ratio does not allow one to derive a unique set of propagation parameters. The radioactive isotope abundances are then used to break the degeneracy. Four radioactive isotopes, ^{10}Be, ^{26}Al, ^{36}Cl, and ^{54}Mn, are commonly used to probe the effective Galactic volume filled with cosmic rays and derive the CR confinement time in the Galaxy. Their half-lives range from 3.07×10^5 yr (^{36}Cl) to 1.60×10^6 yr (^{10}Be), with the shortest half-life being most sensitive to the local structure.

of CR nuclei with the interstellar gas (Strong *et al.*, 2000, 2004; Porter *et al.*, 2008). Positron annihilation in flight (continuum) may contribute in the MeV range (Aharonian and Atoyan, 2000; Beacom and Yüksel, 2006). That contribution can be determined from a comparison of model predictions to the data obtained by INTEGRAL, COMPTEL, and EGRET [and now by Fermi/LAT launched in June 2008 (Atwood *et al.*, 2009)]. The analysis of the INTEGRAL data shows that most of the emission between 50 keV and ~1 MeV (Bouchet *et al.*, 2008) is produced via inverse-Compton scattering of background photons off CR electrons (Porter *et al.*, 2008) and that CR positrons in distant regions of the Galaxy (including the direction of the Galactic center) are mostly secondary (see also Sec. II.C.1).

3. Pulsars, millisecond pulsars, and magnetars

A large fraction of high-energy sources in the Milky Way consists of rapidly rotating magnetized neutron stars, which belong to several subclasses: rotation powered pulsars (including Crab-like and Vela-like pulsars), accretion powered pulsars [including millisecond (ms) pulsars[11]] and strongly magnetized rotating objects (including soft γ-ray repeaters and magnetars). All these objects have been the subject of intense observational and theoretical work [see reviews by Rudak (2001), Seiradakis and Wielebinski (2004), Lorimer (2005), Harding and Lai (2006), and references therein]. Typical values of their main properties (magnetic field intensity, rotation period, activity lifetime, estimated birthrate, and total number in the Milky Way) are provided in Table VIII.

The high-energy radiation and/or a high magnetic field ($B_* \geq 10^{12}$ G) of those objects are associated with intense e^--e^+ pair creation. The pairs are further accelerated in parallel electric fields in the polar caps or in the outer gaps close to the light cylinder.[12] The γ-γ interaction of secondary photons produced by the primary particles yields a pair cascade; its particles can eventually escape into the pulsar wind. Pair creation is accompanied by different high-energy photon production channels that directly contribute to the pair cascade: curvature radiation, magnetic inverse-Compton scattering, synchrotron radiation, and photon splitting.

It suffices for a few charged particles to be accelerated up to high Lorentz factors to initiate an e^--e^+ pair cascade either above the polar caps (Harding, 1981) or in a part of the outer magnetosphere close to the frontier of the open magnetic field lines region called the outer gap (Cheng *et al.*, 1986). In the outer gap model of Zhang and Cheng (1997), primary e^--e^+ pairs have a typical energy $E_p \simeq 5 \times 10^6 P^{1/3}$ MeV (where P is the pulsar's period in seconds). Photons with energy $E > E_{\rm crit} \simeq 3B_{12}^{-1}$ MeV (see Sec. IV.B.1.b) will generate a pair cascade involving a total of $N_{e^\pm} = E_p/E_{\rm crit}$ pairs, most of which will be reflected by the magnetic mirror effect and then move toward the light cylinder.

TABLE VIII. Properties of magnetized neutron stars [data for pulsars and ms pulsars are from Lorimer (2005) and for magnetars from Gill and Heyl (2007), although Keane and Kramer (2008) suggest somewhat higher birthrates].

		Pulsars	ms pulsars	Magnetars
Magn. field	$\langle B\rangle$ (G)	10^{12}	3×10^8	3×10^{14}
Period	$\langle P\rangle$ (s)	0.5	3×10^{-3}	10
Birthrate	R (yr^{-1})	1.5×10^{-2}	10^{-5}	2×10^{-3}
Lifetime	$\langle\tau\rangle$ (yr)	10^7	3×10^9	2×10^4
Total number	N	1.5×10^5	3×10^4	40
e^+ yield[a]	$\dot{n}_{e^\pm}$ (s^{-1})	4×10^{37}	5×10^{37}	4×10^{40}
Total e^+ yield[b]	$\dot{N}_{e^\pm}$ (s^{-1})	5×10^{42}	1.5×10^{42}	1.6×10^{42}

[a]Individual source yield from Eq. (9).
[b]Galactic yield from $\dot{N}_{e^\pm} = \dot{n}_{e^\pm} R\langle\tau\rangle$, assuming $\xi = 1$.

In terms of the surface magnetic field and the pulsar period the total e^+ production rate of the cascade is

$$\dot{n}_{e^\pm} \simeq 2.8 \times 10^{37}\ B_{d,12}^{10/7}\ P^{-8/21}\ \mathrm{s}^{-1}, \tag{9}$$

where $B_{d,12}$ is the dipole magnetic field in 10^{12} G. In the case of ms pulsars the dipole assumption at the stellar surface is not valid anymore and the magnetic field should be rescaled as $B_d \rightarrow B_d(R_*/\ell)^3$, where R_* is the star radius and $\ell \sim 1$ km is the curvature radius of the magnetic field in the stellar surface [approximately equal to the stellar crust radius (Wang *et al.*, 2006)]. The effective rate of positrons injected into the pulsar wind is a fraction ξ of $\dot{n}_{e^\pm}$. This fraction is probably lower than 1 in normal pulsars and close to 1 in ms pulsars: Due to the lower magnetic field of the latter ($B \sim 10^{8-9}$ G), the light cylinder is much closer to the neutron star surface and particles are expected to escape more easily (Wang *et al.*, 2006). Note that in the extreme magnetic field conditions of magnetars the production of most of the e^+-e^- pairs is probably suppressed (Harding and Lai, 2006).

The total Galactic injection rate $\dot{N}_{e^\pm}$ of one particular class (normal pulsars, ms pulsars, magnetars) is $\dot{N}_{e^\pm} = \dot{n}_{e^\pm} N$, where $\dot{n}_{e^\pm}$ is the average e^+ production rate of one source and $N = R\langle\tau\rangle$ is the number of sources in the Galaxy (where R is the birthrate, and $\langle\tau\rangle$ is the typical lifetime of the sources, see Table VIII).

In view of their young age, pulsars and magnetars are expected to have a radial distribution closely following the one of the star formation rate (Fig. 10), a small scale height (~ 100 pc) and an insignificant population in the bulge. Millisecond pulsars are expected to have a different radial distribution, since they originate in binary systems of all ages. For that reason, their radial distribution should be closer to the one of SNIa (Fig. 10), their scale height[13] >300 pc, and they should have a substantial bulge component, albeit with a bulge-to-disk ratio $B/D < 0.5$.

The main problem with compact magnetized objects as candidate e^+ sources is the expected high energy of the produced positrons [$E \sim 30$ MeV (de Jager and Djannati-Ataï, 2008], which violates the constraint from the continuum MeV emission observed in the inner Galaxy.

[11]ms pulsars spin up by accreting angular momentum from a companion star.

[12]The light cylinder is the surface inside which the closed field lines have a rotation velocity smaller than the speed of light; it separates the region of closed and open magnetic field lines.

[13]Story *et al.* (2007) adopted a scale height of 200 pc for ms pulsars, but in view of the age of those systems, and the additional effect of a kick velocity from the explosion, this should be >300 pc.

4. X-ray binaries and microquasars

X-ray binaries involve a compact object (neutron star or black hole, hereafter the primary) accreting matter from a normal star (the secondary) through an accretion disk. They are classified as high mass (HMXRBs) or low mass (LMXRBs) depending on whether the mass of the secondary is of a spectral type earlier or later than B (heavier or lighter than $\sim 4M_{\odot}$, respectively). About 300 XRBs are currently detected in the Galaxy, for a total x-ray luminosity of $\sim 10^{39}$ erg s^{-1}; their luminosity function suggests, however, that there are more than 1000 of them. LMXRBs are ~ 10 times brighter on average and slightly more numerous than HMXRBs. The corresponding scale heights are ~ 410 pc in the former case and ~ 150 pc in the latter (Grimm *et al.*, 2002).

Some XRBs exhibit radio emission, which is usually attributed to synchrotron radiation emitted by leptons (electrons, and perhaps positrons); leptons are launched along diametrically opposite jets fueled by the accretion energy. If the jets are confirmed by imaging, the system is called a microquasar (μQ), for it has a structure similar to quasars (the latter being about 10^6 times larger and brighter (Mirabel, 2008, and references therein).

The physics of microquasars is extremely complex and there is no generally accepted model at present. Empirical evidence suggests that at high accretion rates, x-ray emission peaks at ~ 1 keV (*high-soft* state), whereas at low accretion rates x-ray emission appears at higher energies, with a power-law spectrum and an exponential cutoff at ~ 100 keV (*low-hard* state; see, e.g., McClintock and Remillard (2006). It is expected that a persistent jet will be present in the low-hard state (Fender *et al.*, 2004) and correlations between the radio and x-ray luminosity and the accretion activity have been proposed [see, e.g., Corbel *et al.* (2003)]. It should be noted that the issue of positron production in microquasars suffers from two major uncertainties: (i) while electrons are certainly responsible for the observed synchrotron emission, it is not yet clear whether the positively charged component of the jets consists mainly of ions or positrons; and (ii) even if positrons are largely present, it is not yet known whether the e^--e^+ pairs of the jets are ejected at ultrarelativistic velocities or not; current wisdom is that the jets are mildly relativistic (Gallo *et al.*, 2003) but alternative views have been expressed [see, e.g., Foellmi *et al.* (2008)]. This has obvious implications for the in-flight e^+ annihilation and the production of >1 MeV γ-ray continuum.

Positrons can be pair created in the vicinity of the compact object, either in the hot inner accretion disk, in the x-ray corona surrounding the disk, or at the base of the jets; the latter may channel a fraction of the e^--e^+ pairs out of the system. Alternatively, if the jets consist mainly of relatively cold e^--e^+ or e^--p plasma, they may create new e^--e^+ pairs at the termination shock with the ISM. Heinz and Sunyaev (2002) noticed that the total kinetic luminosity of microquasar jets in the Galaxy, evaluated at $L_{\rm kin} \sim 3 \times 10^{38}$ erg s^{-1}, can produce up to $4 \times 10^{43} e^+$ s^{-1}, i.e., more than required from observations. This estimate requires $\sim 5\%$ of the kinetic power to be converted to e^--e^+ pairs, i.e., a reasonable conversion efficiency.

Soon after the first data release of the 511 keV image by SPI/INTEGRAL, Prantzos (2004) noticed that (i) the observed distribution of LMXRBs in the Galaxy is strongly peaked toward the central regions (Grimm *et al.*, 2002), similar to that of the 511 keV emission, and (ii) their total x-ray luminosity is $\sim 10^{39}$ erg s^{-1}, 100 times larger than the corresponding mass energy of the observed $10^{43} e^+$ s^{-1} in the Galaxy. He also noticed, however, that most of the strongest sources (accounting for 80% of the total Galactic x-ray flux) are evenly distributed in the Galactic plane, with no preference for the bulge; he concluded that, if the positron emissivity scales with their x-ray flux, then LMXRBs cannot be the origin of the bulge Galactic positrons. The argument is invalid, however, if the time scale for the variability of the x-ray flux is much smaller than the slowing down time scale of the positrons, and/or if positrons annihilate far away from their sources.

Various features of the scenario of microquasars as positron producers were studied by Guessoum *et al.* (2006), on the basis of (i) existing theoretical models (see, e.g. Beloborodov (1999) and Yamasaki *et al.* (1999)] and (ii) global energetic considerations (of XRB luminosities correlated to jet power and to positron ejection rates). They found that such considerations lead to average values up to $10^{41} e^+$ s^{-1} for a jet. Interestingly enough, this is roughly the current upper limit for e^+ production rates in XRBs with SPI/INTEGRAL (see Table 1 in Guessoum *et al.*, 2006). If 100 microquasars exist in the Milky Way (not an unreasonable extrapolation from their currently known population of two dozen), then these objects may contribute substantially to the observed 511 keV emission. The distribution of the known microquasars shows indeed some clustering toward the inner galaxy, but the data are insufficient for statistically significant conclusions.

A similar investigation was performed by Bandyopadhyay *et al.* (2009), who considered hadronic jets (also containing e^--e^+ pairs) launched by all LMXRBs, down to the lowest x-ray luminosities. Extrapolating from the results of recent deep x-ray surveys of the central bulge, they estimated that a bulge population of 300–3000 LMXRBs would inject mass in jets at a rate of 10^{17}–10^{18} g s^{-1}; the observed e^+ production (= annihilation) rate of 2×10^{43} s^{-1} requires then a yield of 40–400 e^--e^+ pairs per proton. As an example they discussed observations of the giant galaxy M87, and they argued that such a high ratio is justified by the observational finding that the jet plasma in that galaxy is cold, i.e., the energy spectrum of the electrons has no measurable low-energy cutoff and it is thus dominated by low-energy particles (electrons and positrons). They also argued that this effect allows one to satisfy the observational constraint in the MeV range (see Sec. II.B.2). However, an analysis of the M87 jet by Dunn *et al.* (2006) concluded that the jet is e^--e^+ dominated only under the assumption of a low-energy cutoff $E_{\rm min} \sim 0.5$ MeV, but higher $E_{\rm min}$ (implying smaller pair fractions per proton) cannot be excluded and are even suggested by polarization measurements. It is clear then that neither the energies nor the abundance of positrons in the jets are known at present.

Note that in both Guessoum *et al.* (2006) and Bandyopadhyay *et al.* (2009) the bulge-to-disk ratio can be reproduced only if it is assumed that a fraction of the disk positrons do not annihilate in the disk, but leave it altogether.

These arguments will be discussed in Sec. IV.D along with the claim of Weidenspointner *et al.* (2008a) that their recent finding of asymmetric 511 keV emission from the inner disk (see Sec. II.B.3) favors LMXRBs in the hard state as the e^+ sources.

5. Positron production by the Galactic black hole

As already discussed in Sec. II.B, the SMBH in the GC had been suggested already in the 1980s as a e^+ source, on the basis of the variability found in the HEAO-3 data by Riegler *et al.* (1981). Variability is not an issue anymore, but the first year data of SPI/INTEGRAL revived the idea of the SMBH as a e^+ source because of the difficulty met by other candidate sources to explain the 511 keV image.

Compared to the situation in the 1980s, the SMBH models have to cope with two new requirements:

(i) The emission does not originate from a point source in the GC, but from a region extended over the whole bulge. This implies that positrons from the central source have to travel distances comparable to the bulge radius, i.e., ~2 kpc.

(ii) Sgr A^*, the multiwavelength emission source at the GC, is notoriously weak [see, e.g., Eckart *et al.* (2008)]: its x-ray luminosity is $\sim 10^{35}$ erg s^{-1} and its bolometric luminosity is estimated to be $\sim 10^{36}$ erg s^{-1}, i.e., $\sim 3 \times 10^{-9}$ times the corresponding Eddington luminosity.[14] The x-ray emissivity of Sgr A^* is $\sim 10^4$ times weaker than the combined emissivity of the population of Galactic XRBs (see Sec. IV.B.4) or even some individual XRBs; if positron production is correlated to x-ray emissivity, it is difficult to conceive Sgr A^* as an important e^+ source.

It turns out that a viable solution may emerge, satisfying both constraints, if one drops the assumption of steady state (i.e., equality between e^+ production and annihilation rates): since positrons need time to slow down and to fill the bulge, one may invoke a much higher activity of Sgr A^* in the past. The question is then whether that high activity was due to a rare event (in which case the current low activity represents the normal state of Sgr A^*) or whether the past high activity was the norm (in which case today's low activity is of low probability). Proposed models explore both possibilities (Fig. 17):

(a) Tidal disruption of nearby stars and subsequent accretion of their material may boost the activity of Sgr A^* for time scales of 10–100 yr (Rees, 1988). In view of the star density in the vicinity of Sgr A^* such events may occur every $\tau_{cap} \sim 10^4$–10^5 yr [see, e.g., Syer and Ulmer (1999)]. Fatuzzo *et al.* (2001) and Cheng *et al.* (2006, 2007) suggested that such events are at the origin of past high activity of Sgr A^*.

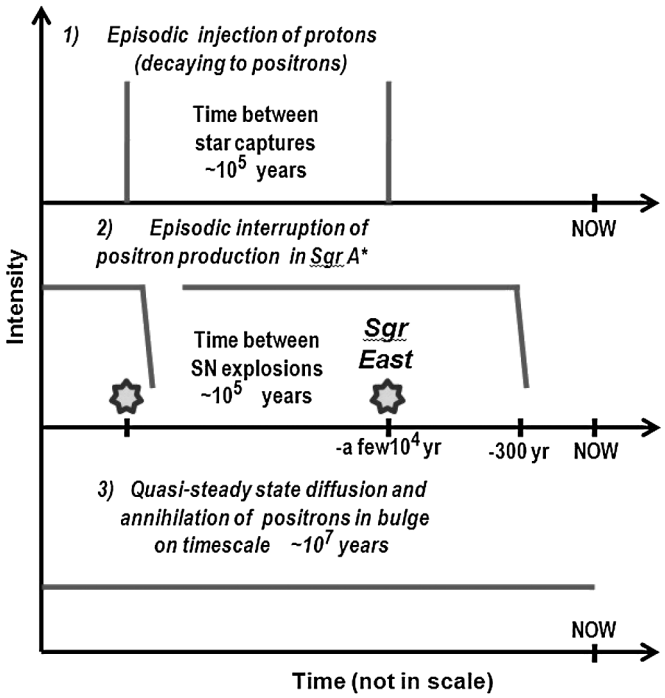

FIG. 17. Illustration of the two schemes conceived for the positron production activity of Sgr A^*. In (1), protons are injected and/or accelerated every $\sim 10^5$ yr following the tidal disruption of a star, and their collisions with the ISM produce positrons (after π^+ decay). In (2), Sgr A^* produces quasicontinuously positrons at a high rate, except when its accretion flow is interrupted by the passage of the shock front of a nearby SN explosion (expected to occur on a time scale of $\sim 10^5$ yr); the last SN explosion created the SN remnant Sgr East 10^4 yr ago and its expansion interrupted the accretion flow 300 yr ago [according to Totani (2006)]. Despite the discontinuous e^+ injection in both cases (1) and (2), the annihilation of positrons and the resulting 511 keV emission are in a quasisteady steady state (3) if positrons diffuse in the bulge, because of the long time scale of the latter process ($\sim 10^7$ yr).

(b) Quasi-steady-state accretion of surrounding gas was $\sim 10^4$ times higher in the past, but it was interrupted by some external factor which destroyed the accretion flow ~300 yr ago (Totani, 2006). This time scale results from the x-ray emission observed from Sgr B and Sgr C (both at distances of ~75 pc from Sgr A^*; see Fig. 18) which has been interpreted as the delayed reflexion of (a much stronger) past emission from Sgr A^* [see, e.g., Markevitch *et al.* (1993), Murakami *et al.* (2000), Revnivtsev *et al.* (2004), and Koyama *et al.* (2006)]. Building on those ideas, Totani (2006) suggested that it is the expansion of the SN remnant Sgr East which destroyed the high accretion flow. The age of that remnant (a few 10^4 yr) is smaller than the estimated time scale between two SN explosions in the GC vicinity ($\sim 10^5$ yr), but the probability that we observed Sgr A^* just 300 yr after its crossing by the expanding shell of Sgr East is rather small (~1%, Totani, 2006).

It should be noted that the time scale for variability of 511 keV emission is the longer of the two time scales τ_{prod} (for variability of e^+ production in the above models) and

[14]The Eddington luminosity is the limiting value for which gravitational attraction of a point source of mass M (accreting from surrounding material) is matched by repulsive radiation pressure due to accretion luminosity L. It is given numerically by $L_{Edd} \sim 1.3 \times 10^{38}\ (M/M_\odot)$ erg s^{-1} (assuming spherical symmetry and Thompson scattering of radiation).

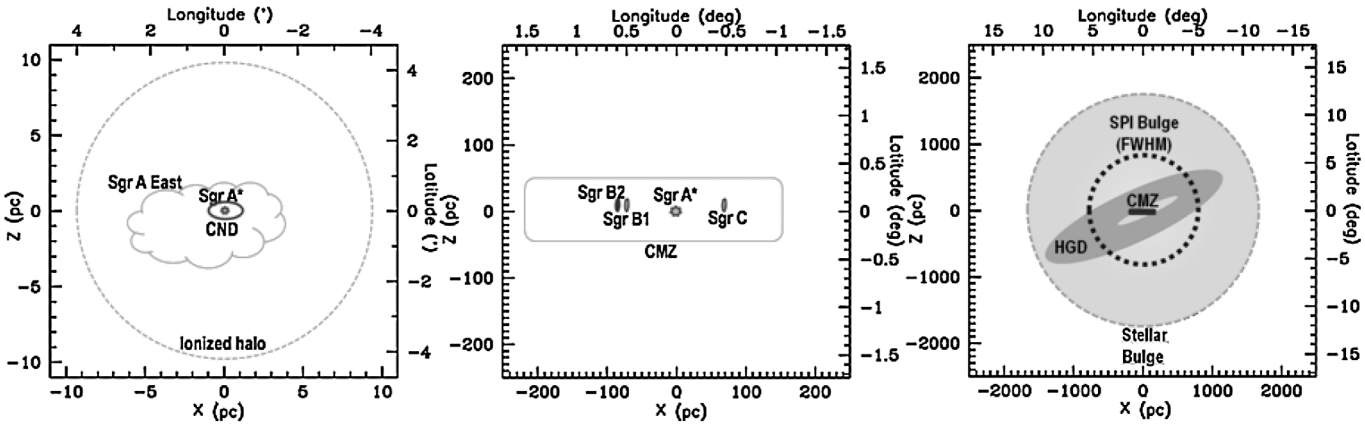

FIG. 18. Schematic representation of the inner Galaxy at different linear (bottom and left axis) and angular (top and right axis) scales. The main features discussed in Sec. IV.B.4 (SMBH scenario) appear on the figures, as, e.g., CND (circumnuclear disk, left panel), CMZ (central molecular zone, middle panel), and the tilted HGD (holed gaseous disk, containing atomic and molecular gas, right panel). If indeed Sgr A^* is the main positron source, (most of) its positrons have to diffuse through the CMZ into the bulge. Notice that the size of the CMZ corresponds to the size (FWHM) of the inner bulge in the first model of SPI data fitting (Table I). The size of the outer SPI bulge in that same model is indicated by a dotted circle in the rightmost panel.

$\tau_{\rm ann}$ (for e^+ slow down and annihilation). The former is $\sim 10^5$ yr, while the latter depends strongly on the physical conditions of the ISM (Sec. V). However, if the positrons survive annihilation in the GC vicinity and manage to fill the bulge (and this is a big if), the corresponding diffusion time scale can be estimated by quasilinear diffusion theory as $\tau_{\rm diff} \sim 10^7$ yr [see, e.g., Jean *et al.* (2006)]. It is this long time scale that determines variability of 511 keV emission and makes it essentially constant (Fig. 17), despite the variability of the e^+ production rate in both cases (a) and (b). We shall discuss the problem of e^+ propagation in the bulge (a crucial issue for all models producing bulge positrons in the SMBH) in Sec. VI.

Production of positrons can be envisioned by either (a) collisions of protons accelerated by the SMBH with the ISM and subsequent π^+ decay or, (b) direct pair production (see Sec. IV.B.1). We briefly present a few models which constitute specific realizations of the aforementioned ideas.

a. Production of positrons via p-p collisions

Models of this class usually try to simultaneously reproduce observations of 511 keV emission from the bulge and of higher energy γ rays from the central regions. Such emission has been detected at $E_\gamma > 500$ MeV with EGRET/CGRO (Mayer-Hasselwander *et al.*, 1998) and at TeV energies with various instruments [Aharonian *et al.* (2004, 2006), and references therein].

The generally large time scale for e^+ thermalization and annihilation (see Sec. V) creates problems for any scheme trying to simultaneously explain current observations of 511 keV and higher energy γ rays, if accelerated protons are assumed to be at the origin of both emissions. This was realized by Fatuzzo *et al.* (2001), who explored the fate of positrons produced by energetic protons, required to explain the GeV emission detected by EGRET from the source 2EG J1746-2852; the latter is located in the inner arcmin of the Galaxy and its γ-ray emissivity is associated with proton acceleration in Sgr East by Melia *et al.* (1998). Fatuzzo *et al.* (2001) found that in the physical conditions of Sgr East, the e^+ thermalization time scale is much longer than the age of Sgr East (or that the current e^+ thermalization and/or annihilation rate is much lower than the e^+ production rate, which is inferred from the high-energy γ-ray emissivity of 2EG J1746-2852). They concluded that recently accelerated protons in Sgr *A* East cannot be the source of the observed annihilation radiation, unless some more efficient e^+ cooling mechanism is at work. Alternatively, they suggested that more positrons from previous episodes of activity in the Galactic center (i.e., from tidal disruption of stars) have been "stockpiled" in that region and are annihilating now.

Cheng *et al.* (2006) further explored those ideas, but they considered in more detail the propagation of protons and positrons in the Galactic bulge. They found that in the case of an energetic but rare event (such as the disruption of a $50M_\odot$ star, releasing 10^{54} erg in energetic protons every $\sim 10^7$ yr) it is impossible to explain simultaneously the 511 keV and high-energy γ-ray emissions: Although positrons take a long time to diffuse and annihilate, protons interact rapidly and the corresponding γ-ray emission fades out in less than 10^5 yr. In a subsequent version of that work, Cheng *et al.* (2007) returned to the idea proposed by Fatuzzo *et al.* (2001), namely, that the observed 511 keV emission results from the annihilation of positrons produced and stockpiled in the bulge by dozens of tidally disrupted low-mass stars in the past $\sim 10^7$ yr: Each one of those events is less energetic ($\sim 10^{52}$ erg) but more frequent (corresponding time scale $\sim 10^5$ yr) than the rare massive star disruption. Because of the short time scale of e^+ production with respect to the time scale of e^+ annihilation, the resulting 511 keV emission is quasisteady (see Fig. 17). Thus, although the invoked e^+ production event is of low probability (small frequency), the observed intensity of the 511 keV emission is not.

Obviously, most of the positrons are produced in the high-density region where protons interact. Cheng *et al.* (2007) argued that positrons do not annihilate in those regions, but they avoid them (because of the screening effect produced by magnetohydrodynamic waves excited near molecular clouds)

and they propagate through the intercloud medium. In general, models where positrons result from the production and decay of π^+ will have typical energies of ~30 MeV, resulting in too much emission at >MeV energies from in-flight annihilation. Chernyshov *et al.* (2010) found that this difficulty may be circumvented if the magnetic field in the Galactic bulge is high enough (> 0.4 mG), because in that case positrons lose their energy rapidly (before significant in-flight annihilation) through synchrotron emission; this cooling process takes place within the time scale of e^+ production, i.e., long before e^+ annihilation, and should be currently undetectable in radio. However, as discussed in Sec. III.D, observations do not favor, at present, such high values for the magnetic field of the inner Galaxy.

b. e^+-e^- pair production by photons

As in the case of XRBs, pair production around the Galactic supermassive black hole may occur either in the inner hot accretion disk, in a corona above it, or in the jets; the latter case has not been considered up to now, in the absence of relevant observational evidence in Sgr A^*.

Beloborodov (1999) studied a detailed model of pair production, resulting from collisions of γ rays from the hot inner disk with x rays from the outer disk; the resulting e^+-e^- pairs are blown outward from the radiation pressure of the disk, in a mildly relativistic wind. The model is not specifically designed for the case of Sgr A^* but rather for extragalactic black holes in active galactic nuclei, but its results can be extrapolated to the case of Sgr A^*. The maximum pair production is obtained for a dense, optically thick, wind. In that case positrons annihilate mostly *inside* the wind flow and produce a very broad annihilation line, unlike the one observed with SPI/INTEGRAL. Positrons can escape and annihilate in the ISM in the case of a less dense, optically thin, wind but in that case their production rate is substantially smaller.

Totani (2006) considered pair production in the hot, inner accretion disk during past phases of higher activity in Sgr A^*. The invoked past accretion rate $\dot{m} \sim 10^{-4} M_\odot/\mathrm{yr}$ is not extravagant and could easily result from the material released by the regular tidal disruption of nearby low-mass stars [as in Cheng *et al.* (2007)] or from winds of nearby massive stars (Quataert, 2004), although Totani (2006) assumed that it originated from the ionized ''halo'' surrounding Sgr A^* (see Fig. 18, left panel). Totani (2006) considered pair production in the framework of the so-called radiatively inefficient advection flow (RIAF) model for accretion disks; this model, decoupling accretion from emerging luminosity, has been applied with considerable success to the case of Sgr A^* [see, e.g., Yuan *et al.* (2004), and Xu *et al.* (2006)). Totani (2006) found that the very high temperatures of the inner disk ($T \sim 10^{11}$ K) implied by the RIAF models are essential for a high rate of e^+ production, which he evaluated up to $\sim 10^{43} e^+ \mathrm{s}^{-1}$, i.e., close to the observationally inferred annihilation rate.

In all models of e^+ production from Sgr A^*, e^+ annihilation occurs on much longer time scales than e^+ production and varies much less in time than the latter. An advantage of direct pair-production models with respect to those involving energetic proton collisions is the low energy of the positrons produced, allowing them to satisfy the constraint of the observed MeV continuum.

In all cases, it has to be demonstrated that positrons may diffuse from Sgr A^* throughout the bulge without excessive annihilation in the dense inner regions (the circumnuclear disk), which would give a strong, pointlike emission. On the other hand, the latest analysis of SPI data suggests a narrow bulge component (Table I), the size of which (3° FWHM) corresponds to the size of the CMZ: ~1/3 of the bulge positrons may annihilate there and the remaining 2/3 may diffuse in the outer bulge (11° FWHM in Table I, see also Fig. 18). This picture may have difficulties, however, with the results of the spectroscopic analysis of SPI (see Sec. V.E) which finds that bulge positrons annihilate mostly in a warm medium (neutral or ionized), not in a molecular one.

C. Dark matter and "nonstandard" models

1. General properties of dark matter particles

In the past 40 years or so, particle physicists searched for possible DM candidates meeting three basic requirements, namely, stability (at least on time scales comparable to the age of the Universe), charge neutrality (to avoid electromagnetic, ELM, interactions and prevent DM from shining), and with a non-negligible mass (so that it can contribute gravitationally)[15]. The absence of electric charge favors DM models with weak interactions. However, weakly interacting particles may suffer from a prohibitive ''free-streaming'' effect,[16] depending on their mass: for example, if DM is composed of massless neutrinos, the formation of Milky Way size galaxies is strongly suppressed. Hence, there is a lower limit on the mass of weakly interacting DM candidates to explain the formation of the smallest objects observed in the Universe, which is of approximately a few keV. This leads to the notion of WIMPs and the idea of *collisionless dark matter*. The existence of WIMPs with a mass in the GeV–TeV range is compatible with the absence of signal in present DM direct detection experiments. However, the fact that none of these experiments has observed a positive signal yet (Baudis, 2007)[17] may lead to different interpretations, as discussed below.

If the DM number density today n_{dm} were similar to the relativistic particle density ($n_\gamma \sim 400\ \mathrm{cm}^{-3}$ for photons), the DM mass-energy density $\rho_{\mathrm{dm}} \simeq m_{\mathrm{dm}} n_{\mathrm{dm}}$ would exceed the critical density ρ_c by several orders of magnitude, for DM particle masses $m_{\mathrm{dm}} > 1$ keV. Given that particles lighter than keV are forbidden by the free-streaming argument, DM particles which have been in thermal equilibrium with

[15]These criteria are, in fact, supported by recent observations (assuming a Friedman-Robertson-Walker universe). For example, extrapolation of the physics of ordinary baryons to DM suggests that DM ELM interactions should damp the DM primordial fluctuations on a cosmological scale and prevent the formation of small-scale structures (smaller than a Milky Way size galaxy).

[16]Free streaming refers to the motion of noninteracting particles endowed with some initial velocity across the Universe. It has the effect of erasing irregularities on scales smaller than the free-streaming length.

[17]Apart, perhaps, from DAMA/LIBRA (Bernabei *et al.*, 2003).

radiation at some stage of the cosmic evolution should subsequently disappear. This may occur in two ways: either through an extremely small decay rate, which ensures a lifetime comparable to the age of the Universe (and thus implies quasistability) or through annihilation processes.

The latter mechanism has received a lot of attention in the last three decades. The requirement $\rho_{\rm dm} \sim \rho_c$ implies that the annihilation cross section of DM particles should be comparable to the weak interaction cross section; see, e.g., Hut (1977), Pryor *et al.* (1980), and Abbott and Sikivie (1983).[18] In some cases, this requirement can also be used to constrain the DM mass. As pointed out by Hut (1977) and Lee and Weinberg (1977), the annihilation rate ($\langle\sigma v\rangle \propto v^2$) of fermionic particles with typical weak interactions has a square dependence on DM mass, $m_{\rm dm}^2$. The observed $\rho_{\rm dm}$ implies then that DM particles should be heavier than a few GeV. This constitutes an extra motivation for considering WIMPs as DM candidates.

About 25 years ago, such properties (weak but nonnegligible interactions and $m_{\rm dm} > 1$ GeV) suggested that direct detection of DM would be relatively easy. However,

(1) The DM spin-independent interactions with matter (as measured by direct detection experiments) are at least 8 orders of magnitude weaker than the weak interactions (Lemrani, 2006; Angle *et al.*, 2008).
(2) Indirect detection experiments find no "smoking gun "evidence (i.e., the emission of a monochromatic line at an energy $E = m_{\rm dm}$) allowing for a clear identification of $m_{\rm dm}$ (Abdo *et al.*, 2009; Aharonian *et al.*, 2009).
(3) No signature of new physics, which would indirectly validate the existence of DM particles, was found at LEP or TEVATRON (Abbiendi *et al.*, 1999; Piper, 2009).

The aforementioned facts could mean either that DM has much weaker interactions than the standard model or point toward very heavy or very light DM particles.[19] Besides, the absence of ELM interactions could also imply strong interactions but at a different energy scale than previously considered (Boehm, 2008).

The aforementioned constraints, individually taken, can be easily accommodated in existing DM models (e.g., WIMPs). However, when combined together, they actually eliminate many proposed models. For example, to reduce the tension between direct detection experiments, which are now sensitive to elastic cross sections of the order of 10^{-43} cm^2 (corresponding to $\langle\sigma v\rangle \sim 10^{-33}$ cm^3 s^{-1}), and the annihilation rate $\sigma v \sim 3 \times 10^{-26}$ cm^3 s^{-1} imposed by the "relic density" criterion (corresponding to $\sigma \sim 10^{-36}$ cm^2), one often has to "decouple" the corresponding processes (Ellis *et al.*, 2000).[20] The lack of evidence could also mean that $m_{\rm dm} \ll 1$ GeV or $m_{\rm dm} \gg 1$ TeV. In the case of sub-GeV DM, one may naturally circumvent the Hut-Lee-Weinberg limit if DM has been produced out of thermal equilibrium or if it is made of scalar particles with nonchiral couplings to standard model particles. Nonthermal production also helps very heavy DM particles to avoid conflict with the relic density criterion. Thus, the acceptable range for $m_{\rm dm}$ still lies from the sub-eV range (with axions) to several TeV (such as "excited" DM, Kaluza-Klein particles) and, in fact in some case, to even higher masses. Hence, keV, MeV, and sub-TeV candidates (such as, respectively, sterile neutrinos, light dark matter, and neutralinos) remain potential solutions [see, e.g., Bertone (2007)].

Progress in the field of DM may come from indirect detection. Indeed, cosmic-ray spectra "anomalies" (with respect to standard astrophysical predictions) appear puzzling enough (Picozza *et al.*, 2007) to open up new particle physics scenarios (Chang *et al.*, 2008; Adriani *et al.*, 2009). For example, recent results from the PAMELA satellite indicate an excess of CR positrons above 10 GeV over the background expected from CR interactions with interstellar matter (Moskalenko and Strong, 1998), but no corresponding excess in antiprotons.[21] However, the all lepton spectrum as measured by the Fermi-LAT came out flatter than previously thought (Abdo *et al.*, 2009). The sources of these particles (or electrons and positrons) should be less than $\sim$1 kpc away, since electrons and positrons in this energy range suffer heavy energy losses through inverse-Compton and synchrotron processes. Conventional astrophysical sources (e.g., nearby pulsars, see Sec. IV.B.3) could explain these excesses, but the possibility of the first indirect detection of DM annihilation created a lot of excitement in the particle physics community [see Essig *et al.* (2009) and references therein].

The recent excitement illustrates the new trends in the DM particle physics community and shows how far we are from the determination of the nature of DM. This also demonstrates that considering only neutralinos or Kaluza-Klein particles as DM may be too restrictive. In this review, we shall focus only on the DM candidates which have been explicitly invoked to explain the Galactic 511 keV emission.

2. Specific dark matter candidates for e^+ production

Positrons produced by DM annihilation or decay may annihilate *in flight*, before losing a large fraction of their

[18]The abundance of DM particles today Ω_X is fixed in the so-called "freeze-out" epoch, when the expansion rate of the Universe H (a function of Ω_X) equals the DM annihilation rate $\Gamma = n_X\langle\sigma v\rangle$, where n_X is the DM particle abundance and $\langle\sigma v\rangle$ their annihilation cross section; this leads to a "relic" abundance of DM particles of $\Omega_X = f(\langle\sigma v\rangle)$ and for the observed $\Omega_X \sim 0.25$ one obtains $\langle\sigma v\rangle \sim 10^{-26}$ cm^3 s^{-1}, which is close to the value of weak interaction cross sections [the actual value depends on the nature of the DM candidate and its mass, see, e.g., Bertone *et al.* (2004)].

[19]If DM is lighter than a few GeV, its interaction with matter would be essentially "invisible" for current detectors (MeV particles would require, for example, detectors with eV energy threshold, while they are currently in the keV range). If DM particles are too heavy, their number density in our Galaxy is too small to generate a significant number of events in a detector.

[20]This decoupling can be made by invoking either "coannihilation," i.e., annihilation of DM with another particle, present during the dark matter transition to the nonrelativistc regime (Griest and Seckel, 1991), or by fine-tuning the DM parameters so that the annihilation cross section is enhanced but the elastic scattering cross section remains very small.

[21]The balloon-borne experiment ATIC reported an excess of electrons plus positrons in the 300–800 GeV range, but the excess was not confirmed by Fermi-LAT (Abdo *et al.*, 2009) nor by HESS (Aharonian *et al.*, 2009).

energy. In-flight e^+ annihilation provides an additional source of continuum γ-ray emission toward the Galactic center (see Sec. II.C.1) which can be used to constrain the e^+ energy at injection and, consequently, the mass of annihilating or decaying DM particles. Assuming that the contribution of known astrophysical sources to the measured continuum in this energy range is well understood, Beacom and Yüksel (2006) and Sizun *et al.* (2006) obtained a mass upper limit of $m_{\rm dm}\sim$ a few MeV (see Fig. 6). Among the many proposed DM scenarios, those that may satisfy such a constraint can be classified in two main categories:

(i) Light DM particles of ~MeV mass, either *annihilating* (Boehm *et al.*, 2004; Gunion *et al.*, 2006), or *decaying* (Hooper and Wang, 2004; Picciotto and Pospelov, 2005) or even both (Pospelov *et al.*, 2008).

(ii) Heavy DM particles in the ~GeV–TeV range, *deexciting* (or decaying into another particle) with a mass difference of a few MeV between initial and final states (Finkbeiner and Weiner, 2007; Pospelov and Ritz, 2007).

Other, more intricate possibilities, involving dark matter, cosmic strings, primordial black holes, and other exotica, will be briefly presented in Sec. IV.C.3.

Low-mass annihilating DM particles were initially proposed to illustrate a new damping effect,[22] but also as a counter example of the "Hut-Lee-Weinberg limit": Boehm *et al.* (2004) pointed out and Boehm and Fayet (2004) showed that this limit is valid only in the case of fermionic DM candidates interacting with Fermi (i.e., weak) interactions. But, if one or both of those assumptions are relaxed, a very different conclusion may be obtained: For instance, if the DM particle is a scalar (spin 0) which annihilates into a e^--e^+ pair via the exchange of a fermionic particle F, then the relic density criterion constrains the characteristics (mass and couplings) of the F particle instead of the mass of the DM particle. Particles substantially lighter than a few GeV (and down to the MeV range) may then account for the observed dark matter relic density in that case. Such particles are expected to annihilate into e^--e^+ pairs (Fig. 19) either via a heavy charged particle exchange or a new neutral gauge boson (Boehm and Fayet, 2004; Boehm, Ensslin, and Silk, 2004). Boehm and Ascasibar (2004) and Boehm and Silk (2008) found that the properties of such particles, if they are at the origin of the 511 keV line, should affect the value of the fine structure constant. In fact, using this very argument, Boehm and Ascasibar (2004) and Boehm and Silk (2008) excluded DM particles heavier than 7 MeV (assuming a NFW dark matter halo and the corresponding best fit cross section).

The light DM particle idea, at least in it simplest form, was challenged by an analysis of the explosion of supernova SN1987A (Fayet *et al.*, 2006), which puts a lower limit of ~10 MeV to the mass of the particle. Such a limit is very close to the upper limit allowed by the observed ~MeV continuum.

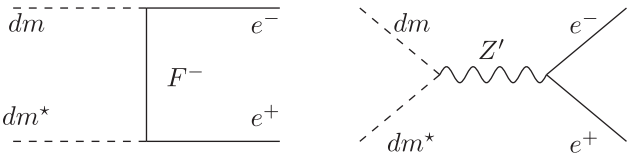

FIG. 19. Possible Feynman diagrams for light annihilating dark matter particles.

Low-mass (< 100 MeV) decaying DM candidates were proposed by several groups, after the release of the 511 keV map by the SPI Collaboration, in order to explain the large amount of low-energy positrons in the Galactic bulge. Decay into e^--e^+ pairs is one of the dominant decay modes of such particles since, apart from the neutrino and photon channels, electrons are the only other kinematically accessible channel. Depending on the model, these particles may [the axinos by Hooper and Wang (2004)] or may not [sterile neutrinos by Picciotto and Pospelov (2005), moduli by Conlon and Quevedo (2007), Kasuya and Kawasaki (2006), and Craig and Raby (2009)] be the major contributors to cosmic DM density.

The second category of DM particle candidates invokes electroweak scale WIMPs, with masses in the 100 GeV–1 TeV range and possessing almost mass degenerate excited states, i.e., the difference between the excited and ground states should be of the order of ~MeV. Finkbeiner and Weiner (2007) noticed that the velocity dispersion of DM particles in the gravitational potential of the inner Galaxy is of the order of a few 100 $\mathrm{km\,s^{-1}}$, endowing a 500 GeV WIMP with a kinetic energy >511 keV. Inelastic scattering between WIMPs could raise one or both of them in their excited state(s) and deexcitation to the ground state could proceed via emission of a e^--e^+ pair. This scenario has also been invoked to explain other observables such as the DAMA/LIBRA signal or the WMAP "haze"[23] (Hooper *et al.*, 2007; Finkbeiner *et al.*, 2008) and the PAMELA e^+ excess (Arkani-Hamed and Weiner). A recent investigation of this idea suggests, however, that the model parameters have to be pushed to their extreme values for the e^+ production rate to agree with observations (Chen *et al.*, 2009). Nonetheless, metastable dark matter could explain the observations, as emphasized by Cline *et al.* (2010), in scenarios with three states of dark matter with small-mass splitting and where the middle state is metastable [based on a mechanism suggested by Chen, Cline, and Frey (2009)].

Independently of their "naturalness" (or lack of) as extensions of the standard model, the various proposed scenarios for DM particles at the origin of the Galactic 511 keV line also differ as to the predicted spatial profile of the resulting e^+ population. Assuming that positrons annihilate close to their production sites, this may constrain and discriminate between the various models.

[22]The mixed damping effect is, in fact, analogous to the "Silk damping," with dark matter playing the role of baryons and neutrinos replacing the photons (Boehm *et al.*, 2001; Boehm and Schaeffer, 2005).

[23]Observations with the Wilkinson microwave anistropy probe (WMAP) revealed an excess of microwave emission in the inner 20° of the Galaxy, which cannot be accounted for by conventional astrophysical explanations, such as thermal bremsstrahlung from hot gas, synchrotron emission, etc.

The rate of positrons produced locally by annihilation, decay, and deexcitation of DM particles is given by $\dot{n}_{e^+}(r) \propto \Gamma_{X\to e^-e^+} n_X(r)$, where $n_X(r)$ is the number density of DM particles at distance r from the Galactic center.[24] The interaction rate $\Gamma_{X\to e^-e^+}$ in the case of decaying DM particles has a maximum value corresponding to the inverse of the age of the Universe. In the case of annihilating or collisionally excited DM particles, $\Gamma_{X\to e^-e^+} = \langle\sigma v\rangle n_X$, where $\langle\sigma v\rangle$ is the annihilation or excitation cross section folded with the velocity distribution of the DM particles.

In the case of decaying DM particles, $\dot{n}(r)_{e^+} \propto n(r)_X$, i.e., the positron production profile closely follows the DM density profile; note that this is also the case for all "conventional" astrophysical sources studied in the previous sections. On the other hand, in the case of annihilating or deexcited DM, $\dot{n}_{e^+}(r) \propto \langle\sigma v\rangle n_X^2(r)$, i.e., the positron profile is generically more centrally concentrated [because of the $n_X^2(r)$ term], but this shape can be also modulated by the possible velocity dependence of the interaction cross section $\sigma(v)$, since the typical particle velocities depend on the gravitational potential $\Phi(r)$ of the DM halo. In the latter case, comparison of the model to the data requires a more elaborate analysis; an example of such an analysis will be given in Sec. IV.D.3.

3. Other exotica

Several rather exotic objects have been invoked as sources of the Galactic positrons producing the 511 keV emisssion. Here we provide a nonexhaustive list of them.

For example, Huh *et al.* (2007) suggested MeV millicharged (fermionic) particles. As in the first version of MeV annihilating dark matter, this scenario assumes a new light [U(1)] boson exchange, called exphoton. Because of the presence of kinetic terms, the dark matter would be millicharged, while the rest of the scenario resembles the fermionic candidates introduced by Boehm and Fayet (2004). The required parameter range to explain the 511 keV line appears to be compatible with the constraints from the relic density requirement and collider experiments.

The idea of Q balls in gauge mediated supersymmetry breaking scenarios was proposed by Kasuya and Takahashi (2005). Q balls can be depicted as stable localized field configurations, their stability being guaranteed by a conserved charge Q associated with a U(1) symmetry. For example, Q could be the electric charge; in Kasuya and Takahashi (2005), Q is, in fact, the lepton number. These objects may have a long enough lifetime and yet a small energy density, possibly enabling them to be present in our Galaxy and to explain the 511 keV emission.

Macroscopic objects, such as superconducting dark matter (Oaknin and Zhitnitsky, 2005) or compact composite objects (Zhitnitsky, 2006) were also proposed. These objects are hypothesized to form during the QCD phase transition and could be schematically depicted as "quark" balls. They introduce a link between the dark matter and baryonic energy densities and eventually explain why these two quantities are of the same order of magnitude. Positronium formation happens through electrons or baryonic matter interactions (annihilations) inside the compact composite objects. However, the ability of such a scenario to explain the 511 keV emission was criticized by Cumberbatch *et al.* (2008), who found that positronium formation is hardly possible at all in such objects, if one describes the electrosphere of the nuggets by using a purely relativistic approximation [unlike what was assumed by Oaknin and Zhitnitsky (2005) and Zhitnitsky (2006)].

If a tangle of light superconducting strings exists in the Milky Way, it may also act as a low-energy positron source (Ferrer and Vachaspati, 2005, 2007). If the string curvature radius is smaller than a characteristic scale, the string can move with respect to the magnetized plasma in the Galaxy. The possible interaction of the string with the magnetic field can then generate a current composed of zero modes of charged particles. Owing to this mechanism, positrons could propagate along the string. They eventually leave the string if they become nonrelativistic and scatter with counterpropagating particles in the string. Depending on the string curvature radius, the positrons would then have an energy of $E <$ MeV, although this energy could reach the GeV scale if there are superconducting strings at the TeV scale.

Finally, Titarchuk, and Chardonnet (2006) proposed that x rays from the SMBH collide with 10-MeV γ rays from small-mass black holes (10^{17} g) to give pairs; this can produce about $10^{42} e^+/$s, about an order of magnitude less than needed. This rate is obtained by taking the total x-ray and γ-ray luminosity of the inner GC regions: $L_X \sim 2\times 10^{39}$ ergs/s and $L_\gamma \sim 4\times 10^{38}$ ergs/s (Strong *et al.*, 2000), then assuming the γ radiation comes from an optically thick medium and that its spectrum is therefore a blackbody one with a temperature of $T_\gamma = 10$ MeV; the two energy distributions (x and γ) are convolved to compute the pair-production rate. A simpler scenario, involving evaporating primordial black holes was proposed by Bambi *et al.* (2008).

D. Assessment of sources

In this section we summarized the pros and cons of each one of the candidate positron sources presented so far, in light of the observational constraints of Sec. II.B, namely, (i) the total e^+ annihilation rate ($\gtrsim 2\times 10^{43}$ s^{-1}), (ii) the typical energy of the injected positrons, or the equivalent mass of annihilation DM particles ($<$ 3–7 MeV), and (perhaps, most significantly) (iii) the morphology of the 511 keV emission (with a bulge-to-disk ratio $B/D > 1$ in the case of a thin disk emission). A fourth constraint, namely, the longitudinally asymmetric disk emission, should be added to this list, once robustly established by further data and analysis.

1. Positron annihilation rate

Assuming a steady-state regime, the e^+ annihilation rate has to be equal to the average e^+ production rate during the lifetime of e^+ in the ISM.

The only source definitely known to provide substantial amounts of e^+ at a well-constrained rate is the radioactive decay of ^{26}Al: $0.4\times 10^{43} e^+$ s^{-1}. The decay of ^{44}Ti probably provides another $0.3\times 10^{43} e^+$ s^{-1}. GCRs probably provide

[24] Generally, $n_X(r)$ is assumed to be spherically symmetric; deviations from spherical symmetry, due to triaxiality of the DM halo, are negligible with respect to other uncertainties of the problem.

$0.1 \times 10^{43} e^+$ s^{-1}. Nova models (as constrained against several observables such as ejecta abundances, velocities, etc.) may provide a e^+ yield from ^{22}Na decay not much below the reported value of $10^{41} e^+$ s^{-1}. The e^+ of all other candidate sources is entirely speculative at present. Values discussed in previous sections should be considered as optimistic rather than typical values. Observed upper limits of individual sources [see Table 4 in Knödlseder *et al.* (2005) and Table 1 in Guessoum *et al.* (2006)] are of little help to constrain positron sources. No useful observational constraints exist up to now on the e^+ yields of hypernovae and GRBs, pulsars, ms pulsars, magnetars, LMXRBs, microquasars, the SMBH at the Galactic center, or dark matter annihilation. SNIa remain an intriguing, but serious candidate, with a potential Galactic yield of $2 \times 10^{43} e^+$ s^{-1}.

2. Positron energy

Radioactive decay produces positrons of $E \leq 1$ MeV, naturally fulfilling the observational constraint on continuum γ rays from in-flight annihilation. The same applies to pair creation through γ-γ collisions in the inner accretion disk or at the base of the jets of LMXRBs, microquasars, and the SMBH at the Galactic center. Conversely, pair creation involving very high-energy photons, as in, e.g., pulsars or magnetars, will produce positrons of too high energy. The same holds for energetic p-p collisions in Galactic cosmic rays or in the baryonic jets of LMXRBs, microquasars, and the Galactic SMBH. Those processes produce e^+ of >30 MeV, and thus may be discarded as major e^+ sources in the Milky Way. Also, that same constraint limits the mass of putative decaying or annihilating DM particles to <10 MeV, while it does not constrain the mass of deexciting DM particles.

3. Morphology

None of the e^+ sources studied in this section reproduce the large $B/D \geq 1$ ratio inferred from SPI data, as can be seen in Figs. 20 and 21, where we present flux sky maps and longitude profiles, respectively, comparing the SPI data of Weidenspointner *et al.* (2008a) to various expected source profiles, either theoretical or observed ones. The comparison is made under the explicit assumption that positrons produced from the corresponding sources annihilate close to them.

The best-established e^+ sources, β^+ decay from ^{26}Al and ^{44}Ti produced in massive stars, yield $B/D \leq 0.2$, as derived from the observed distribution of the 1.8 MeV line (normalized here to a total disk emissivity of $0.7 \times 10^{43} e^+$ s^{-1}, see Sec. IV.D.1) (Figs. 20 and 21, top panels). Note that similar profiles are expected for pulsars, magnetars, hypernovae, and γ-ray bursts (albeit with different normalizations).

Binaries involving low-mass stars, such as SNIa, novae, and LMXRBs, are expected to have a steeper longitude profile, with a maximal $B/D \leq 0.5$ (assuming the bulge and disk masses of Sec. III). Using data from Fig. 10 and Table V and adopting an exponential density profile for the bulge (with scale length of 400 pc and normalized to $1.4 \times 10^{10} M_\odot$) one may estimate an expected sky distribution and corresponding longitude profile of SNIa, also displayed in Figs. 20 (middle panel) and 21 (top panel), where it is

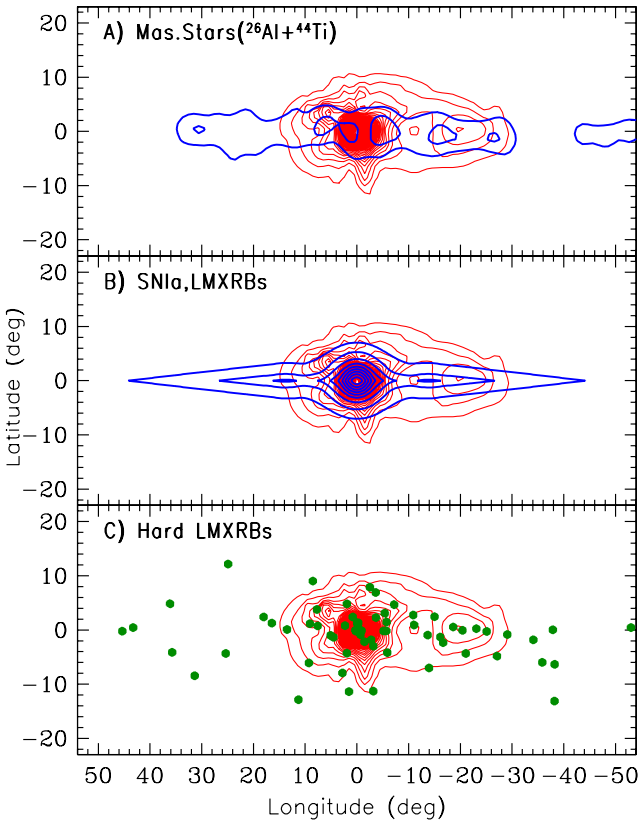

FIG. 20 (color online). Maps of the Galactic 511 keV emission (flux in cm^{-2} s^{-1} sr^{-1}), as observed from SPI (in all panels, thin isocontours from Weidenspointner *et al.*, 2008a) and from observationally based or theoretical estimates. (A) Observed ^{26}Al (and, presumaby, ^{44}Ti) map (from Plüschke *et al.*, 2001); (B) accreting binary systems (SNIa and, presumably, LMXRBs, see text); (C) observed hard LMXRBs (from Bird *et al.*, 2007). The robustly expected e^+ annihilation from radioactivity in the disk (upper panel) is not yet fully seen by SPI.

assumed that the e^+ escape fraction from SNIa is 3%. Figure 21 (top panel) indicates that the theoretically expected SNIa longitude profile resembles the observed profile of LMXRBs [from Grimm *et al.* (2002)]. This similarity reflects the fact that both classes of sources involve an old stellar population, which is proportionally more abundant in the inner Galaxy and the bulge than in the rest of the disk. Novae are also expected, on those grounds, to have a similar distribution (albeit with a much lower normalization constant).

The upper panel of Fig. 21 clearly shows that

(a) The expected outer disk ($l > 20°$) contribution of massive star radioactivity (^{26}Al and ^{44}Ti) is not yet detected, due to insufficient sensitivity; SPI/INTEGRAL or a future instrument should reveal that component, or else it should be concluded that positrons diffuse far away from their sources.
(b) SNIa or LMXRBs or microquasars can explain only about half of the strong 511 keV emission from the inner Galaxy, assuming they produce as many positrons as in Table IX.
(c) Any remaining annihilation γ-ray emission requires a supplementary source (dark matter or the central

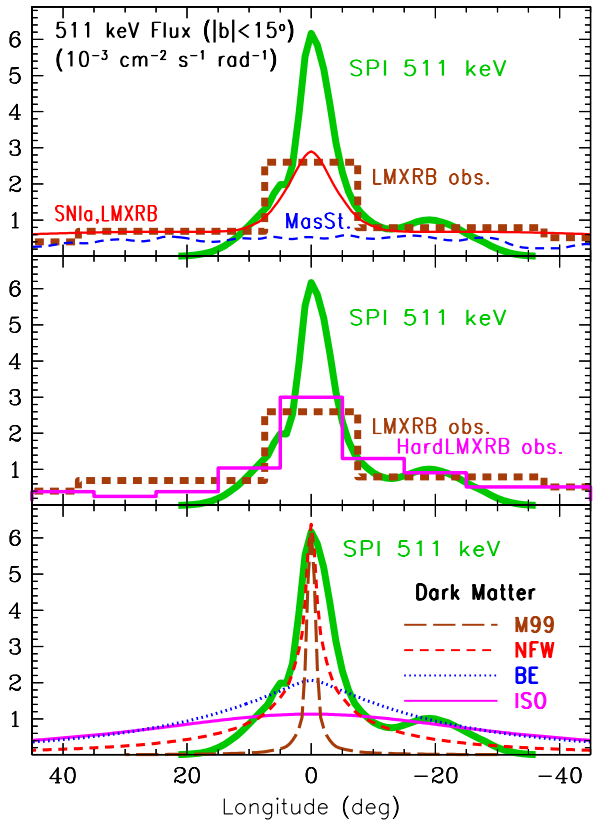

FIG. 21 (color online). Intensity of 511 keV emission as a function of Galactic longitude. All fluxes are integrated for latitudes $|b| < 15°$. In all panels, the thick solid curve corresponds to SPI observations, i.e., the map of Fig. 20. (We note that SPI maps and fluxes are provided here for illustration purposes only; quantitative comparison of model predictions to data should only be made through convolution with the SPI response matrix.). The thick dotted histogram (top and middle panels) is the observed longitude distribution of LMXRBs (from Grimm, *et al.*, 2002); the latter closely resembles the theoretically estimated longitude distribution of SNIa (thin solid curve in the upper panel), which has been normalized to a total emissivity of $1.6 \times 10^{43} e^+$ s^{-1}, with bulge/disk = 0.45 (maximum bulge-to-disk ratio for SNIa from Table V). Also, in the upper panel, the lower dashed curve corresponds to the expected contribution of the ^{26}Al and ^{44}Ti β^+ decay from massive stars. The thin solid histogram in the middle panel is the observed longitude distribution of hard LMXRBs (from Bird *et al.*, 2007) and it has the same normalization as the thick histogram. In the bottom panel, the SPI 511 keV profile is compared to profiles expected from dark matter annihilation (Table VI).

SMBH, provided its positrons can diffuse to kpc distances and fill the bulge); alternatively, it may be assumed that SNIa or LMXRBs or microquasars produce twice as many positrons as assumed in Fig. 21, but half of the disk positrons are transported to annihilate outside the Galactic disk (see Sec. VI.C).

In the middle panel of Fig. 21 we compare the longitude profile of the observed 511 keV emission to the one of the hard LMXRBs (emitting in the 20–100 keV range), as seen with IBIS/INTEGRAL [from Bird *et al.* (2007)]. Weidenspointner *et al.* (2008a) noticed that the latter distribution exhibits a pronounced asymmetry, with source number ratio $N(l < 20°)/N(l > 20°) = 1.7$, which matches the asymmetry well in the 511 keV flux reported in the same paper. They suggested then that hard LMXRBs may be at the origin of the disk emission.

We note that the study of the same SPI/INTEGRAL data by Bouchet *et al.* (2008, 2010) with different methods does not find significant disk asymmetry. Obviously, the important (and intriguing) observational result of Weidenspointner *et al.* (2008a) needs confirmation by further observations or analysis. Assuming the asymmetry is real, what might the implications be? The interpretation of Weidenspointner *et al.* (2008a) implicitly assumes the following:

(i) Positrons annihilate relatively close to their sources, such that the annihilation morphology reflects the source morphology.
(ii) Among all LMXRBs only the bright and hard LMXRBs of the IBIS/INTEGRAL catalog (Bird *et al.*, 2007) are important e^+ contributors.
(iii) Those x-ray bright and hard-spectrum LMXRBs have the same average positron yields, which are therefore not correlated to their currently observed (but known to be widely varying) x-ray luminosities; in that way, the collective e^+ production of hard-spectrum LMXRBs is just proportional to their total number, not to their total x-ray luminosity.

Assumption (i) underlies all efforts to match the observed 511 keV morphology with some particular class of sources. However, if it is adopted, and if it is assumed that the observed disk emission is due to $0.7 \times 10^{43} e^+$ s^{-1} released by hard LMXRBs, one has to explain why the robustly established e^+ production of ^{26}Al and ^{44}Ti is not detected by SPI. Indeed, the corresponding e^+ production rate is quite high (0.7×10^{43} s^{-1}, with small uncertainty) and positrons are released in the dense environment of massive stars and CCSN. In comparison, positrons from LMXRBs are released away from the disk (in view of the ~400 pc scale height), i.e., in less dense environments, and could travel and annihilate farther away from their sources than those of massive star radioactivity. If both radioactivity and LMXRBs release $0.7 \times 10^{43} e^+$ s^{-1}, the former should dominate the observed 511 keV emission (the latter having a lower surface brightness), and no significant asymmetry should be seen (Prantzos, 2008).

Assumption (ii) has been criticized by Bandyopadhyay *et al.* (2009), who noted that a lower sensitivity cutoff than the one of IBIS would lead to a different spatial distribution of the hard LMXRBs, in view of the steeply rising luminosity function of those sources. Besides, in view of the time variability of LMXRBs, the present day asymmetric profile (merely a snapshot in time) does not guarantee that the same morphology characterizes the total number of hard LMXRBs that may contribute to e^+ production during the e^+ lifetime (~10^6 yr). Notice also that in the fourth IBIS source catalog (Bird *et al.*, 2010) there is no strong evidence for a LMXRB distribution asymmetry in the Galactic plane.

Finally, assumption (iii) is far from obvious. This assumption certainly applies to, e.g., SNIa, which are assessed to have an average ^{56}Ni yield of $0.7 M_\odot$ and to constitute a relatively homogeneous class of objects. One may certainly imagine that LMXRBs also produce, on average, the same yield of positrons, at least on time scales comparable to the

TABLE IX. Properties of candidate positron sources in the Milky Way.

Source	Process	$E(e^+)$[a] (MeV)	e^+ rate[b] $\dot{N}_{e^+}$ (10^{43} s^{-1})	Bulge/disk[c] B/D	Comments
Massive stars: ^{26}Al	β^+ decay	~1	0.4	<0.2	$\dot{N}$, B/D: Observationally inferred
Supernovae: ^{24}Ti	β^+ decay	~1	0.3	<0.2	$\dot{N}$: Robust estimate
SNIa: ^{56}Ni	β^+ decay	~1	*2*	<0.5	Assuming $f_{e^+,\mathrm{esc}} = 0.04$
Novae	β^+ decay	~1	*0.02*	<0.5	Insufficient e^+ production
Hypernovae/GRB: ^{56}Ni	β^+ decay	~1	?	<0.2	Improbable in inner MW
Cosmic rays	p-p	~30	0.1	<0.2	Too high e^+ energy
LMXRBs	γ-γ	~1	*2*	<0.5	Assuming $L_{e^+} \sim 0.01\ L_{\mathrm{obs},X}$
Microquasars (μQs)	γ-γ	~1	*1*	<0.5	e^+ load of jets uncertain
Pulsars	γ-γ/γ-γ_B	>30	*0.5*	<0.2	Too high e^+ energy
ms pulsars	γ-γ/γ-γ_B	>30	*0.15*	<0.5	Too high e^+ energy
Magnetars	γ-γ/γ-γ_B	>30	*0.16*	<0.2	Too high e^+ energy
Central black hole	p-p	High	?		Too high e^+ energy, unless $B > 0.4$ mG
	γ-γ	1	?		Requires e^+ diffusion to ~1 kpc
Dark matter	Annihilation	1 (?)	?		Requires light scalar particle, cuspy DM profile
	Deexcitation	1	?		Only cuspy DM profiles allowed
	Decay	1	?		Ruled out for all DM profiles
Observational constraints		<7	2	>1.4	

[a]Typical values are given.
[b]e^+ rates: in roman: observationally deduced or reasonable estimates; in italic: speculative (and rather close to upper limits).
[c]Sources are simply classified as belonging to either young ($B/D < 0.2$) or old (< 0.5) stellar populations.

positron annihilation time scale. However, if LMXRB positrons are produced in the inner accretion disks by processes depending on parameters of the binary system (e.g., temperature, depending on black hole mass) then only a few of those systems may be important e^+ producers; their spatial distribution may not be represented at all by the one of all hard LMXRBs.

The morphology of the observed 511 keV emission provides also some interesting constraints in the case of dark matter particles as positron sources (under the assumption of negligible e^+ propagation). An illustration of such an analysis is provided by Ascasibar *et al.* (2006), who convolved the positron maps predicted for various light DM particle scenarios and types of DM halo profiles with the response function of SPI. Comparison to the data showed that (i) particle candidates with velocity dependent cross sections are excluded as the main source of 511 keV emission, (ii) fermionic DM candidates are also excluded, since they need to exchange too light charged particles, and (iii) decaying dark matter cannot be the main source of low-energy positrons, because the resulting flux profile is too flat, compared to SPI data. Note that this latter feature is a generic property of all models involving decaying particles, where the positron production (and annihilation) rate is proportional to the DM density profile: even "cuspy" profiles, such as the NFW (see Fig. 12), do not provide a γ-ray flux profile sufficiently peaked toward the inner Galaxy. Annihilating or deexciting DM produces positrons at a rate proportional to the square of the DM density profile (see Sec. IV.C.2) and leads to a much more peaked γ-ray profile. Ascasibar *et al.* (2006) found that light scalar annihilating particles remain as a possible candidate, provided the DM halo is at least as cuspy as the NFW profile with $\gamma \sim 1$ (see bottom panel of Fig. 21); however, as stressed in Sec. III.E, astrophysical evidence favors flatter DM halo profiles.

The proximity of the Galactic center and the expected high density of DM particles there make it the prime target for the detection of all kinds of radiation emitted indirectly by DM (either decaying, annihilating, or deexciting). However, because of the uncertainties presently affecting the density profile of DM halos (see Sec. III.E) and the possible contamination of the signal by more conventional astrophysical sources, other potential targets have been sought. The dwarf spheroidal (dSph) satellites of the Milky Way, with their high mass-to-light ratio and relative proximity, may constitute such targets. Hooper *et al.* (2004) suggested that the light DM hypothesis could be tested on the nearby (25 kpc) dSph galaxy Sagittarius, which appears to be dominated by dark matter. A search for the expected annihilation signal at 511 keV (Cordier *et al.*, 2004) was unsuccessful.

4. Summary of candidate sources

The main features of the candidate e^+ sources discussed in this section are summarized in Table IX. As already emphasized, e^+ production rates of all those sources are extremely uncertain (except those of ^{26}Al, ^{44}Ti, and GCRs) and the values listed above should be considered as optimistic rather than typical ones. Only in the case of novae may the estimated production value be used to eliminate those sources as important e^+ producers. Source morphology and high energy of produced positrons appear to exclude pulsars, magnetars, and GCRs as major contributors to the observed 511 keV emission from the bulge. Source morphology alone would exclude hypernovae and GRBs. The high energy of produced positrons disfavors ms pulsars, as well as p-p collisions from any source (microquasars, LMXRB jets, the central SMBH). This still leaves several potentially important e^+ contributors, but none of them has the observed morphology of 511 keV emission.

Thus, assuming that positrons annihilate near their sources, one has to conclude that

(i) either an unknown class of sources dominates e^+ production, or

(ii) positrons are produced by a combination of the sources of Table IX, e.g., (a) ^{26}Al + ^{44}Ti for the disk and dark matter for the bulge, or (b) ^{26}Al + ^{44}Ti + LMXRBs (or microquasars) for the disk and the bulge plus a contribution from the central SMBH for the inner bulge, or (c) some other combination.

Alternative (ii) bears an interesting "philosophical" issue: How is it possible that two widely different classes of sources have such similar e^+ yields (to within a factor of a few), as required to fit the observations? However, such "coincidences" are not unusual in astronomy[25] these days.

A more important issue arises in solutions involving the central SMBH as the main e^+ producer within the Galaxy's bulge: If its positrons can diffuse to kpc scales in the dense environment of the inner bulge, then positrons should diffuse to even larger scales in the less dense environment of the disk; this would be even more true outside the spiral arms, where most of the SNIa, LMXRB, and μQ positrons are expected to be released. Positron escape from the disk to the halo would alleviate the morphology problem, by reducing the disk 511 keV emissivity and thus increasing the B/D ratio of those classes of sources. However, although some of the basic physical processes underlying e^+ propagation are well understood, there is no clear global picture of how far positrons can propagate in the magnetized, turbulent ISM of the Galaxy. We turn to those two issues in the next two sections.

V. POSITRON INTERACTIONS WITH MATTER AND ANNIHILATION

Positrons are initially produced with kinetic energies higher than those of the ISM (see previous section). Most of them slow down to low energy before they annihilate with bounded or free electrons of the ISM. However, when their initial kinetic energy is above a tenth of MeV, a significant fraction of them may annihilate in flight. Figure 22 summarizes the processes that lead to γ-ray production from positron annihilation. The following sections list the interactions that are responsible for the energy losses of positrons in the ISM and present the different ways in which they annihilate with electrons.

A. Energy losses

As charged leptons, positrons interact via the electromagnetic force with all basic constituents of the ISM, namely, electrons, ions, atoms, molecules, solid dust grains, photons, and magnetic fields. Since their initial kinetic energy is generally larger than the kinetic energy of the targets in the ISM, positrons lose energy in these interactions. The energy loss rate and the kind of interaction depend on the energy of positrons and the density of target particles. Figure 23 presents the energy loss rate as a function of positron energy;

[25]Among the most famous coincidences are (i) the contributions of baryonic and nonbaryonic matter, as well as those of dark matter and dark energy, to the cosmic density; (ii) the solar abundances of s and r nuclei (both of $\sim 10^{-6}$ by mass fraction); and (iii) the approximately equal contributions of CCSN and SNIa to the solar Fe content.

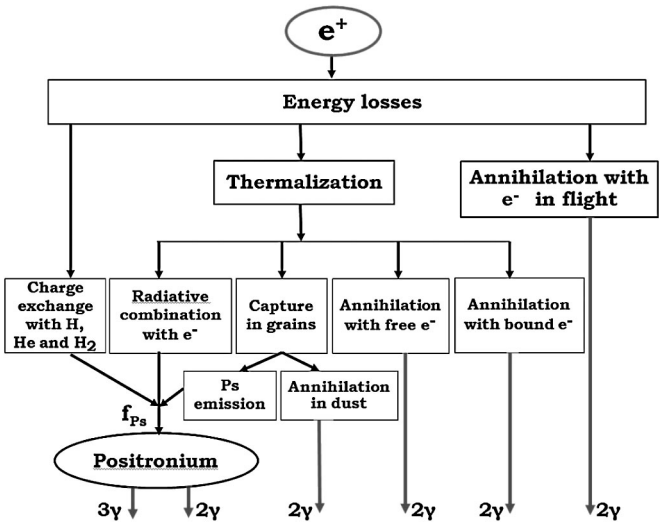

FIG. 22. The processes leading to γ-ray production from positron annihilation. Adapted from Guessoum *et al.*, 1991.

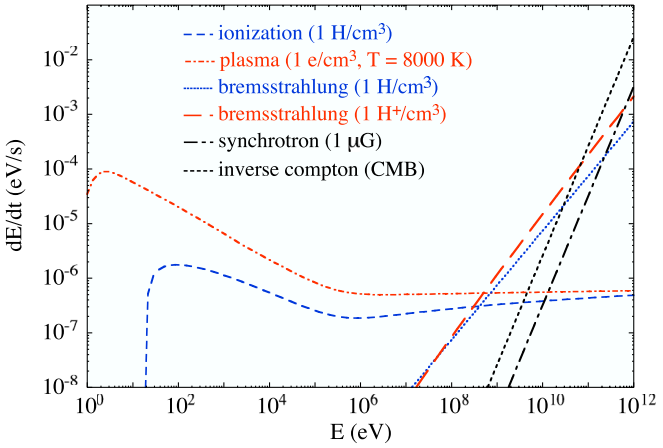

FIG. 23 (color online). Energy loss rate for positrons in ISM conditions. For synchrotron losses, the pitch angle is taken as $\pi/2$.

the contributions of each type of interaction are shown separately.

Ultrarelativistic positrons ($E > 10$ GeV) lose their energy mainly by inverse-Compton scattering with cosmic microwave background (CMB) photons and interstellar radiation fields. When the interaction occurs with an isotropic photon gas in the Thomson scattering regime (i.e., $h\nu \ll m_e c^2$), the energy loss rate (in eV/s) can be calculated from (Blumenthal and Gould, 1970)

$$\left(\frac{dE}{dt}\right)_{\rm IC} = -2.6 \times 10^{-14} u_{\rm rad} \gamma^2 \beta^2, \tag{10}$$

where $u_{\rm rad}$ is the radiation energy density (eV/cm^3), and $\beta = v/c$ is its velocity relative to the speed of light. The radiation energy density depends on the position of the positron in the Galaxy; it ranges from 0.26 eV/cm^3 (CMB) to 11.4 eV/cm^3 in the Galactic center region (Moskalenko *et al.*, 2006).

Ultrarelativistic positrons also lose their energy by emitting synchrotron radiation when they spiral along a magnetic field line. The energy loss rate depends on the magnetic field

intensity, the positron's kinetic energy, and the *pitch angle*.[26] Its expression (in eV/s) is (Blumenthal and Gould, 1970)

$$\left(\frac{dE}{dt}\right)_{\rm SY} = -9.9\times10^{-16}B^2\gamma^2\beta^2\sin^2(\alpha), \quad (11)$$

where B is the magnetic field (in μG) and α is the pitch angle. For a positron moving through a randomly oriented magnetic field, the mean energy loss rate is obtained by replacing $\sin^2(\alpha)$ by its average value 2/3. The synchrotron energy loss rate is proportional to the square of the magnetic field while the inverse-Compton one is proportional to the radiation energy density. Therefore, synchrotron losses dominate for ultrarelativistic positrons in an environment where $B > 6.3\ \mu{\rm G}\ \sqrt{u_{\rm rad}}$, e.g., near pulsars, the Galactic center region, etc.

In the 1–10 GeV energy range, positrons lose their energy mainly by emitting bremsstrahlung radiation in interactions with ions, electrons, and atoms. The energy loss rate depends on the target mass, charge, and density. For relativistic positrons, it is equivalent to the electron one. Methods for calculating the average energy loss rate and the bremsstrahlung energy spectrum are described by Hayakawa (1969), Blumenthal and Gould (1970), and Evans (1975). A recent update, with a more accurate treatment of the differential cross section for electrons with mildly relativistic energies in a fully ionized plasma, was presented by Haug (2004). A good approximation of the bremsstrahlung energy loss rate (in eV/s) of relativistic positrons in a fully ionized gas is (Ginzburg, 1979, p. 408)

$$\left(\frac{dE}{dt}\right)_{\rm BR} = -3.6\times10^{-11}Z(Z+1)n\gamma\left[\ln(2\gamma)-\frac{1}{3}\right], \quad (12)$$

where Z and n are the nuclear charge and the number density (in $\rm cm^{-3}$) of the ion, respectively. In a neutral hydrogen gas, the energy loss rate can be estimated via (Ginzburg, 1979, p. 386)

$$\left(\frac{dE}{dt}\right)_{\rm BR} = An\gamma, \quad (13)$$

where $A = -4.1\times10^{-10}$ for hydrogen and -1.1×10^{-9} for helium.

Below 1 GeV, positrons lose their energy mainly via Coulomb scatterings with free electrons and/or inelastic interactions with atoms and molecules. The former process is a continuous energy loss, whatever the energy of positrons. At high energy, the target electrons can be considered at rest and the energy loss rate depends mostly on their density. Dermer (1985) calculated the rate of *e-e* Coulomb collisions in relativistic thermal plasmas. He also treated the case of collisions in cold plasmas. This energy loss can be approximated by (Ginzburg, 1979, p. 361)

$$\left(\frac{dE}{dt}\right)_{\rm COU} = -7.7\times10^{-9}\frac{n_e}{\beta}\left[\ln\left(\frac{\gamma}{n_e}\right)+73.6\right], \quad (14)$$

where n_e is the electron density.

At low positron energy ($E \lesssim 10kT$, where T is the ambient temperature), the electrons of the ISM cannot be considered at rest anymore. The energy loss rate depends on their temperature and density in the plasma and is given by Book and Ali (1975) and Huba (2006) [see also Murphy, Share *et al.* (2005)].

Inelastic collisions of positrons with atoms and molecules can be considered as a continuous process for a positron energy >1 keV, and the energy loss rate can be evaluated using the Bethe-Bloch formula. The ionization loss is larger than the excitation loss. This energy loss can be approximated by (Ginzburg, 1979, p. 360)

$$\left(\frac{dE}{dt}\right)_{\rm ION} = -7.7\times10^{-9}\frac{nZ}{\beta}\left[\ln\left(\frac{(\gamma-1)(\gamma\beta mc^2)^2}{2I^2}\right)+\frac{1}{8}\right], \quad (15)$$

where n is the neutral atom density, Z is the number of electron of the atom, and I is its ionization potential (e.g., 13.6 eV for H and 24.6 eV for He). Below 1 keV the interaction between positrons and atoms and/or molecules should be estimated via Monte Carlo simulations since positrons release a large fraction of their energy in one interaction and, below ~100 eV, they can pick up an electron from an atom or a molecule to form a positronium in flight (see Table X and the next section). In this case, the cross sections for such collisions should be used in evaluating the energy loss rate [see Guessoum *et al.* (2005)]. The Monte Carlo method to calculate the interaction probability as a function of the positron's energy was presented by Bussard *et al.* (1979).

Equations (10)–(15) allow one to estimate to a good approximation energy losses of positrons. More accurate expressions, valid to energies >1 GeV, are given by Strong and Moskalenko (1998).

B. Annihilation in flight

In this section, we present two kinds of annihilation in flight: (1) direct annihilation of relativistic positrons with electrons and (2) annihilation via positronium produced in interactions of nonrelativistic positrons with atoms and molecules.

1. Direct annihilation in flight

When high-energy positrons ($\gtrsim$10 keV) slow down, they may annihilate in flight with free or bound electrons. The energies of the two photons emitted in this process are

TABLE X. Energy thresholds of inelastic reactions produced by positrons.

Process	Threshold (eV)
$e^+ + {\rm H} \rightarrow {\rm Ps} + {\rm H}^+$	6.8
$e^+ + {\rm H} \rightarrow e^+ + e^- + {\rm H}^+$	13.6
$e^+ + {\rm H} \rightarrow e^+ + {\rm H}^*$	10.2
$e^+ + {\rm H} \rightarrow e^+ + {\rm H}^{**}$	12.1
$e^+ + {\rm He} \rightarrow {\rm Ps} + {\rm He}^+$	17.8
$e^+ + {\rm He} \rightarrow e^+ + e^- + {\rm He}^+$	24.6
$e^+ + {\rm He} \rightarrow e^+ + {\rm He}^*$	21.2
$e^+ + {\rm H}^2 \rightarrow {\rm Ps} + {\rm H}_2^+$	8.6
$e^+ + {\rm H}^2 \rightarrow e^+ + e^- + {\rm H}_2^+$	15.4
$e^+ + {\rm H}_2 \rightarrow e^+ + {\rm H}_2^*$	12.0

[26]The pitch angle of a charged particle is the angle between the vectors of the particle's velocity and of the local magnetic field.

strongly shifted as per the Doppler effect. This produces a continuous spectrum in the energy interval $mc^2/2 \lesssim E_\gamma \lesssim E + mc^2/2$ with E being the total energy of the positron.

The probability that a positron with an initial kinetic energy E_0 annihilates in flight before reaching an energy E is

$$P(E_0, E) = 1 - \exp\left(-n_e \int_E^{E_0} \frac{\upsilon(E')\sigma_a(E')dE'}{|dE'/dt|}\right), \quad (16)$$

where υ and dE'/dt are the positron velocity and the energy loss rate, respectively; n_e is the density of target electrons, and σ_a the annihilation cross section, which can be estimated for kinetic energies larger than 75 keV via (Dirac, 2008)

$$\sigma_a = \frac{\pi r_e^2}{\gamma+1}\left[\frac{\gamma^2+4\gamma+1}{\gamma^2-1}\ln(\gamma+\sqrt{\gamma^2-1}) - \frac{\gamma+3}{\sqrt{\gamma^2-1}}\right], \quad (17)$$

where r_e is the classical electron radius ($r_e = e^2/m_e c^2$); for an evaluation of this cross section below 75 keV, see Gould (1989). The probability $P(E_0, E)$ depends on the energy loss rate and consequently on the physical conditions of the interstellar medium in which the positron propagates. Figure 24 presents the spectra of γ rays emitted by in-flight annihilation of relativistic positrons slowing down in the interstellar medium, for several initial kinetic energies. Figure 25 shows the fraction of positrons annihilating in flight as a function of the initial kinetic energy of positrons, in both a neutral and a fully ionized medium. It is negligible ($\lesssim 4\%$) for energies lower than 1 MeV. Above $\sim$1 GeV, the fraction does not change because the energy loss rate is so large (see Fig. 23) that positrons do not have enough time to annihilate in flight at these energies.

The implications of e^+ annihilation in flight for the observed Galactic MeV emission are further analyzed in Sec. V.E.

2. Positronium formation in flight

When positrons have kinetic energies lower than $\sim$100 eV, they can pick up an electron from an atom or a molecule to form a positronium in flight while they slow down. This reaction, also called charge exchange, is endoenergetic. It can happen as long as the kinetic energy of the positron is larger than the charge exchange threshold energy of Ps formation with the given atom or molecule (see Table. X). This threshold energy is equal to the ionization potential of the atom reduced by the binding energy of the Ps (6.8 eV). The cross sections for positronium formation by charge exchange were measured mostly in rare gases, particularly in helium, and in molecular and atomic hydrogen [see Guessoum *et al.* (2005)].

The fraction of positrons that form a positronium in flight is obtained by Monte Carlo methods which consist of simulating the interactions of positrons with atoms and molecules on the basis of the cross sections and energy loss mechanisms presented in the previous section. This fraction depends on the density, on the temperature, and strongly on the ionization fraction of the medium in which positrons slow down. Figure 26 shows the fraction of positrons forming positronium in flight as a function of the ionized fraction in two

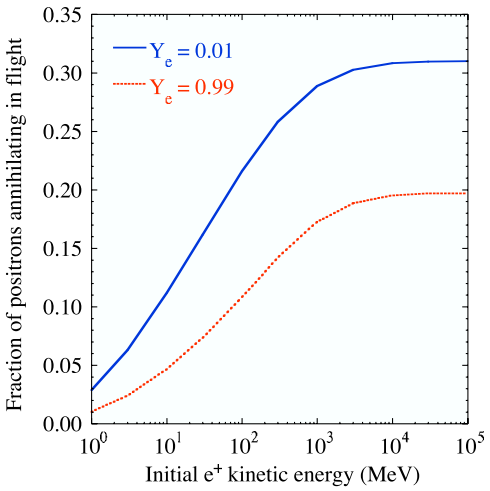

FIG. 25 (color online). Probability for a positron to annihilate in flight as a function of its initial kinetic energy, in a neutral medium (solid line) and an ionized medium (dashed line). Y_e represents the ionization fraction.

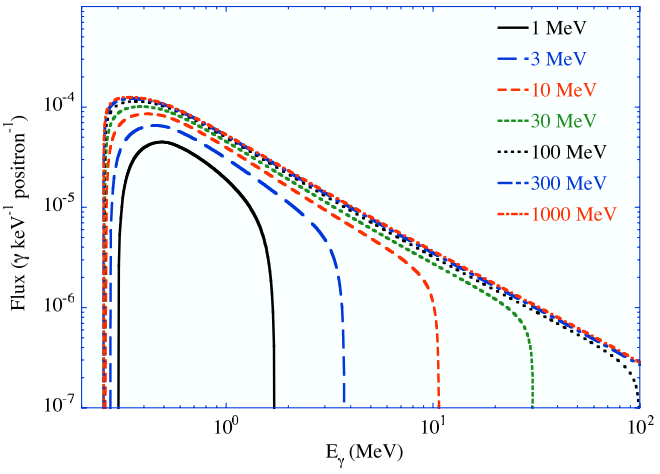

FIG. 24 (color online). γ-ray spectra from the annihilation in flight in the ISM for various initial kinetic energies of positrons.

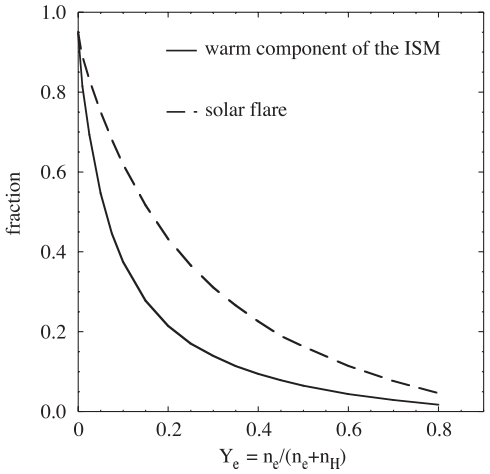

FIG. 26. Fraction of positrons forming positronium in flight by charge exchange with atomic hydrogen as a function of the ionization fraction (Y_e) in a warm component of the interstellar medium (electron density $n_e = 0.1$ cm^{-3}, electron temperature $T_e = 8000$ K) and in a solar flare ($n_e = 5 \times 10^{13}$ cm^{-3}, $T_e = 1.16 \times 10^4$ K).

TABLE XI. Percentage of positrons forming positronium in flight, in totally neutral media.

References	H	H_2	He
Bussard *et al.* (1979)	95	93	—
Brown and Leventhal (1986)	—	89.7 ± 0.3	80.7 ± 0.5
Wallyn *et al.* (1994)	98	90	—
Chapuis *et al.* (1994)	—	—	78
Guessoum *et al.* (2005)	95.5	89.6	81.7

types of media (Murphy, Share *et al.*, 2005). The fraction of positrons that form Ps decreases quickly with increasing values of the ionized fraction not only due to the reduction of the density of neutral H but also because the energy loss rate increases quickly with the ionized fraction (see Fig. 23). It makes the positrons slow down so rapidly that they do not have time to exchange charge with H. Measured (Brown *et al.*, 1984; Brown and Leventhal, 1986) and calculated values of the fraction of positrons forming positronium in flight in H, He, and H_2 are summarized in Table XI.

When the Ps is produced in flight, its kinetic energy is equal to the energy of the positron minus the threshold of the charge exchange reaction. Consequently, the energy of the photons emitted in the annihilation is shifted as per the Doppler effect. The spectral shape of the 511 keV line emitted in the annihilation of p-Ps was also derived from Monte Carlo simulations by extracting the kinetic energy distribution of the produced Ps. The most recent calculations (Guessoum *et al.*, 2005) yield widths of 5.8, 6.4, and 7.4 keV for H, H_2, and He, respectively. The calculated linewidths for He and H_2 are in good agreement with previous measurements (Brown *et al.*, 1984).

For large gas density, the time scale for a Ps to collide with an ambient particle X (atom, electron, photon) may be comparable to or lower than the lifetime of the o-Ps. In that case, the o-Ps can be destroyed ($^3\mathrm{Ps} + X \rightarrow X + e^+ + e^-$) or converted into a p-Ps (spin flip, $^3\mathrm{Ps} + X \rightarrow X + {}^1\mathrm{Ps}$). These processes tend to reduce the contribution of the annihilation via the o-Ps state. They are expected to occur in the solar atmosphere during flares [see Guessoum *et al.* (1997) and Murphy Share *et al.* (2005)] and in nova envelopes (Leising and Clayton, 1987). In such media, the interactions of Ps with components (atoms, electrons, photons) of the plasma must be taken into account in evaluating the proportion of annihilations through the o-Ps and the p-Ps states and is known as "o-Ps quenching."

C. Thermalization

Once the positrons have come down to energies similar to those of the ambient medium, they start to "thermalize," i.e., their energy distribution relaxes to the Maxwellian function which characterizes the interstellar gas (or plasma).[27] The ISM usually consists of a few phases, each with rather well-defined physical characteristics (temperature, density, ionization fraction); see Table IV. The time scale needed for the energetic positrons to relax to the ISM Maxwellian distribution is compared to the time scale for subsequent annihilation processes; if the former time scale is longer than the latter, it would be incorrect to assume a Maxwellian distribution for both the positrons and the ISM when calculating the e^+ annihilation rates.

To tackle this question one may simply estimate the relaxation time scale or perform a full statistical-physics treatment. The former can be simply done by using the energy loss rate $\tau = -[(1/E)(dE/dt)]^{-1}$ or (a simpler but cruder evaluation) $\tau^{-1} = R = \langle n\sigma v\rangle$, taking for the cross section some typical inelastic scattering value. The first formula (using values in Fig. 23 for the energy loss rate) gives $\tau \sim 6 \times 10^7$ s for 1 keV positrons, while using the cruder approach gives $\sim 2 \times 10^7$ s (taking $\sigma \sim 10^{-16}$ cm^2, $E_+ \sim 1$ keV, and $n \sim 1$ cm^{-3}); estimates for the relaxation of positrons from their initial energies of ~MeV is more complicated, both because the particles undergo many different processes and the overall cross section is difficult to estimate, but roughly the two simplistic approaches give time scales $\lesssim 10^{12}$ s. It must be noted that all of these values are much less than typical annihilation time scales in the ISM [see Guessoum *et al.* (2005)], which range around 10^{12}–10^{14} s.

The sophisticated statistical-physics approach is much more rigorous and conclusive, although complicated. A few authors have attempted such treatments, ranging from very broad, highly theoretical (Wolfe and Melia, 2006) to others covering a specific area of application (Crannell *et al.*, 1976), the latter focusing on low-energy (50 eV) positrons produced and annihilated in solar flares. Dermer and Liang (1989) and Nayakshin and Melia (1998) performed thorough statistical-physics treatments for the thermalization of high-energy electrons (and secondarily of positrons), assuming the interaction of the injected particles takes place with a relativistic electron-proton plasma. Baring (1987), modifying a simple treatment by Spitzer (1956), showed how to calculate the relaxation time $\tau(E_e)$ of an electron for any temperature (i.e., relativistic or not). The statistical-physics method uses a Fokker-Planck equation to follow the energetic particles from their injection (at a given time and energy) to their thermalization either with the background plasma and/or gas or with each other, taking into account the various inelastic scattering and loss processes; in this approach, one evaluates the energy and dispersion coefficients $[(1/n_e)(dE/dt)$ and $(1/n_e)[d(\Delta E)^2/dt]$, respectively]. Cheng *et al.* (2006) performed such a treatment for high-energy (30 MeV) positrons, presumably produced by proton-proton collisions at the Galactic center and approaching thermalization with the ISM gas and plasma conditions ($T \sim 10^4$ and 10^6 K, respectively).

These various approaches, heuristic or elaborate, have shown that the positrons do indeed thermalize before the annihilation processes become important, which makes valid and legitimate the usage of Maxwellian distribution functions in the calculations of the rates of annihilation and other processes that the positrons undergo.

D. Annihilation

Positrons annihilate by various processes during the two stages of their "lives": (a) during the slowing-down time (the

[27] It is understood that unless the background medium is in thermodynamical nonequilibrium (occurrence of irregular heating, sudden energy losses, etc.), it will have adopted a Maxwellian energy distribution characterized by temperature T.

process that is referred to as in-flight annihilation, described in Sec. V.B); and (b) after thermalization with the ISM. In this section we consider the latter stage and its processes. As explained in Secs. V.A and V.B, while positrons lose the bulk of their energies from ~1 MeV to ≃ 100 eV, their probability of undergoing "charge exchange" ("picking up" an electron from an atom or molecule and forming a positronium) increases steadily. Thus, by the time they have thermalized with the medium, the probability f_1 that they will have formed a Ps can be as high as 95%, depending on the ionization state of the medium (see Fig. 26).

Depending on the physical conditions of the medium (ionization state, temperature, composition), positrons may undergo a variety of annihilation processes, which are listed here by order of decreasing strength of their cross sections (when the physical conditions allow them to occur): (1) charge exchange (with atoms and molecules); (2) radiative (re)combination with (free) electrons; (3) direct annihilation with free electrons; and (4) direct annihilation with bound electrons (of atoms and molecules). For dust grains, the cross section for collision and annihilation (see below), may be larger than those of some of the above processes; however, when the abundance of dust grains is taken into account, the reaction rate for this process turns out to be smaller than the others', except in rare cases.

The key features of these annihilation processes (see Fig. 27) are the following:

(a) Charge exchange (with H, He, and H_2): although difficult to measure, the cross section for this(ese) process (es) has been obtained by several experimental groups [see Guessoum *et al.* (2005)]; the important feature of that process is its threshold energy (6.8, 17.8, and 8.6 eV, respectively), implying that this reaction (which has by far the highest cross section of all positron annihilation processes) can occur only at temperatures larger than several thousand K; hence this cannot occur in the cold media of the ISM, and, of course, it cannot take place in the hot ISM phase either (because the medium is completely ionized).

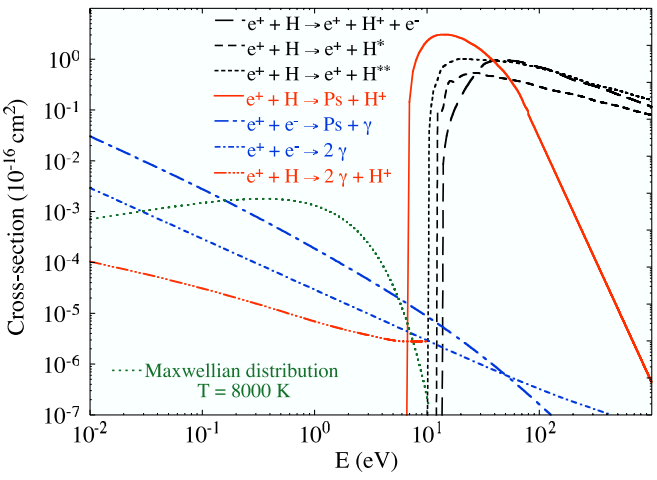

FIG. 27 (color online). Cross sections for ionization, excitation, charge exchange, radiative recombination, and direct annihilation interactions of positrons with atomic hydrogen and free electrons. Also shown is the Maxwellian distribution for a temperature of 8000 K (in arbitrary units).

The width of the line resulting from the annihilation of thermal positrons by charge exchange (decay of Ps) with H or He can be derived from the kinetic energy distribution of the produced Ps. This distribution is obtained simply by computing the charge exchange rate for a population of positrons that follows a Maxwellian distribution. The calculated widths in a warm medium ($T = 8000$ K) are 1.16 and 1.22 keV, for H and He, respectively (Guessoum *et al.*, 2005).

(b) Radiative (re)combination with free electrons: The cross section for this process is too small ($\sim 10^{-20}$ cm^2 at 1 eV) to be measured experimentally; one then has to rely on theoretical calculations, such as the determinations (by different approaches) made by Crannell *et al.* (1976) and by Gould (1989).

(c) Direct annihilation with free electrons: This process has an even smaller cross section (about an order of magnitude less than the previous one at temperatures less than about 10^5 K), hence it is only important in the hot phase of the ISM; the cross section has also been estimated by Crannell *et al.* (1976) and Bussard *et al.* (1979) from the early theoretical work of Heitler (1954).

The width of the line resulting from both radiative combination and direct annihilation of positrons and electrons was calculated by Crannell *et al.* (1976) using a simple argument of thermal broadening due to the pair's center-of-mass motion; they obtained the simple expression $\Gamma_{\mathrm{rc,dae}} = 1.1 \times (T/10^4)^{1/2}$ keV, which applies to both processes.

(d) Direct annihilation with bound electrons: The cross sections (for H, He, and H_2) are the weakest of all (see Fig. 27), but they become important by default at very low temperatures (in the cold phases of the ISM) where free electrons do not exist and the charge exchange (with atoms and molecules) cannot take place due to the threshold energies, which are (at about 10 eV) much too large compared to the particles' average thermal energies of ~0.01 eV. The first work that performed a calculation of this cross section is that of Bhatia *et al.* (1977); more detailed calculations, taking into account short range interactions between the positron and the target electron (e.g., virtual formation of positronium), were performed by Armour *et al.* (1990) and Igarashi *et al.* (2002), for positrons colliding with H and H_2, respectively.

The widths of the lines resulting from these processes have been measured by Brown and Leventhal (1986) for H and by Iwata (1997) for He and H_2; the values obtained were 1.56, and 2.50, and 1.71 keV for H, He, and H_2, respectively. These values have a very weak dependence on the temperature.

(e) Annihilation on dust grains: The importance of this process was first pointed out by Zurek (1985), who stressed the important effect this process would have on the Ps formation fraction, which is a quantity that can be inferred from observational data (see Sec. II.A) and thus represent an important constraint on models; Guessoum *et al.* (1991) then refined the calculation of the rate, adding electric-charge and positron-grain reflection effects, on the one hand, and spectral considerations (linewidth and effect on the overall calculated spectrum). Guessoum *et al.* (2005) have performed the most extensive astrophysical treatment of this process to date, despite the dearth of some crucial information on the processes, considering the materials that constitute the dust grains; in particular, the widths of the lines resulting from the annihilation

of positrons inside the grain (after capture) and from the decay of the positronium which is formed in or on the grain and ejected out have been evaluated to $\Gamma_{\mathrm{Ps,in}} \approx 2.0$ keV and $\Gamma_{\mathrm{Ps,out}} \approx 1.4$ keV, respectively. This is important in that it affects the amount of dust one will infer from the Galactic positron annihilation line spectra [see the discussion by Guessoum *et al.* (2004, 2005)]; note, incidentally, that due to the fact that Ps inside the grain undergoes "pick-off" annihilation, it always gives two photons, never three.

The corresponding reaction rates, taking into account the (Maxwellian) energy distribution of the particles (positrons, electrons, atoms, or molecules) and the abundance and density of each species, are given by

$$r_p = n\langle \sigma v \rangle = \int_{E_T}^{\infty} \frac{2}{\sqrt{\pi}} \frac{\sqrt{E}}{(kT)^{3/2}} e^{-E/kT} \sigma(E) v dE. \quad (18)$$

The reaction rates then allow one to determine the fraction of positrons which annihilate through each process, $f_p = r_p/\Sigma r_p$ (the index p generically refers to a process), and these fractions are then used to determine the spectrum of emission in a given physical medium.

The spectrum of γ-ray emission includes contributions from various processes: Each one of them consists of either a Gaussian function describing the line emission at 511 keV with a given line width (FWHM denoted by Γ) or a Gaussian [denoted below by $G(E, E', \Gamma)$, of variable E' and center E] and an ortho-positronium continuum (at $0 < E < 511$ keV), the latter given by the Ore and Powell (1949) function $P_t(E)$. The spectrum is then given by

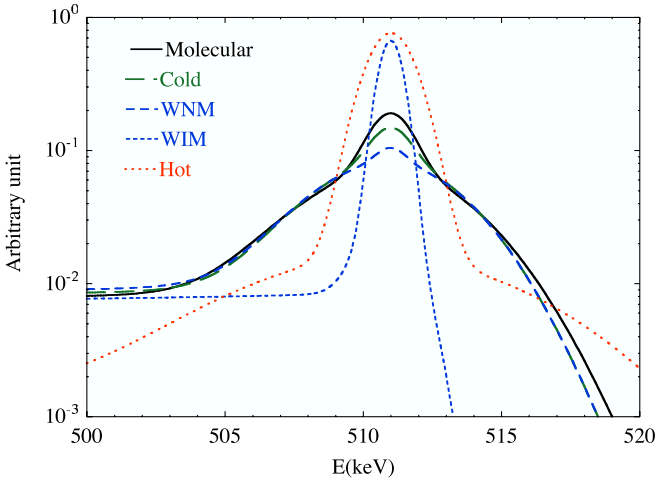

FIG. 28 (color online). Annihilation spectra for the five ISM phases. Adopted temperatures (see Table IV) are 10 K (molecular), 80 K (cold), 8000 K (WNM and WIM), and 10^6 K (hot) and ionization fractions are 0 for the neutral phases (molecular, cold, and WNM) and 1 for the ionized phases (WIM and hot).

$$\begin{aligned} S(E) = \int dE' \Big[3 \times \frac{3}{4} P_t(E') + 2 \times \frac{1}{4} \delta(E' - E_0) \Big] \{ & X f_{1,\mathrm{H/H_2}} G(E, E', \Gamma_{\mathrm{if,H/H_2}}) + Y \times f_{1,\mathrm{He}} G(E, E', \Gamma_{\mathrm{if,He}}) \\ & + (1 - X f_{1,\mathrm{H/H_2}} - Y f_{1,\mathrm{He}}) [f_{\mathrm{ce,H/H_2}} G(E, E', \Gamma_{\mathrm{ce,H/H_2}}) + f_{\mathrm{ce,He}} G(E, E', \Gamma_{\mathrm{ce,He}}) + f_{\mathrm{rce}} G(E, E', \Gamma_{\mathrm{rce}}) \\ & + f_{\mathrm{gr,out}} G(E, E', \Gamma_{\mathrm{gr,out}})] \} + 2(1 - X f_{1,\mathrm{H/H_2}} - Y f_{1,\mathrm{He}}) [f_{\mathrm{dae}} G(E, E_0, \Gamma_{\mathrm{dae}}) + f_{\mathrm{da,H/H_2}} G(E, E_0, \Gamma_{\mathrm{da,}H/\mathrm{H_2}}) \\ & + f_{\mathrm{da,He}} G(E, E_0, \Gamma_{\mathrm{da,He}}) + f_{\mathrm{gr,in}} G(E, E_0, \Gamma_{\mathrm{gr,in}})], \end{aligned} \quad (19)$$

where X and Y are the relative abundances of H (H_2) and He (90% and 10%, respectively, by number) and f_1 is the fraction of positrons forming positronium in flight. The spectra are presented in Fig. 28 for each phase of the ISM. In neutral media the line is broad due to the annihilation of Ps formed in flight. The width of the line is ~1 keV in the warm ionized phase where positrons annihilate mainly by radiative recombination with electrons. The contribution of the annihilation of positrons in grains is negligible in all the media except in the hot phase where it produces the ~2 keV width line superimposed on the broad line (~11 keV). The latter results from positrons that annihilate directly or via the radiative recombination process with electrons at a $T \sim 10^6$ K.

The "global" spectrum of annihilation of positrons in the ISM is then constructed by combining the spectra for each phase, considering the relative contributions (densities and filling factors) of each. For this, a model of the ISM, similar to those briefly sketched in Sec. III [see, e.g., Ferrière (1998, 1999, 2001), and McKee and Ostriker (1977)] is needed. The resulting global spectra can then be compared with the observational data. Of course, it would be at least as interesting and useful to compare the individual phase spectra with observational data, but this has been impossible so far, because of insufficient spatial resolution and sensitivity of the detectors.

E. Spectral analysis of observed emission

The previous sections described the annihilation processes and the resulting characteristics of the possible annihilation emissions. One must distinguish the emission produced by the in-flight annihilation of relativistic positrons, which is characterized by a continuous spectrum in the MeV domain (see Sec. V.B.1) from the 511 keV line and o-Ps continuum emissions produced in the annihilation of low-energy positrons (see Secs. V.B.2 and V.D).

As already discussed in Sec. II.B.2, the observed MeV continuum in the direction of the inner Galaxy significantly constrains the energies of injected positrons: They have to be lower than a few MeV, otherwise the continuum emission would be much higher than observed by COMPTEL (see Figs. 6 and 24). This allows one to eliminate several classes of sources in the steady-state regime, such as pulsars, ms pulsars, magnetars, or energetic proton collisions (either

from cosmic rays or from the central black hole), as major positron sources. The same argument was used by Beacom and Yüksel (2006) and Sizun *et al.* (2006) to constraint the mass of the decaying or annihilating dark matter particles which could be the sources of positrons in the spheroid (see Sec. IV.D) to lower than a few MeV. Note that the MeV continuum does not constrain the mass of deexciting dark matter particles, as discussed in Sec. IV.D. Moreover, Chernyshov *et al.* (2010) showed that the injection of positrons with initial kinetic energy higher than several GeV is allowed if the injection is nonstationary (e.g., through intermittent emission from the central black hole) and if the magnetic field is higher than 0.4 mG in this region (see also Sec. IV.B.5).

Concerning the annihilation of low-energy positrons, the shape of the annihilation line and the relative intensity of the o-Ps continuum are closely related to the abundances and thermodynamical conditions (density, temperature, ionization fraction) of the plasma in which positrons annihilate. The broadening of the 511 keV line induced by bulk motions of the gas in which positrons annihilate is not taken into account since we do not expect a significant Doppler shift due to Galactic rotation and/or turbulence in the Galactic center region ($\Delta v \lesssim 100$ km/s, $\Delta E \lesssim 0.17$ keV). Consequently, the spectral characteristics of the annihilation emission offer valuable information on the physical conditions of the ISM where positrons annihilate.

The observed spectrum can be simply characterized by the sum of its independent components: the Gaussians (to describe the 511 keV lines) and the ortho-positronium continuum. The fraction of positrons annihilating via Ps (f_{Ps}) is derived from the ratio of the ortho-positronium flux ($I_{3\gamma}$) to the total line flux ($I_{2\gamma}$) using Eq. (3). The measured characteristics (widths, f_{Ps}) can then be compared with what we expect from the physics of the annihilation of positrons in the ISM (see Sec. V.D).

From the OSSE data, Kinzer *et al.* (1996) inferred a positronium fraction $f_{\mathrm{Ps}} \approx 0.97 \pm 0.03$ in the Galactic center region. Measurements with the Ge detector TGRS onboard the WIND mission (1995–1997) gave a compatible value of 0.94 ± 0.04 (Harris *et al.*, 1998). From the linewidth, (1.8 ± 0.5) keV, and the positronium fraction measurements, Harris *et al.* (1998) concluded that a scenario in which annihilation does not occur either in cold molecular clouds or in the hot phase of the ISM is favored. Using preliminary SPI data of Jean *et al.* (2003) and TGRS data of Harris *et al.* (1998), Guessoum *et al.* (2004) showed that the bulk of the annihilation occurs in warm gas. However, the two groups did not exclude the fact that a significant fraction of the annihilation may occur in hot gas and in interstellar dust.

Another approach consists of fitting annihilation models to the observed spectrum. Churazov *et al.* (2005) fitted the temperature and the ionized fraction of the gas where the annihilation occurs with a measured spectrum based on SPI observations of the Galactic center region. They inferred from their analysis that the spectral parameters of the emission can be explained by positrons annihilating in a warm gas with a temperature ranging from 7000 to 40 000 K and an ionized fraction >1%. However, they did not exclude a combination of warm and cold gases. When a similar analysis was performed using a spectrum measured with 3 times more exposure, a temperature $T = (7.8^{+0.8}_{-0.5}) \times 10^3$ K and an ionized fraction of (10 ± 2)% (see Fig. 29) were obtained (Jean, unpublished).

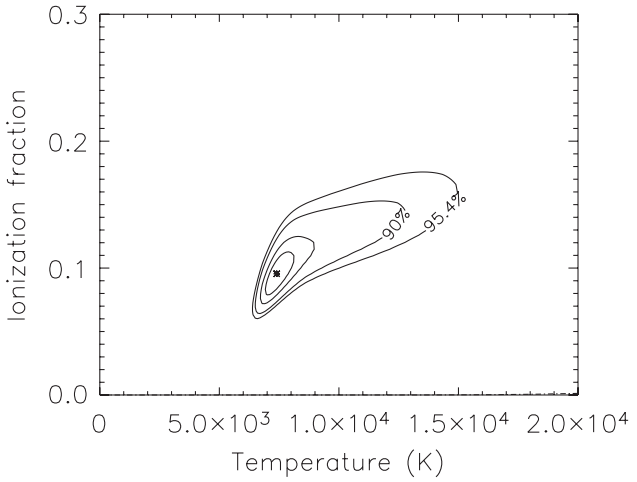

FIG. 29. Confidence regions of the fit of the temperature and ionization fraction to the SPI data obtained after 1 yr of mission. The best fit values are $T = 7800$ K and $y_e = 0.1$.

Instead of fitting the temperature and the ionized fraction to the SPI data, Jean *et al.* (2006) adopted the spectral models for the different ISM phases (see Fig. 30) and adjusted the phase fractions f_i (with $i = \{$molecular, cold, warm neutral, warm ionized, hot$\}$) so as to obtain the best fit to the spectrum measured by SPI. This model is described by

$$S_{\mathrm{ISM}}(E) = I_{e^+e^-} \sum_{i=1}^{5} f_i S_i(E, x_{\mathrm{gr}}), \tag{20}$$

where $S_i(E, x_{\mathrm{gr}})$ is the normalized spectral distribution (in keV^{-1}) of the annihilation photons in phase i, $I_{e^+e^-}$ is the

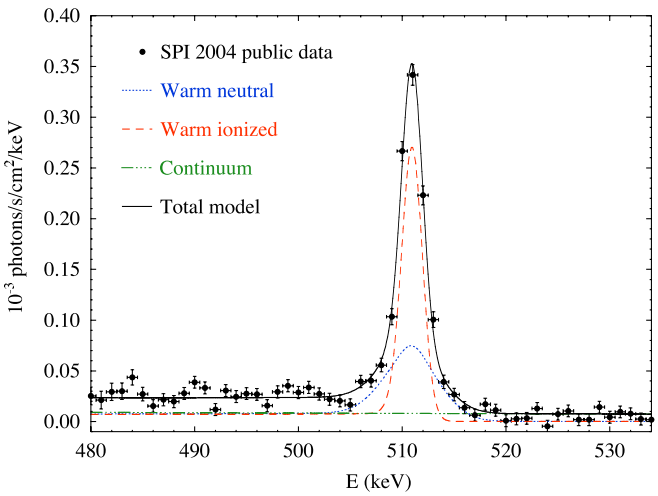

FIG. 30 (color online). Best fit of the spectrum measured by SPI using the warm components of the ISM and the Galactic continuum. Contributions from the molecular, cold, and hot components are not needed to explain the data. From Jean *et al.*, 2006.

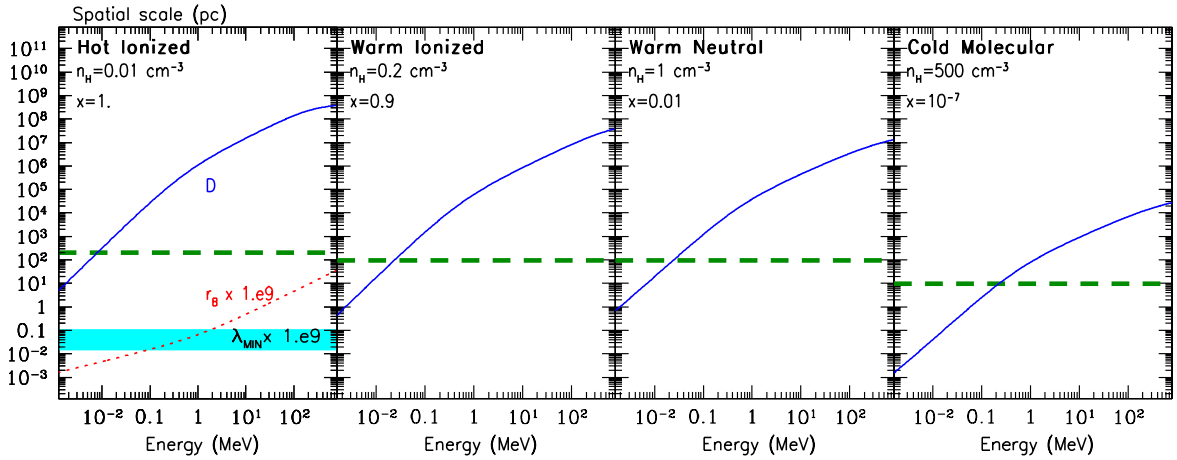

FIG. 31 (color online). Positron stopping distance D in various phases of the ISM (characterized by typical densities n_H and ionization fractions x) as a function of positron energy E. Horizontal dashed lines display typical sizes of the corresponding ISM phases. In the left panel, the lower dashed curve displays positron gyroradius r_g in a magnetic field of $B = 5$ μG, and the shaded area displays the minimum scale length $\lambda_{\rm MIN}$ of MHD Alfvén waves [the latter being calculated by Jean *et al.* (2009)]; both r_g and $\lambda_{\rm MIN}$ are enhanced by a factor of 10^9.

annihilation flux (photons $s^{-1}\,cm^{-2}$), and $x_{\rm gr}$ represents the fraction of dust grains and allows for uncertainties in dust abundance and positron-grain reaction rates ($x_{\rm gr} = 1$ in the standard grain model of Guessoum *et al.*, 2005). With this method, Jean *et al.* (2006) found that $49^{+2}_{-23}\%$ of the annihilation emission comes from the warm neutral phase and $51^{+3}_{-2}\%$ comes from the warm ionized phase. While they may not exclude that up to 23% of the emission might come from cold gas, they have constrained the fraction of annihilation emission from molecular clouds and hot gas to be less than 8% and 0.5%, respectively, and the contribution of grains to be less than 1.2%.

Finally, Guessoum *et al.* (2010) examined the annihilation of positrons on polycyclic aromatic hydrocarbon (PAH) molecules in ISM conditions. They showed that PAHs played a significant role only if their abundances were higher than about 10^{-6} (by number), the low abundances being compensated by the large enhancement in the PAHs' (resonant) annihilation cross sections. They used the 511 keV spectrum measured by SPI (Fig. 30) to constrain the PAH abundance in the bulge and found an upper limit of 4.6×10^{-7}, consistent with results obtained from IR observations on other Galactic regions.

VI. POSITRON PROPAGATION IN THE ISM

While most astrophysical sources are producing relativistic positrons (see Sec. IV), the results of the spectral analysis of the Galactic 511 keV emission (linewidth $\Delta E/E < 0.01$ and positronium fraction $f_{\rm Ps} \sim 97\%$) imply that positrons annihilate at very low energies (see Secs. II and V.E). This implies significant deceleration of positrons on their way to the annihilation sites, through the various energy loss processes summarized in Sec. V. Furthermore, various plasma processes, such as advection due to the Galactic wind, adiabatic deceleration, energy gain due to stochastic acceleration, and diffusion, may significantly affect the propagation of positrons and the extent of the region of e^+ annihilation emission.

There are two distinctly different regimes of positron transport in the ISM: *collisional* and *collisionless*. The former implies Coulomb interactions of positrons with particles in various gas phases of the ISM (in the presence of radiation and magnetic fields), while the latter is essentially due to the scattering off magnetic turbulence in the interstellar plasma. Observations of the solar energetic particles in the heliosphere reveal that their transport is indeed dominated by the scattering off fluctuating magnetic fields (see Sec. VI.B.1).

In the collisional regime, positrons change their momentum and lose their energy through collisions with gas particles while propagating along magnetic field lines in the ISM. Figure 31 shows the *stopping distances* $D = \int_0^E v(E')dE'/\dot{E}'$ [where $v(E)$ is positron's velocity and $\dot{E}'$ represents the sum of energy losses of Sec. V.A] in the various phases of the ISM. For MeV positrons, D is much larger than the typical size of HIM, WIM, and WNM phases, and comparable to the size of CMM phase (horizontal lines in Fig. 31)[28]. Therefore, in the collisional regime, only the CMM phase may be efficient in stopping MeV positrons.

In the case of a magnetized plasma, positrons are spiraling along the magnetic field lines. The gyroradius of a positron with Lorentz factor γ is $r_g \sim 1.7 \times 10^9\, B^{-1}_{\mu\rm G}(\gamma^2 - 1)^{1/2}$ cm, where the local mean magnetic field $B_{\mu\rm G}$ is expressed in μG. For typical values of the Galactic B field (1–10 μG, see Sec. III.D), r_g is many orders of magnitude smaller than λ_C in all ISM phases. In a magnetized, turbulent plasma, the most efficient of collisionless processes is scattering off magnetic fluctuations of size $r_B \simeq r_g$, which induce *resonant* pitch-angle scattering of positrons [see, e.g., Kulsrud (2005), and references therein], or *nonresonant* interactions with fluctuations on scales just above r_g [see, e.g., Ragot (2005) and Toptygin (1985)]. The transport of energetic ($>$ GeV) GCR is driven by such collisionless processes (see Sec. IV.B.2), but in the case of MeV positrons the situation

[28]For a complete description of the ISM gas phases, see Sec. III.B

is not clear, because there is no observational evidence on the level of intestellar turbulence at such small scales (although one may reasonably expect that it can be quite high in the vicinity of some positron sources, e.g., supernovae).

Because of the lack of observational evidence on the dominant regime of propagation of low-energy positrons, in this section we consider both regimes (see Secs. VI.A and VI.B, respectively). Some implications of this analysis for the spatial morphology of the Galactic 511 keV emission are presented in Sec. VI.C.

A. Transport by collisions

The propagation of positrons in different gas phases in the collisional regime is thoroughly studied in the recent work of Jean *et al.* (2009), with a Monte Carlo code describing e^+ "cooling" and annihilation.[29] The Monte Carlo simulation consists of calculating the trajectory of positrons (injected through a point source) along magnetic field lines, taking into account collisions that change their pitch angle and energy. Their initial velocity distribution is assumed to be isotropic, so the cosine of their initial pitch angle is distributed uniformly between -1 and 1. The initial kinetic energy of positrons is in the range 10 keV $< E <$ 10 MeV (appropriate for radioactivity emitted positrons). The simulation provided the spatial position of positrons at the end of their life. Analysis of a large number of test particles leads to the spatial distribution of the annihilation sites.

The simulations show that the spatial field-aligned distributions of positrons at the end of their life are nearly uniform out to the maximum distance traveled along the field lines (corresponding to initial zero pitch angle). This implies that the pitch angle does not change significantly during the slowing-down period. For a given density, the most significant effect on positron propagation is found to be due to the variation of the ionization fraction in the neutral gas (warm neutral, cold neutral, and molecular): As the ionization fraction increases, Coulomb scattering quickly becomes the dominant process of e^+ energy losses.

Figure 32 shows the spatial extents of the final (before annihilation) distribution of positrons along and perpendicular to the regular magnetic field, respectively, as a function of their initial kinetic energy, for each ISM phase. The extent along the regular magnetic field corresponds to approximately twice the maximum distance traveled by positrons and gives the size of the annihilation site (even though positrons originate from a point source). A "realistic" Galactic magnetic field was assumed, composed of an average magnetic uniform field B plus a random field of intensity $\delta B \simeq B$, due to the turbulent motions of the gas (see Sec. III.D). The effective distances traveled by positrons (i.e., in a straight line from their initial to final position) following the chaotic field lines are smaller than in the case of a simple, uniform magnetic field, but only by 25%. The reason for such a surprisingly small effect is that, because of the assumed injection scale of turbulence from supernovae (10–100 pc) and the adopted turbulence power spectrum (Fig. 11), the number of small-scale fluctuations interacting with positrons is quite small. For that reason, the distances calculated by Monte Carlo simulations for a realistic Galactic magnetic field in Fig. 32 are quite similar to the stopping distances D calculated semianalytically for a uniform average magnetic field in Fig. 31. In other words, the magnetic field rapidly orients the motion of randomly injected positrons along its direction and MeV positrons travel an effective distance $\sim S \sim 10n^{-1}$ kpc [where n (cm^{-3}) is the ISM density] from their origin before stopping by Coulomb collisions. As already stressed, these distances are larger than typical sizes of the warm ISM phases where Galactic positrons annihilate, according to the spectral analysis of 511 keV

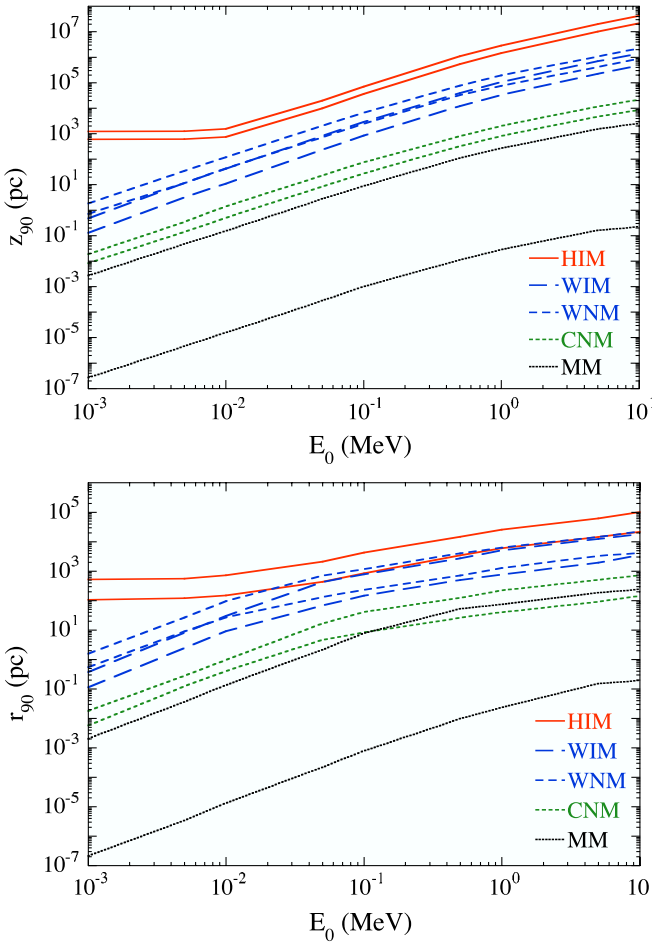

FIG. 32 (color online). Minimum and maximum extents of the spatial distributions of 1 MeV positrons slowing down to 100 eV, along (top panel) and perpendicular (bottom panel) to the regular Galactic magnetic field, taking into account the turbulent behavior of the field lines as well as realistic values for the density in each ISM phase. From Jean *et al.*, 2009.

[29]The process of e^+ cooling encompasses two distinctly different phases: slowing down and thermalization. During the slowing-down period, the e^+ kinetic energy is above the charge-exchange threshold and the particles cool through binary or Coulomb interactions. Once the e^+ kinetic energy is between the charge-exchange energy and the thermal energy of the gas, the particles enter into a thermalization phase where the elastic and/or Coulomb interactions dominate. The thermalization ends once the e^+ kinetic energy becomes close to the gas thermal energy and positrons annihilate. Jean *et al.* (2009) found that the slowing-down process is always the longer of the two.

emission (see Sec. V.E). This may imply either that the adopted model for turbulence is inadequate [for instance, turbulence can show anisotropic or intermittent behavior, instead of the isotropic turbulence cascade assumed by Jean *et al.* (2009)] or that positron transport (at least, in the warm phases) is dominated by collisionless processes. The latter issue is discussed in the next section.

B. Wave-particle interactions and collisionless transport

In the case of weak homogeneous turbulence, electromagnetic fluctuations over several orders of magnitude in wavelength, homogenously distributed in space, the wave-particle interactions and collisionless charged particle transport are rather well understood. Since the gyroradii of particles in interstellar magnetic fields are usually much smaller than the relevant spatial scales, one may use the so-called ''gyrophase averaged distribution'' of particles, which depends on four variables: time t, spatial coordinate s along the field lines, momentum p, and pitch angle μ. The evolution of the particle distribution $f(t, s, p, \mu)$ can be described by a Fokker-Planck equation (Melrose, 1980), while the injected spectrum of positrons and its spatial distribution depend on the nature of the e^+ source (see Sec. IV).

Positrons undergo pitch-angle scattering described by the angular diffusion coefficient $D_{\mu\mu}$ and stochastic acceleration by interaction with plasma turbulence, described by the momentum diffusion coefficient D_{pp}. In collisionless turbulent interstellar plasmas, the kinetic coefficients in the Fokker-Planck equation are dominated by resonant wave-positron interactions involving both *cyclotron* and *Cherenkov* resonances[30] (Melrose, 1980), and they can be evaluated in the ''quasilinear'' theory, valid in the weak turbulence regime.[31]

Magnetohydrodynamical (MHD) waves[32] are of prime interest for the transport of low-energy positrons. They can exist only at frequencies lower than the proton cyclotron frequency $\Omega_{\rm cp} = (qB/m_p c)$, where q is the elementary charge, and m_p is the proton mass. They are damped either by collisional effects (mainly viscous friction and ion-neutral collisions) at low frequencies or by the Landau damping[33] (due to thermal protons) at frequencies approaching $\Omega_{\rm cp}$. Higher-frequency waves are potentially important as well. However, whistler waves produced by electron-proton plasma instabilities, which are the most interesting waves in this frequency domain, are right-handed polarized; therefore, they cannot be in resonance with positrons, unless positron or proton flows generate their own waves. We shall restrict our analysis to MHD waves with frequency $\omega \ll \Omega_{\rm se}$, where $\Omega_{\rm se} = \Omega_{\rm ce}/\gamma$ and $\Omega_{\rm ce} = qB/m_e c$ are the synchrotron and the cyclotron frequencies of the positron, respectively.

Collisionless processes may result in efficient deceleration, or cooling, of fast positrons [see, e.g., Petrosian and Bykov (2008), and references therein]. The collisionless positron scattering due to particle-wave interaction is efficient in warm ionized phases of the ISM where the wave damping is not too strong [see, e.g., Kulsrud (2005)]. Moreover, *adiabatic deceleration* of positrons in jets or expanding shells (for example in SNRs) results in positron cooling, even without Coulomb collisions; this occurs if the positron mean free path, which is dominated by e^+ scattering by waves, is shorter than the typical scale of bulk plasma motion.[34] Hence, wave-particle interactions, both resonant and adiabatic nonresonant, could result in particle deceleration or reacceleration, depending strongly on the local conditions. Poor knowledge of those local conditions (concerning essentially the small-scale magnetic turbulence in the ISM) imposes a case by case study and precludes any generic conclusions to be drawn. Studies of wave-positron interactions have then to rely either on *in situ* measurements in the solar wind (see Sec. VI.B.1) or on theoretical modeling of the properties of the MHD turbulence (see Sec. VI.B.2).

1. Local e^+ transport in the ISM and reacceleration

In the solar wind, the only natural laboratory for direct study of the propagation effects, sub-MeV electrons and positrons resonantly interact with waves of high enough frequencies that contain only a small fraction of energy of the turbulent wave cascade [see, e.g., Ragot (2005)]. At 1 AU from the Sun,[35] the solar wind turbulence steepens at a cutoff scale $V_A/\Omega_{\rm ce} \sim 10^7$ cm, where the Alfvén velocity $V_A \sim 2.1 \times 10^5 B_{\mu\rm G}\, n^{-1/2}\,\mathrm{cm\,s^{-1}}$ and $n(\mathrm{cm^{-3}})$ is the local plasma density. This means that for pitch angles $\mu \leq V_A/v$ (where v is the positron velocity) sub-MeV particles can no longer gyroresonate with waves in the inertial range of the solar wind turbulence. However, if nonresonant magnetosonic (i.e. fast) waves of lower frequencies are present in the solar wind,

[30]The *electron cyclotron resonance* involves the gyromotion of electrons (or positrons) perpendicular to the magnetic field: The transverse electric field associated with the wave rotates at the same velocity and in the same direction with the particles, which absorb its energy and accelerate. The *Cherenkov resonance* involves particle motion along the magnetic field lines.

[31]To calculate the diffusion coefficients beyond the quasilinear approach (e.g., for particle transport and acceleration by strong turbulent fluctuations) the renormalization equations were developed by Bykov and Toptygin (1993) and Zank *et al.* (2004), assuming that the particle propagation regime is diffusive.

[32]Under MHD waves we mean shear Alfvén waves and fast magnetosonic waves. Because the phase velocity of the magnetosonic mode is almost always larger than the Alfvén velocity V_A, the magnetosonic wave is often called the ''fast'' hydromagnetic wave. The dynamics of the third MHD mode, the ''slow'' wave, has been shown to be entirely controlled by the Alfvén wave cascade by Lithwick and Goldreich (2001); the slow wave spectrum is basically the same as the Alfvén wave spectrum.

[33]Landau damping occurs due to the energy exchange between a wave with phase velocity v_P and particles with velocity $v \simeq v_P$, which can interact strongly with the wave. Particles with $v < v_P$ will be accelerated by the wave electric field, while those with $v > v_P$ will be decelerated, losing energy to the wave.

[34]The adiabatic deceleration of a positron diffusing in an expanding shell has a typical time scale $\tau_{\rm ad} \sim |\nabla \cdot \bar{\mathbf{U}}(\mathbf{r}, t)|^{-1}$, where $\bar{\mathbf{U}}(\mathbf{r}, t)$ is the bulk plasma velocity. The cooling time in expanding wind, shell, or jet [with $\nabla \cdot \bar{\mathbf{U}}(\mathbf{r}, t) > 0$] can be much shorter than the Coulomb stopping time in a rarefied plasma.

[35]One astronomical unit (AU) $= 1.5 \times 10^8$ km, the Earth-Sun distance.

they could dominate the propagation of sub-MeV particles [see, e.g., Ragot (2006) and Toptygin (1985)]. Depending on the level of nonresonant fast-mode wave turbulence and the injection distribution of electrons, this can induce diffusion in energy space, i.e., Fermi reacceleration of sub-MeV electrons in the inner heliosphere (Ragot, 2006). The conditions for efficient reacceleration can be estimated as follows:

If positron velocities are above the thermal electron velocities, the ratio of the energy diffusion rate D_{pp}/p^2 and the positron pitch-angle scattering rate $D_{\mu\mu}$ (both in s^{-1}) is

$$(D_{pp}/p^2)D_{\mu\mu}^{-1} \approx (V_A/v)^2 \ll 1 \tag{21}$$

[see, e.g., Petrosian and Bykov (2008), and references therein]. The reacceleration effect is non-negligible when the reacceleration time scale is shorter than the energy loss time scale (or the e^+ propagation time scale). Stated differently, the acceleration rate D_{pp}/p^2 must exceed the momentum loss rate $\dot{p}_L/p = [dE/dt]/(m_e v^2 \gamma)$, where, apart from fastly expanding regions, the energy loss rate of sub-MeV particles is dominated by Coulomb losses [Eq. (14)]. Therefore, for reacceleration to be important, the positron scattering rate by MHD waves $D_{\mu\mu}$ must satisfy the condition

$$D_{\mu\mu} > 0.02\beta^{-1}\gamma^{-1}\frac{n_e^2}{B_{\mu G}^2}\ (s^{-1}), \tag{22}$$

which corresponds to a particle mean free path $\lambda(= 1/3vD_{\mu\mu}^{-1})$ satisfying

$$\lambda < 0.1\beta^2\gamma\frac{B_{\mu G}^2}{n_e^2}\ (\text{AU}). \tag{23}$$

In the solar wind, the electron mean free path λ reaches a plateau at energies $\sim$1 MeV with λ about 0.01–1 AU (Ragot, 1999), depending on the parameters chosen for the interplanetary medium (IPM). This is comparable to typical values of λ estimated from observations of electrons propagating in the inner heliosphere (see Fig. 33). Interestingly, those observations show no dependence on electrons' rigidity (or momentum). This can be interpreted as an indication that

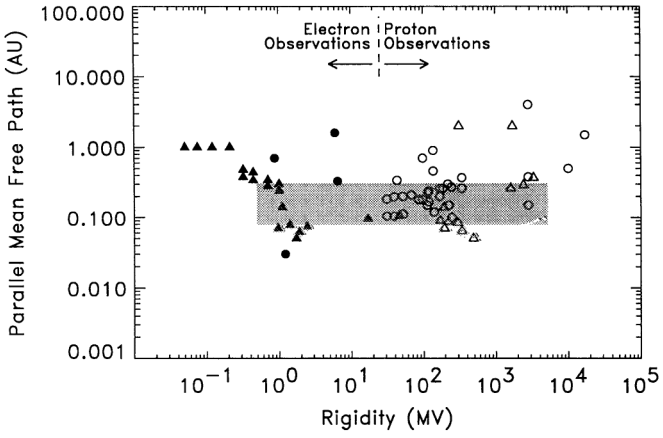

FIG. 33. Mean free path of energetic particles parallel to the magnetic field direction, as a function of particle rigidity in the interplanetary medium; circles and upward pointing triangles denote the measured values and upper limits, respectively. From Bieber *et al.*, 1994.

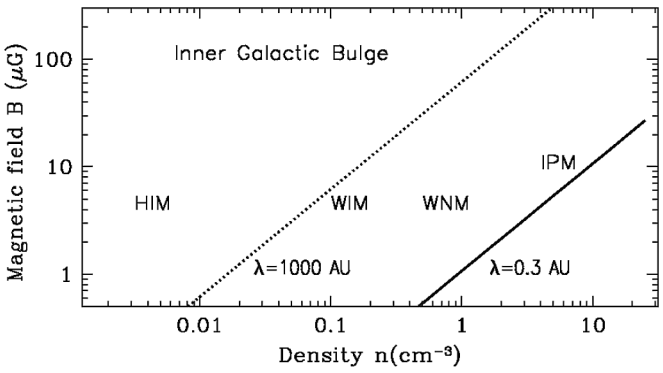

FIG. 34. Regions of the ISM in the B vs n (magnetic field vs number density) plane. Physical conditions for HIM, WIM, WNM, and the inner bulge are discussed in Sec. III, while IPM stands for the interplanetary medium. The two lines correspond to Eq. (23) for MeV positrons, with the particle mean free path $\lambda = 0.3$ AU (solid line, appropriate for the interplanetary medium from Fig. 33), and $\lambda = 1000$ AU (dotted line, provided for illustration purposes only, since its value is unknown in the ISM). In regions of the ISM found to the left of those lines, reacceleration effects may be important for positrons (provided there is a sufficient level of small-scale turbulence), as suggested from observations of the IPM.

reacceleration of low-energy particles is important in the case of the solar wind [for further discussion, see Dröge (2000) and Shalchi *et al.* (2006)].

In the ISM, Eq. (23) implies that the effect of reacceleration is expected to be important in the tenuous phases filled with strong MHD turbulence. Figure 34 shows the ISM parameter space (number densities versus mean magnetic fields) where MeV positrons may be affected by reacceleration, depending on their mean free path λ, which depends in its turn on the level of MHD turbulence. Reacceleration becomes progressively important in regions of low density and/or high magnetic field (such as those of the inner bulge), resulting in longer thermalization time scales for positrons and increasing the sizes of corresponding e^+ annihilation regions.

Unfortunately, our knowledge of the small-scale ISM turbulence is limited at present. While the quasilinear theory provides a simple analytical description of charged particle transport, recent test-particle simulations revealed some problems of this approach [see, e.g., Tautz *et al.* (2006)]. In particular, while nonlinear effects were shown to be essential for particle transport in MHD turbulence (Matthaeus *et al.*, 2003; Zank *et al.*, 2004; le Roux and Webb, 2007), test-particle simulations of the coefficient D_{pp} do not exist at present. Therefore, one has to rely on simulations of $D_{\mu\mu}$ and use that quantity in order to estimate D_{pp} from Eq. (21); in their turn, simulations of $D_{\mu\mu}$ require assumptions on the polarization and spectral properties of MHD waves.

The aforementioned uncertainties affect any attempt to evaluate the propagation of MeV positrons in the Galaxy without detailed information on the magnetic fluctuation spectra in the propagation region. In recent work, Higdon *et al.* (2009) adopted a particular model calculation of the charged particle mean free path in the interplanetary medium (in the quasilinear regime), which they extrapolated to the conditions of the ISM (see Sec. VI.C for details of their

model). However, in view of the different conditions, density, magnetic field, and unknown level of small-scale turbulence, in the bulge, such a calculation appears rather arbitrary (although not necessarily wrong). Their model can be considered as a quantitative illustration of a possible scenario, the plausibility of which remains to be shown.

Note that small-scale MHD waves can be injected into the ISM *in situ* by a variety of *kinetic instabilities.* A kinetic instability may be locally triggered, for instance, by the streaming (through the ISM) of cosmic rays with bulk velocity larger than a few times the local Alfvén speed (Wentzel, 1974). Such streaming instability is expected to develop in the intercloud medium and may provide particle reacceleration, compensating for the strong ionization losses inside molecular clouds. In other terms, low-energy cosmic rays scatter off their self-generated waves and are, therefore, pushed outside molecular clouds (Skilling and Strong, 1976). The waves thus generated can help to confine the positrons in the warm phases around the molecular clouds. To our knowledge the only work discussing the effect of penetration of leptons in a molecular cloud was due to Morfill (1982), but it was restricted to electrons and its ability to confine positrons within the ionized phases of the ISM is questionable (Jean *et al.*, 2009). Higdon *et al.* (2009) proposed an alternative mechanism in which positrons scatter off their own self-generated waves. It is possible that kinetic instabilities play a key role in the observed e^+ annihilation (mostly) in the warm phases of the ISM.

2. Global positron transport

The description of positron transport on a small scale $r_g < L < \lambda$ (where $\lambda \sim v D_{\mu\mu}^{-1}$ is the positron mean free path) requires the solution of the Fokker-Planck equation. On much larger spatial scales ($L > \lambda$) the pitch-angle distribution is nearly isotropic. This justifies the use of a simplified Fokker-Planck equation, in the so-called *diffusion approximation*; the corresponding equation is called the *diffusion-advection equation* (Bykov and Toptygin, 1993; Bykov, 2001). If the amplitude of velocity fluctuations is $u > v\lambda/L$, the particle transport is dominated by the turbulent advection.

It is important to note that only compressible large-scale turbulent motions provide efficient reacceleration (Bykov and Toptygin, 1993). In the regime dominated by turbulent advection (TA), the reacceleration rate can be approximated as $D_{\text{pp-TA}} \approx (u/9L)p^2$ (Bykov and Toptygin, 1993, 2001). The reacceleration effect is important if $D_{\text{pp-TA}}/p^2 > \dot{p}_L/p$, where the stopping rate due to Coulomb collisions $\dot{p}_L/p$ is discussed in Sec. VI.B.1. Therefore, particle reacceleration significantly affects the global positron propagation in the bulge if the amplitude of compressible turbulence u_{50} (measured in units of 50 km/s) and the energy containing scale L_{50} (measured in units of 50 pc) satisfy the condition[36]

$$u_{50}/L_{50} > 300\frac{n}{\beta^3\gamma}. \tag{24}$$

A word of caution is in order here. The reacceleration effect, in principle, could boost a substantial amount of mildly relativistic MeV positrons to ultrarelativistic energies. It might, therefore, lead to violation of the limit on γ-ray continuum emission from in-flight annihilation of positrons imposed by Beacom and Yüksel (2006), which was discussed in Sec. IV. In the GC vicinity and in the presence of a strong magnetic field, the severe synchrotron-Compton losses of relativistic positrons can make it impossible to accelerate them to energies above a few MeV by the Fermi-type mechanism. In the absence of synchrotron-Compton losses the differential spectral index of the Fermi reaccelerated positron momentum distribution $N(p) \propto p^{-a}$ can be approximated as $a = -1/2 + \sqrt{9/4 + 36(L/R)/2}$, where R is the minimal size of the confinement region (if anisotropic); in the bulge R is likely below 1 kpc and it is much less in the disk. Exact estimates of the positron spectra can be done only if one knows the energy (or momentum) dependence of the positron mean free path in the MeV regime, which is governed by yet uncertain small-scale magnetic fluctuations in the regions of interest.

The question of whether MHD cascades may extend over several orders of magnitude on spatial scales is still a matter of active debate. Electron density power spectra in the local ISM have been measured down to scales of 10^{10} cm [see, e.g., Armstrong *et al.* (1995)]. It was established that radio scattering in the interstellar plasma implies widespread inhomogeneities in density with a power-law spatial spectrum and suggests a turbulent origin. Observations suggest that the small-scale plasma turbulence is often highly anisotropic and clumpy (Shebalin *et al.*, 1983; Desai and Fey, 2001; Brisken *et al.*, 2010); its fluctuations are likely to concentrate in filamentary density structures aligned by the local magnetic field [see, e.g., Higdon (1984)]. Since the scattering becomes isotropic if the irregularities are uniformly distributed over many length scales of the magnetic field, Rickett and Coles (2004) concluded that the plasma turbulence is distributed intermittently.

To estimate the positron scattering effect from the electron density measurements one has to assume a relationship between the amplitudes of density and magnetic field fluctuations. Fluctuations due to magnetosonic waves could contribute to nonresonant scattering of MeV particles or, if they survive down to small scales, to resonant scattering. However, if the observed electron density fluctuations are simply due to entropy-type (''isobaric'') fluctuations, they are inefficient in e^+ scattering.

Depending on the ISM phase, the MHD waves can suffer from collisionless or collisional damping. Jean *et al.* (2009) concluded that in the neutral atomic and molecular phases of the ISM the Alfvén and fast magnetosonic wave cascades are both cut off by ion-neutral collisions, on scales considerably larger than the gyroradius of MeV positrons; therefore, MHD waves cannot resonantly interact with positrons. The situation is different in the ionized phases of the ISM, where the Alfvén wave cascade suffers insignificant (collisional) damping down to the thermal proton Coulomb mean free path.[37]

[36] In case of important energy losses, other than from Coulomb collisions, higher values of u_{50}/L_{50} than given in Eq. (24) are required.

[37] On smaller scales, the cascade enters the collisionless regime and is cut off by linear Landau damping around the proton inertial length c/ω_{pp} (where $\omega_{\text{pp}} = 4\pi n_H e^2/m_p$).

TABLE XII. Collionless and collisional transport processes in ISM phases (see Table IV). Y (N) means that the process can (cannot) take place. NR (R) stands for nonresonant (resonant) MHD motions at large scales. Streaming modes are generated through the streaming instability produced by the CRs propagating away from their sources. The streaming processes not yet studied in depth are indicated with question marks.

Transport processes	ISM phase CM	CN	WN	WI	HI
NR MHD modes: Large scale	N	N	N	Y	Y
R MHD modes Alfvén	N	N	N	Y	Y
R MHD modes fast MS	N	N	N	N (Y)	N (Y)
Streaming modes	Y?	Y?	Y?	Y	Y
Collisions	Y	Y	Y	Y	Y

This leaves some room for possible resonant interactions of the Alfvén wave cascade with positrons,[38] but the effect has not been properly investigated.

In summary, contrary to the case of the solar wind (where nonresonant compressible perturbations may control the positron mean free path), the cascade of MHD waves in the ISM (injected at scales $L_{\rm inj} \sim 10$–100 pc by supernovae) is expected to be damped at scales well above r_g. Small-scale MHD (and whistler) waves could be generated by anisotropic distributions of energetic particles, through streaming instabilities, but the waves could be damped by ion-neutral collisions as well (Higdon *et al.*, 2009); in any case, the effects have not been studied in detail up to now. Streaming instabilities could help to confine positrons at the border of the molecular clouds, thus enhancing the fraction of positrons that annihilate in warm phases. In ISM regions of low density (and/or high magnetic field) with even a moderate level of MHD turbulence (see Fig. 34), particle reacceleration could substantially suppress the positron stopping by Coulomb collisions (even in the absence of any other cooling effect, e.g., adiabatic losses), thus providing a possibility to largely extend the volume filled with annihilating positrons. Most of the current models rely on quasilinear wave treatment, but nonlinear effects could substantially change some estimates. Note that, in general, a quasihomogeneous distribution of the sources of turbulence is assumed, although the intermittency effects (due to, e.g., large-scale ISM shocks) can modify the analysis. In Table XII we list processes that are potentially important for positron propagation in the ISM [see also Jean *et al.* (2009)] and which require further investigation. Our current understanding of MeV positron propagation does not allow one to conclude whether such positrons undergo strong diffusion or essentially free propagation.

[38]Note that theoretical considerations show that the energy transfer in the Alfvén cascade proceeds mostly through the interaction of oppositely propagating wave packets. The distortion of the wave packets during the interaction produces anisotropic fluctuations elongated along the mean magnetic field (Lithwick and Goldreich, 2001). Using numerical simulation, the magnetosonic cascade has been found to keep its isotropy along the whole range of spatial scales (Yan and Lazarian, 2004). In the case of strong anisotropy of the cascade, the scattering efficiency of MeV positrons by small-scale Alfvén waves could be considerably reduced while the effect of magnetosonic waves could be enhanced.

C. Implications of e^+ propagation for 511 keV emission

The implications of low-energy positron transport for the Galactic 511 keV emission were raised by Prantzos (2006), who pointed out that the morphology of the 511 keV emission does not necessarily reflect the morphology of the underlying e^+ source distribution. He noticed that e^+ from SNIa are released in the hot and rarefied ionized medium, since the scale height of SNIa is considerably larger than the scale height of the disk of cool, dense, gas (see Fig. 10). The e^+ propagation distances are then quite large (Fig. 31), allowing e^+ from the disk to annihilate far away from their sources (perhaps in the halo, where a low surface brightness emission should be expected); this fact may considerably reduce the bulge-to-disk ratio of 511 keV emission of any class of astrophysical e^+ sources, thus alleviating the morphology problem discussed in Sec. IV.D. Models of cosmic-ray propagation in the Galaxy (such as those described in Sec. IV.B.2) usually adopt an isotropic diffusion coefficient. Gebauer and de Boer (2009) recently introduced an anisotropic diffusion coefficient in the GALPROP code to simulate the advection of cosmic rays by a Galactic wind. They found that, by adopting observationally derived wind velocities, their scheme naturally produces large escape fractions ($> 50\%$) of positrons from the disk.

Furthermore, Prantzos (2006) suggested that if the halo magnetic field of the Milky Way has a strong poloidal component, as suggested by several [see, e.g., Prouza and Šmída (2003), Han (2004), and Fig. 35, top panel], then some positrons escaping the disk may be channeled into the bulge and annihilate there, enhancing even more the bulge-to-disk e^+ annihilation ratio; he noticed that, in that case, positrons from SNIa may suffice to explain quantitatively both the total observed e^+ annihilation rate ($\sim 2 \times 10^{43} e^+$ s^{-1}) and the corresponding bulge-to-disk ratio, provided that the escaping e^+ fraction from SNIa is $\sim 4\%$. As discussed in Sec. III.D, it is rather unlikely, although it cannot yet be ruled out, that the poloidal component of the regular Galactic magnetic field is close to a dipole. Observations of external spirals suggest rather an X-shaped halo field (see, e.g., Fig. 35, bottom panel), in which case it would be difficult for disk positrons to find their way into the bulge. Still, the issue is of considerable interest and urgently calls for a better assessment of the poorly known global configuration of the Galactic magnetic field.

Higdon *et al.* (2009) suggested that positron propagation may be the key for understanding not only the spatial morphology of the 511 keV emission, but also its spectral properties. They made the bold assumption that radioactivity (from ^{26}Al, ^{44}Ti, and, mostly, ^{56}Co, see Sec. IV.A) is the sole e^+ source in the Galaxy. They considered (i) a fairly detailed description of the various phases of the ISM (Sec. III.B) and (ii) a particular phenomenological model of collisionless scattering of MeV positrons by turbulent fluctuations of the ISM that was used to describe energetic particle (electron or proton) propagation in the interplanetary medium. Depending on the nature of the medium, positrons are assumed to propagate either by diffusion along magnetic flux tubes (in ionized media, where turbulence cascades down to the gyroradius r_g) or by streaming with mean velocity $v = \beta c$ (in neutral media, where turbulence is quenched by ion-neutral collisions at scales $\gg r_g$).

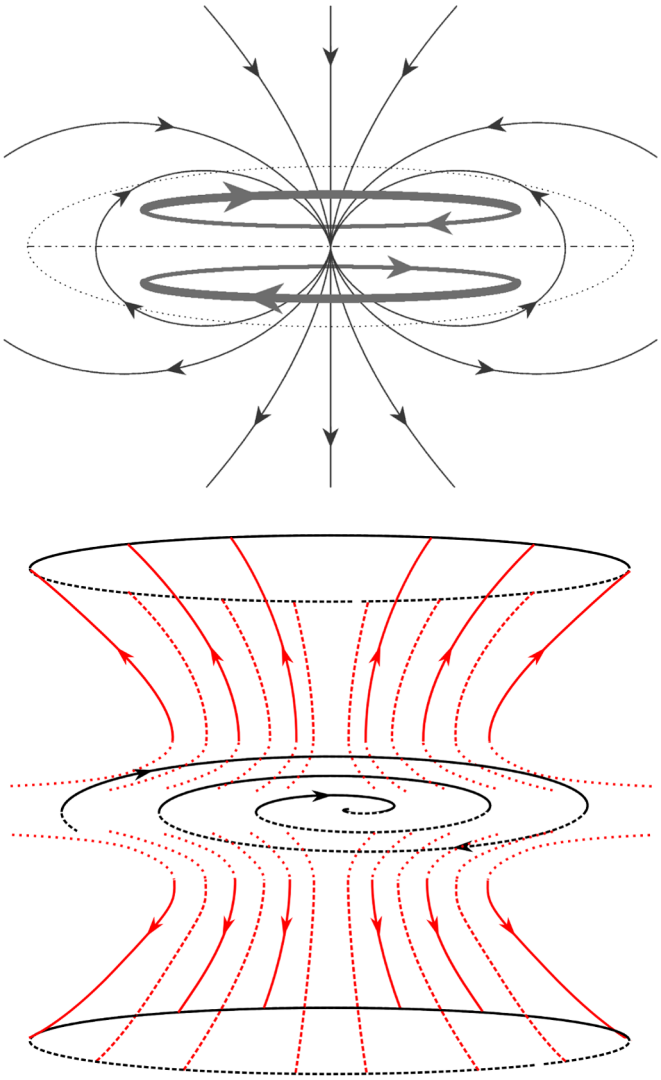

FIG. 35 (color online). Possible configurations of the large-scale magnetic field of the Milky Way. Top panel: As derived from Faraday polarization measurements of the MW, according to Han (2004). Bottom panel: Sketch of the observable components of the large-scale magnetic field of the disk galaxy NGC253 (which shows, however, signs of starburst activity, unlike the Milky Way); the halo magnetic field is even and pointing outward, whereas the dotted parts are not observed. From Heesen *et al.*, 2009.

Putting together the aforementioned ingredients, Higdon *et al.* (2009) proceeded in an impressive calculation of positron production rates from radioactivity along the Galaxy, typical distances of e^+ propagation in the corresponding ISM phases and probabilities that positrons will finally annihilate in one or another of those phases. In the end, they found excellent agreement with each and every observable of the 511 keV emission available so far (see Sec. II.D): spatial morphology, i.e., bulge-to-disk annihilation ratio, spectral futures (including a narrow and a broad 511 keV line), and even the claimed asymmetry between fluxes from negative and positive longitudes; they explain the latter as due to the corresponding overall asymmetry of the spiral-arm pattern of the Milky Way disk, as viewed from the Sun.

The work of Higdon *et al.* (2009) constituted the first study of Galactic e^+ production, propagation, and annihilation in a global framework, trying to include all (or most of) the various aspects of this complex topic and to account for all the available observational data. However, its extremely precise "predictions" for the various properties of the 511 keV emission (which fit extremely well, to better than 10%, each and every observable), concealed the various uncertainties of the problem. For instance, it is assumed that most Galactic positrons result from ^{56}Co produced in SNIa: but, as discussed in Sec. IV.A.4, recent observations suggest that the e^+ escape fraction from such objects is very small, at least at late times. Only an early e^+ escape (due, perhaps, to 3D effects, not yet theoretically treated and unobservable at present) could make SNIa plausible e^+ sources again. And even if that were the case, the poorly known SFR of the bulge does not allow one to estimate the SNIa rate of that region to better than a factor of 2 (see Table V). The same criticism applies to their treatment of e^+ propagation. Their prescription for deriving the e^+ mean free path is, strictly speaking, valid in the framework of interplanetary plasma, while the properties of the ISM and magnetic fields in the inner Galactic regions are too poorly understood to allow for any strong conclusions on the nature of turbulence there. For instance, reacceleration, which extends the e^+ annihilation zone, is expected to be particularly efficient in the ionized, low-density, medium of the bulge (see Sec. VI.B.1). As for the claim that the observed spatial asymmetry of the 511 keV emission is simply due to the corresponding asymmetry of the spiral arms as viewed by the Sun, it is apparently in contradiction with the fact that no such strong asymmetry is observed in the 1.8 MeV emission of ^{26}Al (a product of massive stars), which should be a direct tracer of spiral arms, since ^{26}Al nuclei travel much slower than positrons.

One of the most interesting results of the work of Higdon *et al.* (2009) is, perhaps, their prediction of a spatial differentiation between the broad and narrow 511 keV line components, revealed by the spectral analysis of SPI data (see Sec. II.C). The former should occur in the "middle bulge" (the region of radius $0.5 < r < 1.5$ kpc, according to the authors' terminology), through in-flight positronium formation, while the latter occurs in the "inner bulge" ($r <$ 0.5 kpc) through positronium formation at thermal energies. An analogous spatial differentiation is predicted to exist between the bulge and disk 511 keV line components. It is unlikely that such predictions will be checked with INTEGRAL/SPI observations, but they certainly hold important clues to positron propagation issues.

In a companion paper, Lingenfelter *et al.* (2009) argued that, since the Higdon *et al.* (2009) model (with propagation of radioactively produced positrons from SNIa) can fully account for the observations, dark matter should be excluded as a major positron source. However, such a conclusion is premature, since it is not yet clear whether positrons from SNIa escape at all. It is true that, since the confirmation of the disk 511 keV emission, DM has lost a lot of its "appeal" as a positron source, but it cannot yet be excluded as such, at least for the bulge: Indeed, in that case e^+ propagation merely smears out the spatial profile of the 511 keV emission, and even decaying DM cannot be

excluded then (contrary to the arguments of Sec. IV.D, which neglect positron propagation).

VII. SUMMARY AND PERSPECTIVES

The Galactic 511 keV emission from e^+ annihilation is the first γ-ray line detected from outside the Solar System. Its unambiguous identification came soon after its detection, with high-resolution Ge detectors aboard balloon experiments. However, its spatial morphology remained elusive for almost three decades after its first detection. Only long running experiments aboard satellites could tackle this issue, in view of the importance of the treatment of the background at those energies (mostly created inside the detectors by cosmic-ray interactions). Observations in the 1990s by OSSE/CGRO offered the first hints for an abnormally high bulge-to-disk ratio (compared to the situation at any other wavelength). That property was firmly established only after observations in the 2000s with SPI/INTEGRAL, which further detected for the fist time an unambiguous disk emission. The latter appears to be asymmetric, according to Weidenspointner *et al.* (2008a), with emission from negative longitudes being 80% brighter than from positive ones; however, that claim is not supported by a different analysis (Bouchet *et al.*, 2008, 2010) and has yet to be confirmed.

According to the latest imaging analysis of SPI data (Weidenspointner *et al.*, 2008a), the total Galactic e^+ annihilation rate is at least $\dot{N}_{e^+} \sim 2 \times 10^{43}$ s^{-1}, with a luminosity bulge-to-disk ratio $B/D = 1.4$. This model (see Table I) is further refined by considering a narrow (FWHM = 3°) and a broad (FWHM = 11°) bulge, the former contributing to ~35% of the total bulge emission. However, the data analysis also allows for other morphologies, involving extended regions of low surface brightness but high total emissivity, e.g., a halo of total $\dot{N}_{e^+} \sim 3 \times 10^{43}$ s^{-1} and a thin disk of $\dot{N}_{e^+} \sim 5 \times 10^{42}$ s^{-1}, leading to a high $B/D \sim 6$ (see Table I). Obviously, the poorly known configuration of the Galactic 511 keV emission precludes at present the formulation of definitive statements about the origin of annihilating positrons.

Information on the origin of those positrons is also obtained via the spectral analysis of the 511 keV emission: The observed flux at ~MeV energies from the inner Galaxy constrains the initial energy of the positrons to less than a few MeV (otherwise the emission from in-flight annihilation would exceed the observed flux). Moreover, the spectral analysis provides important information on the physical properties of the e^+ annihilation sites. The large positronium fraction $f_{Ps} \sim 94\%$–97% implies that positrons annihilate mostly at low energies, since direct annihilation cross sections are important only at high energies (see Sec. V.D). The overall spectral shape suggests that annihilation occurs mostly in warm ($T \sim 8000$ K) media, at about equal amounts in neutral and ionized phases but it cannot be excluded that less than 23% of annihilation occurs in the cold neutral medium ($T \sim 80$ K; see Sec. V.E). Annihilation in the neutral media may account for the presence of a broad 511 keV line component (FWHM ~ 5 keV) and the annihilation in the warm ionized medium for the narrow one (FWHM ~ 1 keV).

Among the various astrophysical sources of positrons proposed so far, the only one known with certainty to release e^+ in the ISM is β^+ radioactivity of ^{26}Al; the observed intensity of its characteristic 1.8 MeV emission in the Galaxy corresponds to ~(3–4) $\times 10^{42} e^+$ s^{-1} (see Sec. II.C.2). A similar amount is expected from the decay of ^{44}Ti, on the grounds of nucleosynthesis arguments (see Sec. IV.A.2). Both radionuclides are produced mostly in massive stars and their positrons should be released along the Galactic plane, as traced by the 1.8 MeV emission; they could thus account for the observed disk 511 keV emission.

Radioactivity of ^{56}Co from SNIa was traditionally considered to be the major e^+ producer in the Galaxy. Both the typical ^{56}Ni yield of a SNIa and the Galactic SNIa rate are rather well constrained, resulting in $5 \times 10^{44} e^+$ s^{-1} produced inside SNIa. If only $f_{esc} \sim 4\%$ of them escape the supernova to annihilate in the ISM, the observed total e^+ annihilation rate can be readily explained. However, observations of two SNIa, interpreted in the framework of 1D (stratified) models, suggest that the positron escape fraction is negligible at late times. On the other hand, both observations of early spectra and 3D models of SNIa suggest that a sizable fraction of ^{56}Ni is found at high velocity (close to the surface), perhaps making the escape of ^{56}Co positrons easier (see Sec. IV.A.4). In our opinion, SNIa remain a serious candidate, with a potential Galactic yield of $2 \times 10^{43} e^+$ s^{-1}. But the expected spatial distribution of SNIa in the Galaxy corresponds to a much smaller B/D ratio than that of the observed 511 keV profile.

Most of the other astrophysical candidates can be constrained to be only minor e^+ sources, on the basis of either weak e^+ yields (novae, Galactic cosmic rays), high e^+ energy (compact objects, such as pulsars or magnetars), spatial morphology of sources (hypernovae, γ-ray bursts), or a combination of those features (e.g., cosmic rays), as discussed in Sec. IV.D. Only two astrophysical candidates remain as potentially important contributors: LMXRBs (or the microquasar variant of that class of sources, Sec. IV.B.3) and the supermassive black hole at the Galactic center (see Sec. IV.B.4). It should be stressed that there is no evidence that either of those sources produces positrons and the e^+ yields evaluated by various authors are close to upper limits rather than typical values (see Sec. IV.D.1). Furthermore, because of the current low activity of the central MBH (much lower than that of LMXRBs), it has to be assumed that the source was much more active in the past, thus dropping the assumption of "steady state" between e^+ production and annihilation, which is likely in all other cases.

The observed spatial distribution of LMXRBs is similar to the theoretically derived one for SNIa (see Sec. IV.D.3), as expected, since both classes of sources have old and young stellar components; however, none of them has the large B/D ratio of the observed 511 keV emission. The only hint that LMXRBs may contribute to, at least, the disk 511 keV emission stems from the asymmetric distribution of the hard LMXRBs in the third IBIS catalog, of similar magnitude to the detected 511 keV emission. However, the former asymmetry is not confirmed (the fourth IBIS catalog shows no strong evidence for such an asymmetry) and even if the 511 keV asymmetry is confirmed by future analysis, there is

considerable debate on whether such a similarity has a causal origin or is just fortuitous (see Sec. IV.D.3).

Dark matter has been proposed as an alternative e^+ source, at least for the bulge 511 keV emission; in principle, it could complement disk emission originating from radioactivity of ^{26}Al and ^{44}Ti or ^{56}Co. Observations of the MeV continuum from the inner Galaxy constrain the large phase space of DM properties. The mass of annihilating or decaying DM particles should be smaller than a few MeV, otherwise their in-flight annihilation would overproduce the MeV continuum (see Secs. II.C.1 and IV.B.1). Scalar light DM particles with fermionic interactions still appear as possible candidates; alternatively, the collisional deexcitation of heavy (100 GeV) DM particles could provide the required positrons, provided the energy separation between their excited levels is in the MeV range (see Sec. IV.C). On the other hand, the observed spatial profile of the 511 keV emission constrains the production mode of DM positrons, if it is assumed that they annihilate close to their production region: only cuspy profiles are allowed in the case of annihilating or deexciting DM particles (for which $\rho_\gamma \propto \rho_{\rm DM}^2$), while decaying DM particles (for which $\rho_\gamma \propto \rho_{\rm DM}$) are excluded (see Sec. IV.D.3). The problem is that observations of external galaxies suggest rather flat, not cuspy, DM profiles (see Sec. III.E).

Positrons produced in the hot, tenuous plasma filling the bulge (either from SNIa, LMXRBs, or DM) have to travel long distances before slowing down and annihilating. This is corroborated by the spectral analysis, which suggests that positrons annihilate in warm gas: such gas is filling mostly the inner bulge. Positron propagation thus appears unavoidable, undermining the assumption that the e^+ production and annihilation profiles are correlated, at least in the bulge. A similar situation should hold for positrons produced away from the plane of the disk (i.e., from SNIa or LMXRBs), which is also dominated by hot, tenuous gas. The situation is less clear for positrons produced by massive star radioactivity, in the plane of the disk and inside spiral arms: Although some of them may fill hot bubbles and cavities created by the SN explosions and ultimately escape from the disk, another fraction may annihilate in close-by dense molecular clouds. Propagation of MeV positrons in the ISM may then hold the key to understanding the 511 keV emission. It depends on the physical properties of the ISM (density, ionization, Sec. V), but also on the properties of turbulence and magnetic field configuration (see Sec. VI). Preliminary attempts to evaluate the extent of positron propagation (see Sec. VI.A) and their implications for the Galactic 511 keV emission (see Sec. VI.C) are promising in that respect, but the situation is far from clear at present: The entanglement between the various uncertainties (concerning e^+ sources, e^+ propagation, and annihilation sites) does not allow any strong conclusions to be drawn.

Almost 40 years after its discovery, the origin of the first extrasolar γ-ray line remains unknown. Progress in the field requires advances in several directions:

(i) Observations of 511 keV emission: What is the true spatial distribution of the emission? How far do the spheroid and disk extend? Are there yet undetected regions of low surface brightness? Is the disk emission asymmetric indeed? How do the 1.8 MeV and 511 keV disk emissions compare to each other? A much deeper exposure of the Galaxy and a better understanding of the backgrounds will be required to tackle those issues. Even if INTEGRAL's mission is extended to 2014, it may not provide the answers; unfortunately, no other mission of similar scope is on the horizon.

(ii) Physics of e^+ sources: What is the escaping fraction of e^+ in SNIa? What is the SNIa rate in the inner (star forming) and in the outer (inactive) bulge? What are the e^+ yields, activity time scales, and spatial distribution in the inner bulge of LMXRBs or microquasars? How can the past level of activity of the central supermassive black hole be reliably inferred?

(iii) Positron propagation: What is the large-scale configuration of the Galactic magnetic field? What are the properties of interstellar plasma turbulence and how do they affect the positron transport? What are the dominant propagation modes of positrons and what is the role of reacceleration?

The many facets of the Galactic 511 keV emission make this problem one of the most intriguing problems in high-energy astrophysics today and for many years to come.

ACKNOWLEDGMENTS

This work was largely performed in the framework of the ISSI (International Space Science Institute at Bern) program for International Team work (ID No. 110). We are grateful to ISSI for generous support and for the hospitality of its staff. I. V. M. acknowledges support from NASA Grant No. NNX09AC15G. A. M. B. was supported by RBRF Grant No. 11-02-12082 and the RAS Presidium Programm. He also acknowledges the Joint Supercomputing Centre (JSCC RAS), the Supercomputing Centre at Ioffe Institute, and the program "Particle Acceleration in Astrophysical Plasmas" at KITP. We are grateful to Martin Pohl and Peter Kalberla, who kindly provided us with their data files, and to P. Sizun, R. Murphy, and V. Heesen for providing updated figures. We thank V. Dogiel and the other two (anonymous) referees for their careful reading of the manuscript and their constructive reports.

REFERENCES

Abbiendi, G., *et al.* (OPAL Collaboration), 1999, Eur. Phys. J. C **6**, 01.
Abbott, L. F., and P. Sikivie, 1983, Phys. Lett. **120B**, 133.
Abdo, A. A., *et al.* (The Fermi LAT Collaboration), 2009, Phys. Rev. Lett. **102**, 181101.
Adriani, O., *et al.*, 2009, Nature (London) **458**, 607.
Agaronyan, F. A., and A. M. Atoyan, 1981, Sov. Astron. Lett. **7**, 395.
Aharonian, F., *et al.*, 2009, Astron. Astrophys. **508**, 561.
Aharonian, F., *et al.*, 2006, Astrophys. J. **636**, 777.
Aharonian, F., *et al.*, 2004, Astron. Astrophys. **425**, L13.
Aharonian, F., *et al.*, 2006, Astron. Astrophys. **449**, 223.
Aharonian, F. A., and A. M. Atoyan, 2000, Astron. Astrophys. **362**, 937.
Albernhe, F., J. F. Leborgne, G. Vedrenne, D. Boclet, P. Durouchoux, and J. M. da Costa, 1981, Astron. Astrophys. **94**, 214.
Alvarez-Muñiz, J., R. Engel, and T. Stanev, 2002, Astrophys. J. **572**, 185.

Anantharamaiah, K. R., A. Pedlar, R. D. Ekers, and W. M. Goss, 1991, Mon. Not. R. Astron. Soc. **249**, 262.
Anderson, C. D., 1932, Science **76**, 238.
Angle, J., *et al.*, 2008, Phys. Rev. Lett. **100**, 021303.
Arkani-Hamed, N., and N. Weiner, 2008, J. High Energy Phys., 104.
Armour, E. A. G., D. J. Baker, and M. Plummer, 1990, J. Phys. B **23**, 3057.
Armstrong, J. W., B. J. Rickett, and S. R. Spangler, 1995, Astrophys. J. **443**, 209.
Arnett, W. D., 1977, NASA Conference Publication Vol. 2, p. 257.
Arnett, W. D., 1982, Astrophys. J. **253**, 785.
Arnett, W. D., J. N. Bahcall, R. P. Kirshner, and S. E. Woosley, 1989, Annu. Rev. Astron. Astrophys. **27**, 629.
Arvanitaki, A., S. Dimopoulos, S. Dubovsky, P. W. Graham, R. Harnik, and S. Rajendran, 2009, Phys. Rev. D **80**, 055011.
Ascasibar, Y., P. Jean, C. Boehm, and J. Knoedlseder, 2006, Mon. Not. R. Astron. Soc. **368**, 1695.
Atwood, W. B., *et al.*, 2009, Astrophys. J. **697**, 1071.
Bambi, C., A. D. Dolgov, and A. A. Petrov, 2008, Phys. Lett. B **670**, 174.
Bandyopadhyay, R. M., J. Silk, J. E. Taylor, and T. J. Maccarone, 2009, Mon. Not. R. Astron. Soc. **392**, 1115.
Baring, M., 1987, Mon. Not. R. Astron. Soc. **228**, 695.
Bartelmann, M., 2010, Rev. Mod. Phys. **82**, 331.
Baudis, L., 2007, arXiv:0711.3788.
Beacom, J. F., and H. Yüksel, 2006, Phys. Rev. Lett. **97**, 071102.
Beck, R., 2001, Space Sci. Rev. **99**, 243.
Beck, R., 2008, AIP Conf. Proc.**1085**, 83.
Bell, E. F., *et al.*, 2008, Astrophys. J. **680**, 295.
Beloborodov, A. M., 1999, Mon. Not. R. Astron. Soc. **305**, 181.
Berezinskii, V. S., S. V. Bulanov, V. A. Dogiel, V. L. Ginzburg, and V. S. Ptuskin, 1990, *Astrophysics of Cosmic Rays* (North-Holland, Amsterdam, 1990).
Bernabei, R., *et al.*, 2003, arXiv:astro-ph/0311046.
Bertone, G., 2007, arXiv:0710.5603.
Bertone, G., D. Hooper, and J. Silk, 2004, Phys. Rep. **405**, 279.
Bertone, G., A. Kusenko, S. Palomares-Ruiz, S. Pascoli, and D. Semikoz, 2006, Phys. Lett. B **636**, 20.
Beuermann, K., G. Kanbach, and E. M. Berkhuijsen, 1985, Astron. Astrophys. **153**, 17.
Bhatia, A. K., R. J. Drachman, and A. Temkin, 1977, Phys. Rev. A **16**, 1719.
Bieber, J. W., W. H. Matthaeus, C. W. Smith, W. Wanner, M.-B. Kallenrode, and G. Wibberenz, 1994, Astrophys. J. **420**, 294.
Bienaymé, O., C. Soubiran, T. V. Mishenina, V. V. Kovtyukh, and A. Siebert, 2006, Astron. Astrophys. **446**, 933.
Binney, J. J., and N. W. Evans, 2001, Mon. Not. R. Astron. Soc. **327**, L27.
Bird, A. J., *et al.*, 2010, Astrophys. J. Suppl. Ser. **186**, 1.
Bird, A. J., *et al.*, 2007, Astrophys. J. Suppl. Ser. **170**, 175.
Blackett, P. M. S., and G. P. S. Occhialini, 1933, Proc. R. Soc. A **139**, 699.
Blandford, R., and D. Eichler, 1987, Phys. Rep. **154**, 1.
Blasi, P., 2009, Phys. Rev. Lett. **103**, 051104.
Blattnig, S. R., S. R. Swaminathan, A. T. Kruger, M. Ngom, and J. W. Norbury, 2000, Phys. Rev. D **62**, 094030.
Blinnikov, S. I., F. K. Röpke, E. I. Sorokina, M. Gieseler, M. Reinecke, C. Travaglio, W. Hillebrandt, and M. Stritzinger, 2006, Astron. Astrophys. **453**, 229.
Blumenthal, G. R., S. M. Faber, R. Flores, and J. R. Primack, 1986, Astrophys. J. **301**, 27.
Blumenthal, G. R., and R. J. Gould, 1970, Rev. Mod. Phys. **42**, 237.
Boehm, C., 2008, in *Reviews in Modern Astronomy*, edited by S. Röser, Cosmic Matter No. 20 (Wiley, New York), p. 107 .
Boehm, C., and Y. Ascasibar, 2004, Phys. Rev. D **70**, 115013.
Boehm, C., T. A. Ensslin, and J. Silk, 2004, J. Phys. G **30**, 279.
Boehm, C., and P. Fayet, 2004, Nucl. Phys. **B683**, 219.
Boehm, C., P. Fayet, and R. Schaeffer, 2001, Phys. Lett. B **518**, 8.
Boehm, C., D. Hooper, J. Silk, M. Casse, and J. Paul, 2004, Phys. Rev. Lett. **92**, 101301.
Boehm, C., and R. Schaeffer, 2005, Astron. Astrophys. **438**, 419.
Boehm, C., and J. Silk, 2008, Phys. Lett. B **661**, 287.
Book, D. L., and A. W. Ali, 1975, A Collection of Plasma Physics Formulas and Data, Technical Report.
Bouchet, L., E. Jourdain, J.-P. Roques, A. Strong, R. Diehl, F. Lebrun, and R. Terrier, 2008, Astrophys. J. **679**, 1315.
Bouchet, L., *et al.*, 1991, Astrophys. J. **383**, L45.
Bouchet, L., J. P. Roques, and E. Jourdain, 2010, Astrophys. J. **720**, 1772.
Boulanger, F., A. Abergel, J.-P. Bernard, W. B. Burton, F.-X. Desert, D. Hartmann, G. Lagache, and J.-L. Puget, 1996, Astron. Astrophys. **312**, 256.
Boulanger, F., P. Cox, and A. P. Jones, 2000, in *Infrared Space Astronomy, Today and Tomorrow*, edited by F. Casoli, J. Lequeux, and F. David (EDP Science, Les Ulis, Paris), p. 251.
Boulanger, F., and M. Perault, 1988, Astrophys. J. **330**, 964.
Bravo, E., and D. García-Senz, 2006, Astrophys. J. **642**, L157.
Breit, G., and J. A. Wheeler, 1934, Phys. Rev. **46**, 1087.
Briggs, M. S., D. E. Gruber, J. L. Matteson, and L. E. Peterson, 1995, Astrophys. J. **442**, 638.
Brisken, W. F., J. Macquart, J. J. Gao, B. J. Rickett, W. A. Coles, A. T. Deller, S. J. Tingay, and C. J. West, 2010, Astrophys. J. **708**, 232.
Bronfman, L., R. S. Cohen, H. Alvarez, J. May, and P. Thaddeus, 1988, Astrophys. J. **324**, 248.
Brown, B. L., and M. Leventhal, 1986, Phys. Rev. Lett. **57**, 1651.
Brown, B. L., M. Leventhal, A. P. Mills, Jr., and D. W. Gidley, 1984, Phys. Rev. Lett. **53**, 2347.
Brown, J. C., M. Haverkorn, B. M. Gaensler, A. R. Taylor, N. S. Bizunok, N. M. McClure-Griffiths, J. M. Dickey, and A. J. Green, 2007, Astrophys. J. **663**, 258.
Burton, W. B., and H. S. Liszt, 1992, Astron. Astrophys. Suppl. Ser. **95**, 9.
Bussard, R. W., R. Ramaty, and R. J. Drachman, 1979, Astrophys. J. **228**, 928.
Bykov, A. M., 2001, Space Sci. Rev. **99**, 317.
Bykov, A. M., and I. N. Toptygin, 1993, Phys. Usp. **36**, 1020.
Bykov, A. M., and I. N. Toptygin, 2001, Astron. Lett. **27**, 625.
Canter, K. F., A. P. Mills, Jr., and S. Berko, 1975, Phys. Rev. Lett. **34**, 177.
Case, G. L., and D. Bhattacharya, 1998, Astrophys. J. **504**, 761.
Cassé, M., B. Cordier, J. Paul, and S. Schanne, 2004, Astrophys. J. **602**, L17.
Chan, K.-W., and R. E. Lingenfelter, 1993, Astrophys. J. **405**, 614.
Chang, J., *et al.*, 2008, Nature (London) **456**, 362.
Chapuis, C. G. L., P. Wallyn, and P. Durouchoux, 1994, Astrophys. J. Suppl. Ser. **92**, 545.
Chen, F., J. M. Cline, A. Fradette, A. R. Frey, and C. Rabideau, 2009, arXiv:0911.2222.
Chen, F., J. M. Cline, and A. R. Frey, 2009, Phys. Rev. D **79**, 063530.
Cheng, K. S., D. O. Chernyshov, and V. A. Dogiel, 2006, Astrophys. J. **645**, 1138.
Cheng, K. S., D. O. Chernyshov, and V. A. Dogiel, 2007, Astron. Astrophys. **473**, 351.
Cheng, K. S., C. Ho, and M. Ruderman, 1986, Astrophys. J. **300**, 500.
Cheng, L. X., M. Leventhal, and D. M. Smith, 1997, Astrophys. J. **481**, L43.

Cheng, L. X., M. Leventhal, and D. M. Smith, 1998, Astrophys. J. **503**, 809.

Chernyshov, D. O., K. Cheng, V. A. Dogiel, C. Ko, and W. Ip, 2010, Mon. Not. R. Astron. Soc. **403**, 817.

Chupp, E. L., D. J. Forrest, and A. N. Suri, 1975, in *Solar Gamma-, X-, and EUV Radiation*, edited by S. R. Kane, IAU Symposium Vol. 68 (D. Reidel Publishing Co., Dordrecht), p. 341.

Churazov, E., R. Sunyaev, S. Sazonov, M. Revnivtsev, and D. Varshalovich, 2005, Mon. Not. R. Astron. Soc. **357**, 1377.

Chuss, D. T., J. A. Davidson, J. L. Dotson, C. D. Dowell, R. H. Hildebrand, G. Novak, and J. E. Vaillancourt, 2003, Astrophys. J. **599**, 1116.

Clayton, D. D., 1973, Nature (London) **244**, 137.

Clayton, D. D., 1984, Astrophys. J. **280**, 144.

Cline, J. M., A. R. Frey, and F. Chen, 2010, arXiv:1008.1784.

Combes, F., 1991, Annu. Rev. Astron. Astrophys. **29**, 195.

Conlon, J. P., and F. Quevedo, 2007, J. Cosmol. Astropart. Phys., 019.

Corbel, S., M. A. Nowak, R. P. Fender, A. K. Tzioumis, and S. Markoff, 2003, Astron. Astrophys. **400**, 1007.

Cordes, J. M., and T. J. W. Lazio, 2002, Astrophysics arXiv:astro-ph/0207156.

Cordier, B., D. Attié, M. Cassé, J. Paul, S. Schanne, P. Sizun, P. Jean, J.-P. Roques, and G. Vedrenne, 2004, in *Proceedings of the 5th INTEGRAL Workshop on the INTEGRAL Universe*, edited by V. Schoenfelder, G. Lichti, and C. Winkler, ESA Special Publication (ESA, The Netherlands), Vol. 552, p. 581.

Craig, N. J., and S. Raby, 2009, arXiv:0908.1842.

Crannell, C. J., G. Joyce, R. Ramaty, and C. Werntz, 1976, Astrophys. J. **210**, 582.

Crocker, R. M., D. I. Jones, F. Melia, J. Ott, and R. J. Protheroe, 2010, Nature (London) **463**, 65.

Crutcher, R. M., 1999, Astrophys. J. **520**, 706.

Crutcher, R. M., 2007, EAS Publications Series **23**, 37.

Crutcher, R. M., D. A. Roberts, D. M. Mehringer, and T. H. Troland, 1996, Astrophys. J. **462**, L79.

Cumberbatch, D. T., J. Silk, and G. D. Starkman, 2008, Phys. Rev. D **77**, 063522.

Dame, T. M., 1993, in *Back to the Galaxy*, edited by S. S. Holt and F. Verter, AIP Conf. Proc. No. 278 (AIP, New York), p. 267.

Darnley, M. J., *et al.*, 2006, Mon. Not. R. Astron. Soc. **369**, 257.

Daugherty, J. K., and A. K. Harding, 1983, Astrophys. J. **273**, 761.

de Jager, O. C., and A. Djannati-Ataï, 2008, arXiv:0803.0116.

della Valle, M., and M. Livio, 1998, Astrophys. J. **506**, 818.

Dermer, C. D., 1985, Astrophys. J. **295**, 28.

Dermer, C. D., and E. P. Liang, 1989, Astrophys. J. **339**, 512.

Desai, K. M., and A. L. Fey, 2001, Astrophys. J. Suppl. Ser. **133**, 395.

de Shong, J. A., R. H. Hildebrand, and P. Meyer, 1964, Phys. Rev. Lett. **12**, 3.

Deutsch, M., 1951, Phys. Rev. **82**, 455.

Dickey, J. M., and F. J. Lockman, 1990, Annu. Rev. Astron. Astrophys. **28**, 215.

Diehl, R., *et al.*, 1995, Astron. Astrophys. **298**, 445.

Diehl, R., *et al.*, 2006, Nature (London) **439**, 45.

Diehl, R., and M. Leising, 2009, Proc. Sci., INT008.

Dirac, P., 2008, Proc. Cambridge Philos. Soc. **26**, 361.

Dirac, P. A. M., 1931, Proc. R. Soc. A **133**, 60.

Dröge, W., 2000, Astrophys. J. **537**, 1073.

Dunn, R. J. H., A. C. Fabian, and A. Celotti, 2006, Mon. Not. R. Astron. Soc. **372**, 1741.

Dunphy, P. P., E. L. Chupp, and D. J. Forrest, 1983, AIP Conf. Proc. **101**, 237.

Dwek, E., R. G. Arendt, M. G. Hauser, T. Kelsall, C. M. Lisse, S. H. Moseley, R. F. Silverberg, T. J. Sodroski, and J. L. Weiland, 1995, Astrophys. J. **445**, 716.

Eckart, A., *et al.*, 2008, arXiv:0810.0168.

Ellis, J. R., A. Ferstl, and K. A. Olive, 2000, Phys. Lett. B **481**, 304.

Ellis, S. C., and J. Bland-Hawthorn, 2009, Astrophys. J. **707**, 457.

Essig, R., N. Sehgal, and L. E. Strigari, 2009, Phys. Rev. D **80**, 023506.

Evans, R. D., 1975, *The Atomic Nucleus* (McGraw-Hill, New York).

Fatuzzo, M., F. Melia, and J. Rafelski, 2001, Astrophys. J. **549**, 293.

Fayet, P., D. Hooper, and G. Sigl, 2006, Phys. Rev. Lett. **96**, 211302.

Fender, R. P., T. M. Belloni, and E. Gallo, 2004, Mon. Not. R. Astron. Soc. **355**, 1105.

Ferrer, F., and T. Vachaspati, 2005, Phys. Rev. Lett. **95**, 261302.

Ferrer, F., and T. Vachaspati, 2007, Int. J. Mod. Phys. D **16**, 2399.

Ferrière, K., 1998, Astrophys. J. **497**, 759.

Ferrière, K., W. Gillard, and P. Jean, 2007, Astron. Astrophys. **467**, 611.

Ferrière, K. M., 1999, in *New Perspectives on the Interstellar Medium*, edited by A. R. Taylor, T. L. Landecker, and G. Joncas, Astronomical Society of the Pacific Conference Series, Vol. 168 (Astronomical Society of the Pacific, San Francisco), p. 333.

Ferrière, K. M., 2001, Rev. Mod. Phys. **73**, 1031.

Figer, D. F., 2008, arXiv:0803.1619.

Figer, D. F., R. M. Rich, S. S. Kim, M. Morris, and E. Serabyn, 2004, Astrophys. J. **601**, 319.

Finkbeiner, D. P., N. Padmanabhan, and N. Weiner, 2008, Phys. Rev. D **78**, 063530.

Finkbeiner, D. P., and N. Weiner, 2007, Phys. Rev. D **76**, 083519.

Flynn, C., J. Holmberg, L. Portinari, B. Fuchs, and H. Jahreiß, 2006, Mon. Not. R. Astron. Soc. **372**, 1149.

Foellmi, C., P. O. Petrucci, J. Ferreira, and G. Henri, 2008, arXiv:0810.0108.

Freudenreich, H. T., 1998, Astrophys. J. **492**, 495.

Frick, P., R. Stepanov, A. Shukurov, and D. Sokoloff, 2001, Mon. Not. R. Astron. Soc. **325**, 649.

Gallo, E., R. P. Fender, and G. G. Pooley, 2003, Mon. Not. R. Astron. Soc. **344**, 60.

Gardner, B. M., D. J. Forrest, P. P. Dunphy, and E. L. Chupp, 1982, AIP Conf. Proc. **83**, 144.

Gebauer, I., and W. de Boer, 2009, arXiv:0910.2027.

Gehrels, N., S. D. Barthelmy, and B. J. Teegarden, 1991, Astrophys. J. **375**, L13.

Gentile, G., C. Tonini, and P. Salucci, 2007, Astron. Astrophys. **467**, 925.

Gilfanov, M., and Á. Bogdán, 2010, Nature (London) **463**, 924.

Gilfanov, M., E. Churazov, and R. Sunyaev, 1994, Astrophys. J. Suppl. Ser. **92**, 411.

Gill, R., and J. Heyl, 2007, Mon. Not. R. Astron. Soc. **381**, 52.

Gillessen, S., F. Eisenhauer, S. Trippe, T. Alexander, R. Genzel, F. Martins, and T. Ott, 2009, Astrophys. J. **692**, 1075.

Gilmore, G., and N. Reid, 1983, Mon. Not. R. Astron. Soc. **202**, 1025.

Gil-Pons, P., E. García-Berro, J. José, M. Hernanz, and J. W. Truran, 2003, Astron. Astrophys. **407**, 1021.

Ginzburg, V. L., 1956, Nuovo Cimento, Suppl. X **3**, 38.

Ginzburg, V. L., 1979, *Theoretical Physics and Astrophysics*, International Series in Natural Philosophy (Pergamon, Oxford).

Gleeson, L. J., and W. I. Axford, 1968, Astrophys. J. **154**, 1011.

Goldsmith, P. F., 1987, in *Interstellar Processes*, edited by D. J. Hollenbach and H. A. Thronson, Jr., Astrophysics and Space Science Library, Vol. 134 (Springer, Germany), p. 51.

Goldwurm, A., *et al.*, 1992, Astrophys. J. **389**, L79.

Gómez-Gomar, J., J. Isern, and P. Jean, 1998, Mon. Not. R. Astron. Soc. **295**, 1.
Gondolo, P., and J. Silk, 1999, Phys. Rev. Lett. **83**, 1719.
Gould, R. J., 1989, Astrophys. J. **344**, 232.
Gray, A. D., L. E. Cram, R. D. Ekers, and W. M. Goss, 1991, Nature (London) **353**, 237.
Greggio, L., 2005, Astron. Astrophys. **441**, 1055.
Greiner, W., 2003, *Quantum Electrodynamics* (Springer, Berlin).
Griest, K., and D. Seckel, 1991, Phys. Rev. D **43**, 3191.
Grimm, H.-J., M. Gilfanov, and R. Sunyaev, 2002, Astron. Astrophys. **391**, 923.
Groenewegen, M. A. T., A. Udalski, and G. Bono, 2008, Astron. Astrophys. **481**, 441.
Guessoum, N., P. Jean, and W. Gillard, 2005, Astron. Astrophys. **436**, 171.
Guessoum, N., P. Jean, and W. Gillard, 2010, Mon. Not. R. Astron. Soc. **402**, 1171.
Guessoum, N., P. Jean, J. Knödlseder, V. Lonjou, P. von Ballmoos, and G. Weidenspointer, 2004, in *Proceedings of the 5th INTEGRAL Workshop on the INTEGRAL Universe*, edited by V. Schoenfelder, G. Lichti, and C. Winkler, ESA Special Publication (ESA, The Netherlands), Vol. 552, p. 57.
Guessoum, N., P. Jean, and N. Prantzos, 2006, Astron. Astrophys. **457**, 753.
Guessoum, N., R. Ramaty, and R. E. Lingenfelter, 1991, Astrophys. J. **378**, 170.
Guessoum, N., J. G. Skibo, and R. Ramaty, 1997, in *The Transparent Universe*, edited by C. Winkler, T. J.-L. Courvoisier, and P. Durouchoux, ESA Special Publication (ESA, The Netherlands), Vol. 382, p. 113.
Guibert, J., J. Lequeux, and F. Viallefond, 1978, Astron. Astrophys. **68**, 1.
Gunion, J. F., D. Hooper, and B. McElrath, 2006, Phys. Rev. D **73**, 015011.
Han, J., 2002, in *Astrophysical Polarized Backgrounds*, edited by S. Cecchini, S. Cortiglioni, R. Sault, and C. Sbarra, AIP Conf. Proc. No. 609 (AIP, New York), p. 96.
Han, J. L., 2004, in *The Magnetized Interstellar Medium*, edited by B. Uyaniker, W. Reich, and R. Wielebinski (Max Planck Institut fur Radioastronomie, Bonn), p. 3.
Han, J. L., K. Ferrière, and R. N. Manchester, 2004, Astrophys. J. **610**, 820.
Han, J. L., R. N. Manchester, E. M. Berkhuijsen, and R. Beck, 1997, Astron. Astrophys. **322**, 98.
Han, J. L., R. N. Manchester, A. G. Lyne, G. J. Qiao, and W. van Straten, 2006, Astrophys. J. **642**, 868.
Han, J. L., R. N. Manchester, and G. J. Qiao, 1999, Mon. Not. R. Astron. Soc. **306**, 371.
Harding, A. K., 1981, Astrophys. J. **247**, 639.
Harding, A. K., and D. Lai, 2006, Rep. Prog. Phys. **69**, 2631.
Harris, M. J., G. H. Share, and M. D. Leising, 1994a, Astrophys. J. **433**, 87.
Harris, M. J., G. H. Share, and M. D. Leising, 1994b, Astrophys. J. **420**, 649.
Harris, M. J., B. J. Teegarden, T. L. Cline, N. Gehrels, D. M. Palmer, R. Ramaty, and H. Seifert, 1998, Astrophys. J. **501**, L55.
Haug, E., 2004, Astron. Astrophys. **423**, 793.
Hayakawa, S., 1969, *Cosmic Ray Physics. Nuclear and Astrophysical Aspects*, Interscience Monographs and Texts in Physics and Astronomy (Wiley-Interscience, New York).
Haymes, R. C., G. D. Walraven, and C. A. Meegan, 1975, Astrophys. J. **201**, 593.
Heesen, V., R. Beck, M. Krause, and R.-J. Dettmar, 2009, Astron. Astrophys. **494**, 563.
Heiles, C., and T. H. Troland, 2005, Astrophys. J. **624**, 773.
Heinz, S., and R. Sunyaev, 2002, Astron. Astrophys. **390**, 751.
Heitler, W., 1954, *Quantum Theory of Radiation*, International Series of Monographs on Physics (Clarendon, Oxford), 3rd ed.
Helmi, A., 2004, Astrophys. J. **610**, L97.
Hernanz, M., 2005, in *The Astrophysics of Cataclysmic Variables and Related Objects*, edited by J.-M. Hameury, and J.-P. Lasota, Astronomical Society of the Pacific Conference Series (Astronomical Society of the Pacific, San Francisco), Vol. 330, p. 265.
Hernanz, M., and J. José, 2006, New Astron. Rev. **50**, 504.
Higdon, J. C., 1984, Astrophys. J. **285**, 109.
Higdon, J. C., R. E. Lingenfelter, and R. E. Rothschild, 2009, Astrophys. J. **698**, 350.
Holmberg, J., and C. Flynn, 2004, Mon. Not. R. Astron. Soc. **352**, 440.
Hooper, D., D. P. Finkbeiner, and G. Dobler, 2007, Phys. Rev. D **76**, 083012.
Hooper, D., and L.-T. Wang, 2004, Phys. Rev. D **70**, 063506.
Hooper, D., *et al.*, 2004, Phys. Rev. Lett. **93**, 161302.
Huba, J. D., 2006, a collection of plasma physics formulas and data, NRL plasma formulary, Tech. Rep., Naval Research Laboratory.
Huh, J.-H., J. E. Kim, J.-C. Park, and S. C. Park, 2007, 0711.3528.
Hut, P., 1977, Phys. Lett. **69B**, 85.
Iben, Jr., I., and A. V. Tutukov, 1984, Astrophys. J. Suppl. Ser. **54**, 335.
Igarashi, A., M. Kimura, and I. Shimamura, 2002, Phys. Rev. Lett. **89**, 123201.
Inoue, M., and H. Tabara, 1981, Publ. Astron. Soc. Jpn. **33**, 603.
Isern, J., E. Bravo, and A. Hirschmann, 2007, in *The Multicolored Landscape of Compact Objects and Their Explosive Origins*, AIP Conf. Proc. No. 924 (AIP, New York), p. 210.
Iwamoto, K., F. Brachwitz, K. Nomoto, N. Kishimoto, H. Umeda, W. R. Hix, and F.-K. Thielemann, 1999, Astrophys. J. Suppl. Ser. **125**, 439.
Iwata, K., 1997, Positron annihilation on atoms and molecules, Ph.D. thesis, University of California, San Diego.
Iyudin, A. F., *et al.*, 1994, Astron. Astrophys. **284**, L1.
Jean, P., W. Gillard, A. Marcowith, and K. Ferrière, 2009, Astron. Astrophys. **508**, 1099.
Jean, P., J. Knödlseder, W. Gillard, N. Guessoum, K. Ferrière, A. Marcowith, V. Lonjou, and J. P. Roques, 2006, Astron. Astrophys. **445**, 579.
Jean, P., *et al.*, 2003, Astron. Astrophys. **407**, L55.
Johnson, W. N., F. R. Harnden, and R. C. Haymes, 1972, Astrophys. J. **172**, L1.
Johnson, W. N., and R. C. Haymes, 1973, Astrophys. J. **184**, 103.
Joliot, F., and I. Curie, 1934, Nature (London) **133**, 201.
Jones, F. C., and D. C. Ellison, 1991, Space Sci. Rev. **58**, 259.
Jun, B.-I., and M. L. Norman, 1996, Astrophys. J. **472**, 245.
Jung, G. V., D. J. Kurfess, and W. N. Johnson, R. L. Kinzer, J. E. Grove, M. S. Strickman, W. R. Purcell, D. A. Grabelsky, M. P. Ulmer, 1995, Astrophys. J. **295**, L23.
Jurić, M., *et al.*, 2008, Astrophys. J. **673**, 864.
Kalberla, P. M. W., and L. Dedes, 2008, arXiv:0804.4831.
Kalemci, E., S. E. Boggs, P. A. Milne, and S. P. Reynolds, 2006, Astrophys. J. **640**, L55.
Kamae, T., N. Karlsson, T. Mizuno, T. Abe, and T. Koi, 2006, Astrophys. J. **647**, 692.
Kamae, T., N. Karlsson, T. Mizuno, T. Abe, and T. Koi, 2007, Astrophys. J. **662**, 779.
Kasuya, S., and M. Kawasaki, 2006, Phys. Rev. D **73**, 063007.
Kasuya, S., and F. Takahashi, 2005, Phys. Rev. D **72**, 085015.
Kazantzidis, S., *et al.*, 2004, Astrophys. J. **611**, L73.

Keane, E. F., and M. Kramer, 2008, arXiv:0810.1512.
Kelner, S. R., F. A. Aharonian, and V. V. Bugayov, 2006, Phys. Rev. D **74**, 034018.
Kennicutt, R. C., Jr., 1998, Annu. Rev. Astron. Astrophys. **36**, 189.
Killeen, N. E. B., K. Y. Lo, and R. Crutcher, 1992, Astrophys. J. **385**, 585.
Kim, S.-H., P. G. Martin, and P. D. Hendry, 1994, Astrophys. J. **422**, 164.
Kinzer, R. L., P. A. Milne, and J. D. Kurfess, 2001, Astrophys. J. **559**, 282.
Kinzer, R. L., W. R. Purcell, W. N. Johnson, J. D. Kurfess, G. Jung, and J. Skibo, 1996, Astron. Astrophys. Suppl. Ser. **120**, 317.
Kinzer, R. L., W. R. Purcell, and J. D. Kurfess, 1999, Astrophys. J. **515**, 215.
Klemperer, O., and J. Chadwick, 1934, Proc. Cambridge Philos. Soc. **30**, 347.
Klepikov, N. P., 1954, Zh. Eksp. Teor. Fiz. **26**, 19.
Knödlseder, J., 1999, Astrophys. J. **510**, 915.
Knödlseder, J., *et al.*, 2005, Astron. Astrophys. **441**, 513.
Kothes, R., and W. Reich, 2001, Astron. Astrophys. **372**, 627.
Koyama, K., Y. Hyodo, and T. Inui, 2006, J. Phys. Conf. Ser. **54**, 95.
Kozlovsky, B., R. E. Lingenfelter, and R. Ramaty, 1987, Astrophys. J. **316**, 801.
Kulkarni, S. R., and C. Heiles, 1987, in *Interstellar Processes*, edited by D. J. Hollenbach and H. A. Thronson, Jr., Astrophysics and Space Science Library (Springer, Germany), Vol. 134, p. 87.
Kulsrud, R. M., 2005, *Plasma Physics for Astrophysics* (Princeton University Press, Princeton, NJ).
LaRosa, T. N., C. L. Brogan, S. N. Shore, T. J. Lazio, N. E. Kassim, and M. E. Nord, 2005, Astrophys. J. **626**, L23.
LaRosa, T. N., M. E. Nord, T. J. W. Lazio, and N. E. Kassim, 2004, Astrophys. J. **607**, 302.
Launhardt, R., R. Zylka, and P. G. Mezger, 2002, Astron. Astrophys. **384**, 112.
Lee, B. W., and S. Weinberg, 1977, Phys. Rev. Lett. **39**, 165.
Leibundgut, B., 2001, Annu. Rev. Astron. Astrophys. **39**, 67.
Leising, M. D., and D. D. Clayton, 1987, Astrophys. J. **323**, 159.
Leloudas, G., *et al.*, 2009, arXiv:0908.0537.
Lemrani, R., 2006, Phys. At. Nucl. **69**, 1967.
le Roux, J. A., and G. M. Webb, 2007, Astrophys. J. **667**, 930.
Leventhal, M., 1973, Astrophys. J. **183**, L147.
Leventhal, M., S. D. Barthelmy, and N. Gehrels, 1993, Astrophys. J. **405**, L25.
Leventhal, M., C. J. MacCallum, S. D. Barthelmy, and N. Gehrels, 1989, Nature (London) **339**, 36.
Leventhal, M., C. J. MacCallum, A. F. Huters, and P. D. Stang, 1980, Astrophys. J. **240**, 338.
Leventhal, M., C. J. MacCallum, A. F. Huters, and P. D. Stang, 1982, Astrophys. J. **260**, L1.
Leventhal, M., C. J. MacCallum, A. F. Huters, and P. D. Stang, 1986, Astrophys. J. **302**, 459.
Leventhal, M., C. J. MacCallum, and P. D. Stang, 1978, Astrophys. J. **225**, L11.
Limongi, M., and A. Chieffi, 2006, Astrophys. J. **647**, 483.
Lingenfelter, R. E., J. C. Higdon, and R. E. Rothschild, 2009, Phys. Rev. Lett. **103**, 031301.
Lingenfelter, R. E., and R. Ramaty, 1989, Astrophys. J. **343**, 686.
Lingenfelter, R. E., R. Ramaty, and D. Leiter, 1981, International Cosmic Ray Conference **1**, 112.
Liszt, H. S., 1985, Astrophys. J. **293**, L65.
Liszt, H. S., and W. B. Burton, 1978, Astrophys. J. **226**, 790.
Liszt, H. S., and W. B. Burton, 1980, Astrophys. J. **236**, 779.
Lithwick, Y., and P. Goldreich, 2001, Astrophys. J. **562**, 279.
Lodders, K., 2003, Astrophys. J. **591**, 1220.
López-Corredoira, M., A. Cabrera-Lavers, and O. E. Gerhard, 2005, Astron. Astrophys. **439**, 107.
Lorimer, D. R., 2005, Living Rev. Relativity **8**, 7.
Lyne, A. G., R. N. Manchester, and J. H. Taylor, 1985, Mon. Not. R. Astron. Soc. **213**, 613.
Magkotsios, G., *et al.*, 2008, in *Nuclei in the Cosmos (NIC X)* (Publications of Science (PoS), Trieste, Italy).
Mahoney, W. A., J. C. Ling, A. S. Jacobson, and R. E. Lingenfelter, 1982, Astrophys. J. **262**, 742.
Mahoney, W. A., J. C. Ling, and W. A. Wheaton, 1994, Astrophys. J. Suppl. Ser. **92**, 387.
Maness, H., *et al.*, 2007, Astrophys. J. **669**, 1024.
Mannucci, F., M. Della Valle, N. Panagia, E. Cappellaro, G. Cresci, R. Maiolino, A. Petrosian, and M. Turatto, 2005, Astron. Astrophys. **433**, 807.
Mao, S. A., B. M. Gaensler, M. Haverkorn, E. G. Zweibel, G. J. Madsen, N. M. McClure-Griffiths, A. Shukurov, and P. P. Kronberg, 2010, Astrophys. J. **714**, 1170.
Markevitch, M., R. A. Sunyaev, and M. Pavlinsky, 1993, Nature (London) **364**, 40.
Martinez-Delgado, D., M. A. Gomez-Flechoso, A. Aparicio, and R. Carrera, 2004, Astrophys. J. **601**, 242.
Mathis, J. S., W. Rumpl, and K. H. Nordsieck, 1977, Astrophys. J. **217**, 425.
Matthaeus, W. H., G. Qin, J. W. Bieber, and G. P. Zank, 2003, Astrophys. J. **590**, L53.
Mayer-Hasselwander, H. A., *et al.*, 1998, Astron. Astrophys. **335**, 161.
Mazzali, P. A., F. K. Röpke, S. Benetti, and W. Hillebrandt, 2007, Science **315**, 825.
McClintock, J. E., and R. A. Remillard, 2006, *Compact Stellar X-ray Sources*, edited by W. H. G. Lewin and M. van der Klis (Cambridge University Press, Cambridge, England), p. 157.
McKee, C. F., and J. P. Ostriker, 1977, Astrophys. J. **218**, 148.
McKee, C. F., and J. P. Williams, 1997, Astrophys. J. **476**, 144.
Melia, F., F. Yusef-Zadeh, and M. Fatuzzo, 1998, Astrophys. J. **508**, 676.
Melrose, D. B., 1980, *Plasma Astrohysics* (Gordon and Breach, New York).
Men, H., K. Ferrière, and J. L. Han, 2008, Astron. Astrophys. **486**, 819.
Merritt, D., 2010, arXiv:1001.3706.
Meyer, B. S., 1993, Phys. Rep. **227**, 257.
Milne, D. K., R. T. Stewart, and R. F. Haynes, 1993, Mon. Not. R. Astron. Soc. **261**, 366.
Milne, P. A., D. D. Dixon, M. D. Leising, J. D. Kurfess, M. Leventhal, R. L. Kinzer, S. M. Matz, W. R. Purcell, D. M. Smith, and J. Tueller, 1998, Astro. Lett. & Comm. **38**, 441.
Milne, P. A., *et al.*, 2004, Astrophys. J. **613**, 1101.
Milne, P. A., J. D. Kurfess, R. L. Kinzer, and M. D. Leising, 2001a, AIP Conf. Proc. **587**, 11.
Milne, P. A., J. D. Kurfess, R. L. Kinzer, and M. D. Leising, 2002, New Astron. Rev. **46**, 553.
Milne, P. A., J. D. Kurfess, R. L. Kinzer, M. D. Leising, and D. D. Dixon, 2001b, ESA-SP **459**, 145.
Milne, P. A., L.-S. The, and M. D. Leising, 1999, Astrophys. J. Suppl. Ser. **124**, 503.
Minter, A. H., and S. R. Spangler, 1996, Astrophys. J. **458**, 194.
Mirabel, I. F., 2008, arXiv:0805.2378.
Mirabel, I. F., L. F. Rodriguez, B. Cordier, J. Paul, and F. Lebrun, 1992, Nature (London) **358**, 215.
Mohorovicic, S., 1934, Astron. Nachr. **253**, 93.
Moore, B., *et al.*, 1999, Astrophys. J. **524**, L19.

Morfill, G. E., 1982, Astrophys. J. **262**, 749.
Morris, M., 1990, in *Galactic and Intergalactic Magnetic Fields*, edited by R. Beck, R. Wielebinski, and P. P. Kronberg, IAU Symposium Vol. 140 (Kluwer, Dordrecht, The Netherlands), p. 361.
Morris, M., and E. Serabyn, 1996, Annu. Rev. Astron. Astrophys. **34**, 645.
Moskalenko, I. V., T. A. Porter, and A. W. Strong, 2006, Astrophys. J. **640**, L155.
Moskalenko, I. V., and A. W. Strong, 1998, Astrophys. J. **493**, 694.
Moss, D., and D. Sokoloff, 2008, Astron. Astrophys. **487**, 197.
Motizuki, Y., and S. Kumagai, 2004, New Astron. Rev. **48**, 69.
Murakami, H., K. Koyama, M. Sakano, M. Tsujimoto, and Y. Maeda, 2000, Astrophys. J. **534**, 283.
Murphy, R. J., C. D. Dermer, and R. Ramaty, 1987, Astrophys. J. Suppl. Ser. **63**, 721.
Murphy, R. J., G. H. Share, J. G. Skibo, and B. Kozlovsky, 2005, Astrophys. J. Suppl. Ser. **161**, 495.
Murphy, R. J., J. G. Skibo, G. H. Share, and B. Kozlovsky, 2005, AGU Spring Meeting Abstracts, A9+.
Nadyozhin, D. K., 1994, Astrophys. J. Suppl. Ser. **92**, 527.
Nagataki, S., M.-A. Hashimoto, K. Sato, S. Yamada, and Y. S. Mochizuki, 1998, Astrophys. J. **492**, L45.
Nakanishi, H., and Y. Sofue, 2003, Publ. Astron. Soc. Jpn. **55**, 191.
Nakanishi, H., and Y. Sofue, 2006, Publ. Astron. Soc. Jpn. **58**, 847.
Navarro, J. F., C. S. Frenk, and S. D. M. White, 1997, Astrophys. J. **490**, 493.
Navarro, J. F., A. Ludlow, V. Springel, J. Wang, M. Vogelsberger, S. D. M. White, A. Jenkins, C. S. Frenk, and A. Helmi, 2010, Mon. Not. R. Astron. Soc. **402**, 21.
Nayakshin, S., and F. Melia, 1998, Astrophys. J. Suppl. Ser. **114**, 269.
Nishiyama, S., *et al.*, 2009, Astrophys. J. **690**, 1648.
Nomoto, K., F.-K. Thielemann, and K. Yokoi, 1984, Astrophys. J. **286**, 644.
Nomoto, K., K. Maeda, Y. Mochizuki, S. Kumagai, H. Umeda, T. Nakamura, and I. Tanihata, 2001, in *Gamma 2001: Gamma-Ray Astrophysics*, edited by S. Ritz, N. Gehrels, and C. R. Shrader, AIP Conf. Proc. No. 587 (AIP, New York), p. 487.
Nomoto, K., M. Tanaka, N. Tominaga, and K. Maeda, 2010, New Astron. Rev. **54**, 191.
Novak, G., D. T. Chuss, T. Renbarger, G. S. Griffin, M. G. Newcomb, J. B. Peterson, R. F. Loewenstein, D. Pernic, and J. L. Dotson, 2003, Astrophys. J. **583**, L83.
Oaknin, D. H., and A. R. Zhitnitsky, 2005, Phys. Rev. Lett. **94**, 101301.
Olling, R. P., and M. R. Merrifield, 2001, Mon. Not. R. Astron. Soc. **326**, 164.
Ore, A., and J. L. Powell, 1949, Phys. Rev. **75**, 1696.
Paciesas, W. S., T. L. Cline, and B. J. Teegarden, 1982, Astrophys. J. **260**, L7.
Pannuti, T. G., G. E. Allen, J. C. Houck, and S. J. Sturner, 2003, Astrophys. J. **593**, 377.
Parizot, E., M. Cassé, R. Lehoucq, and J. Paul, 2005, Astron. Astrophys. **432**, 889.
Parker, E. N., 1965, Planet. Space Sci. **13**, 9.
Parthasarathy, M., D. Branch, D. J. Jeffery, and E. Baron, 2007, New Astron. Rev. **51**, 524.
Petrosian, V., and A. M. Bykov, 2008, Space Sci. Rev. **134**, 207.
Phillips, M. M., 1993, Astrophys. J. **413**, L105.
Picciotto, C., and M. Pospelov, 2005, Phys. Lett. B **605**, 15.
Picozza, P., *et al.*, 2007, Astropart. Phys. **27**, 296.
Piper, J. (CDF Collaboration), 2009, 0906.3676.
Plante, R. L., K. Y. Lo, and R. M. Crutcher, 1995, Astrophys. J. **445**, L113.
Plüschke, S., *et al.*, 2001, in *Exploring the Gamma-Ray Universe*, edited by A. Gimenez, V. Reglero, and C. Winkler, ESA Special Publication, Vol. 459 (ESA, Nordwijk, The Netherlands), p. 55.
Pohl, M., P. Englmaier, and N. Bissantz, 2008, Astrophys. J. **677**, 283.
Pollack, J. B., and G. G. Fazio, 1963, Phys. Rev. **131**, 2684.
Porter, T. A., I. V. Moskalenko, A. W. Strong, E. Orlando, and L. Bouchet, 2008, Astrophys. J. **682**, 400.
Pospelov, M., and A. Ritz, 2007, Phys. Lett. B **651**, 208.
Pospelov, M., A. Ritz, and M. B. Voloshin, 2008, Phys. Lett. B **662**, 53.
Potgieter, M. S., 1998, Space Sci. Rev. **83**, 147.
Prantzos, N., 1991, in *Gamma-Ray Line Astrophysics*, edited by P. Durouchoux and N. Prantzos, AIP Conf. Proc. No. 232 (AIP, New York), p. 129.
Prantzos, N., 1993, Astron. Astrophys. Suppl. Ser. **97**, 119.
Prantzos, N., 2004, in *Proceedings of the 5th INTEGRAL Workshop on the INTEGRAL Universe*, edited by V. Schoenfelder, G. Lichti, and C. Winkler, ESA Special Publication (ESA, Nordwijk, The Netherlands), Vol. 552, p. 15.
Prantzos, N., 2006, Astron. Astrophys. **449**, 869.
Prantzos, N., 2008, New Astron. Rev. **52**, 457.
Prantzos, N., and R. Diehl, 1996, Phys. Rep. **267**, 1.
Prouza, M., and R. Šmída, 2003, Astron. Astrophys. **410**, 1.
Pryor, C., M. Davis, M. Lecar, and E. Witten, 1980, Bull. Am. Astron. Soc., **12**, 861.
Ptuskin, V. S., I. V. Moskalenko, F. C. Jones, A. W. Strong, and V. N. Zirakashvili, 2006, Astrophys. J. **642**, 902.
Purcell, W. R., D. A. Grabelsky, M. P. Ulmer, W. N. Johnson, R. .L. Kinzer, J. D. Kurfess, M. S. Strickman, and G. V. Jung, 1994, AIP Conf. Proc. **304**, 403.
Purcell, W. R., L.-X. Cheng, and D. D. Dixon, 1997, Astrophys. J. **491**, 725.
Quataert, E., 2004, Astrophys. J. **613**, 322.
Ragot, B. R., 1999, Astrophys. J. **518**, 974.
Ragot, B. R., 2005, Astrophys. J. **619**, 585.
Ragot, B. R., 2006, Astrophys. J. **642**, 1163.
Ramaty, R., and R. E. Lingenfelter, 1977, Astrophys. J. **213**, L5.
Ramaty, R., R. J. Murphy, B. Kozlovsky, and R. E. Lingenfelter, 1983, Sol. Phys. **86**, 395.
Rand, R. J., and S. R. Kulkarni, 1989, Astrophys. J. **343**, 760.
Rand, R. J., and A. G. Lyne, 1994, Mon. Not. R. Astron. Soc. **268**, 497.
Rattenbury, N. J., S. Mao, T. Sumi, and M. C. Smith, 2007, Mon. Not. R. Astron. Soc. **378**, 1064.
Rees, M. J., 1988, Nature (London) **333**, 523.
Reich, W., 1994, in *The Nuclei of Normal Galaxies: Lessons from the Galactic Center*, edited by R. Genzel, and A. I. Harris, NATO ASIC Proc. Vol. 445 (Kluwer, Dordrecht, The Netherlands), p. 55.
Renaud, M., *et al.*, 2006, Astrophys. J. **647**, L41.
Revnivtsev, M. G., E. M. Churazov, S. Y. Sazonov, R. A. Sunyaev, A. A. Lutovinov, M. R. Gilfanov, A. A. Vikhlinin, P. E. Shtykovsky, and M. N. Pavlinsky, 2004, Astron. Astrophys. **425**, L49.
Rickett, B. J., and W. A. Coles, 2004, in *Bulletin of the American Astronomical Society* (American Astronomical Society, Washington DC), Vol. 36, p. 1539.
Riegler, G. R., J. C. Ling, and W. A. Mahoney, 1981, Astrophys. J. **248**, 13.
Robin, A. C., C. Reylé, S. Derrière, and S. Picaud, 2003, Astron. Astrophys. **409**, 523.
Robitaille, T. P., and B. A. Whitney, 2010, Astrophys. J. **710**, L11.
Röpke, F. K., W. Hillebrandt, W. Schmidt, J. C. Niemeyer, S. I. Blinnikov, and P. A. Mazzali, 2007, Astrophys. J. **668**, 1132.

Röpke, F. K., and J. C. Niemeyer, 2007, Astron. Astrophys. **464**, 683.

Roy, S., A. P. Rao, and R. Subrahmanyan, 2005, Mon. Not. R. Astron. Soc. **360**, 1305.

Rudak, B., 2001, in *Physics and Astrophysics of Ultra-High-Energy Cosmic Rays*, edited by M. Lemoine, and G. Sigl, Lecture Notes in Physics (Springer-Verlag, Berlin), Vol. 576, p. 90.

Ruzmaikin, A. A., D. D. Sokolov, and A. M. Shukurov, 1988, Eds., *Magnetic Fields of Galaxies*, Astrophysics and Space Science Library Vol. 133 (Springer-Verlag, New York).

Salpeter, E. E., 1955, Astrophys. J. **121**, 161.

Savaglio, S., K. Glazebrook, and D. Le Borgne, 2009, Astrophys. J. **691**, 182.

Sawada, T., T. Hasegawa, T. Handa, and R. J. Cohen, 2004, Mon. Not. R. Astron. Soc. **349**, 1167.

Scannapieco, E., and L. Bildsten, 2005, Astrophys. J. **629**, L85.

Schmidt, W., and J. C. Niemeyer, 2006, Astron. Astrophys. **446**, 627.

Schure, K., J. Vink, B. Achterberg, and R. Keppens, 2008, in *37th COSPAR Scientific Assembly, Montréal, Canada.*, COSPAR, Plenary Meeting (Elsevier, Amsterdam), Vol. 37, p. 2791.

Segre, E., 1977, *Nuclei and Particles* (Benjamin, New York).

Seiradakis, J. H., and R. Wielebinski, 2004, Astron. Astrophys. Rev. **12**, 239.

Seitenzahl, I. R., S. Taubenberger, and S. A. Sim, 2009, Mon. Not. R. Astron. Soc. **400**, 531.

Sellwood, J. A., and S. S. McGaugh, 2005, Astrophys. J. **634**, 70.

Shafter, A. W., 1997, Astrophys. J. **487**, 226.

Shalchi, A., J. W. Bieber, W. H. Matthaeus, and R. Schlickeiser, 2006, Astrophys. J. **642**, 230.

Share, G. H., R. L. Kinzer, and J. D. Kurfess, 1988, Astrophys. J. **326**, 717.

Share, G. H., R. L. Kinzer, J. D. Kurfess, D. J. Forrest, E. L. Chupp, and E. Rieger, 1985, Astrophys. J. **292**, L61.

Share, G. H., M. D. Leising, D. C. Messina, and W. D. Purcell, 1990, Astrophys. J. **358**, L45.

Shebalin, J. V., W. H. Matthaeus, and D. Montgomery, 1983, J. Plasma Phys. **29**, 525.

Sim, S. A., and P. A. Mazzali, 2008, Mon. Not. R. Astron. Soc. **385**, 1681.

Sizun, P., M. Cassé, and S. Schanne, 2006, Phys. Rev. D **74**, 063514.

Skilling, J., and A. W. Strong, 1976, Astron. Astrophys. **53**, 253.

Smith, D. M., M. Leventhal, and R. Cavallo, 1996a, Astrophys. J. **458**, 576.

Smith, D. M., M. Leventhal, and R. Cavallo, 1996b, Astrophys. J. **471**, 783.

Smith, D. M., R. P. Lin, and P. Feffer, 1993, Astrophys. J. **414**, 165.

Sofue, Y., M. Honma, and T. Omodaka, 2008, arXiv:0811.0859.

Sollerman, J., *et al.*, 2004, Astron. Astrophys. **428**, 555.

Spano, M., M. Marcelin, P. Amram, C. Carignan, B. Epinat, and O. Hernandez, 2008, Mon. Not. R. Astron. Soc. **383**, 297.

Spitzer, L., 1956, *Physics of Fully Ionized Gases* Physics of Fully Ionized Gases (Interscience Publishers, New York).

Springel, V., S. D. M. White, C. S. Frenk, J. F. Navarro, A. Jenkins, M. Vogelsberger, J. Wang, A. Ludlow, and A. Helmi, 2008, Nature (London) **456**, 73.

Stecker, F. W., 1969, Astrophys. Space Sci. **3**, 579.

Story, S. A., P. L. Gonthier, and A. K. Harding, 2007, Astrophys. J. **671**, 713.

Stritzinger, M., P. A. Mazzali, J. Sollerman, and S. Benetti, 2006, Astron. Astrophys. **460**, 793.

Stritzinger, M., and J. Sollerman, 2007, Astron. Astrophys. **470**, L1.

Strong, A. W., *et al.*, 1994, Astron. Astrophys. **292**, 82.

Strong, A. W., and I. V. Moskalenko, 1998, Astrophys. J. **509**, 212.

Strong, A. W., I. V. Moskalenko, and V. S. Ptuskin, 2007, Annu. Rev. Nucl. Part. Sci. **57**, 285.

Strong, A. W., I. V. Moskalenko, and O. Reimer, 2000, Astrophys. J. **537**, 763.

Strong, A. W., I. V. Moskalenko, and O. Reimer, 2004, Astrophys. J. **613**, 962.

Sullivan, M., *et al.*, 2006, Astrophys. J. **648**, 868.

Sunyaev, R., *et al.*, 1992, Astrophys. J. **389**, L75.

Sunyaev, R., *et al.*, 1991, Astrophys. J. **383**, L49.

Syer, D., and A. Ulmer, 1999, Mon. Not. R. Astron. Soc. **306**, 35.

Tammann, G. A., W. Loeffler, and A. Schroeder, 1994, Astrophys. J. Suppl. Ser. **92**, 487.

Tanaka, M., P. A. Mazzali, S. Benetti, K. Nomoto, N. Elias-Rosa, R. Kotak, G. Pignata, V. Stanishev, and S. Hachinger, 2008, Astrophys. J. **677**, 448.

Tautz, R. C., A. Shalchi, and R. Schlickeiser, 2006, J. Phys. G **32**, 1045.

Taylor, A. R., J. M. Stil, and C. Sunstrum, 2009, Astrophys. J. **702**, 1230.

The, L.-S., D. D. Clayton, R. Diehl, D. H. Hartmann, A. F. Iyudin, M. D. Leising, B. S. Meyer, Y. Motizuki, and V. Schönfelder, 2006, Astron. Astrophys. **450**, 1037.

Thielemann, F.-K., K. Nomoto, and M.-A. Hashimoto, 1996, Astrophys. J. **460**, 408.

Titarchuk, L., and P. Chardonnet, 2006, Astrophys. J. **641**, 293.

Timmes, F. X., S. E. Woosley, D. H. Hartmann, and R. D. Hoffman, 1996, Astrophys. J. **464**, 332.

Toptygin, I. N., 1985, *Cosmic Rays in Interplanetary Magnetic Fields* (D. Reidel Publishing Co., Dordrecht).

Totani, T., 2006, Publ. Astron. Soc. Jpn. **58**, 965.

Travaglio, C., W. Hillebrandt, M. Reinecke, and F.-K. Thielemann, 2004, Astron. Astrophys. **425**, 1029.

Troland, T. H., and C. Heiles, 1986, Astrophys. J. **301**, 339.

Tsuboi, M., M. Inoue, T. Handa, H. Tabara, and T. Kato, 1985, Publ. Astron. Soc. Jpn. **37**, 359.

Uchida, K. I., and R. Guesten, 1995, Astron. Astrophys. **298**, 473.

Vallée, J. P., 2005, Astrophys. J. **619**, 297.

Vedrenne, G., *et al.*, 2003, Astron. Astrophys. **411**, L63.

Von Ballmoos, P., N. Guessoum, P. Jean, and J. Knödlseder, 2003, Astron. Astrophys. **397**, 635.

Wallyn, P., P. Durouchoux, C. Chapuis, and M. Leventhal, 1994, Astrophys. J. **422**, 610.

Wang, W., *et al.*, 2009, Astron. Astrophys. **496**, 713.

Wang, W., C. S. J. Pun, and K. S. Cheng, 2006, Astron. Astrophys. **446**, 943.

Webbink, R. F., 1984, Astrophys. J. **277**, 355.

Weidenspointner, G., C. R. Shrader, and J. Knödlseder, 2006, Astron. Astrophys. **450**, 1013.

Weidenspointner, G., *et al.*, 2008a, Nature (London) **451**, 159.

Weidenspointner, G., G. K. Skinner, P. Jean, J. Knödlseder, P. von Ballmoos, R. Diehl, A. Strong, B. Cordier, S. Schanne, and C. Winkler, 2008b, New Astron. Rev. **52**, 454.

Wentzel, D. G., 1974, Annu. Rev. Astron. Astrophys. **12**, 71.

Whelan, J., and I. J. Iben, 1973, Astrophys. J. **186**, 1007.

Winkler, C., *et al.*, 2003, Astron. Astrophys. **411**, L1.

Wolfe, B., and F. Melia, 2006, Astrophys. J. **638**, 125.

Woosley, S. E., 1993, Astrophys. J. **405**, 273.

Woosley, S. E., and T. A. Weaver, 1994, Astrophys. J. **423**, 371.

Woosley, S. E., and T. A. Weaver, 1995, Astrophys. J. Suppl. Ser. **101**, 181.

Xu, Y.-D., R. Narayan, E. Quataert, F. Yuan, and F. K. Baganoff, 2006, Astrophys. J. **640**, 319.

Yamasaki, T., F. Takahara, and M. Kusunose, 1999, Astrophys. J. **523**, L21.
Yan, H., and A. Lazarian, 2004, Astrophys. J. **614**, 757.
Yanasak, N. E., *et al.*, 2001, Adv. Space Res. **27**, 727.
Yuan, F., E. Quataert, and R. Narayan, 2004, Astrophys. J. **606**, 894.
Yusef-Zadeh, F., and M. Morris, 1987, Astrophys. J. **322**, 721.
Yusef-Zadeh, F., M. Morris, and D. Chance, 1984, Nature (London) **310**, 557.
Zank, G. P., G. Li, V. Florinski, W. H. Matthaeus, G. M. Webb, and J. A. le Roux, 2004, J. Geophys. Res. **109**, 4107.
Zhang, L., and K. S. Cheng, 1997, Astrophys. J. **487**, 370.
Zhitnitsky, A., 2006, Phys. Rev. D **74**, 043515.
Zoccali, M., A. Renzini, S. Ortolani, L. Greggio, I. Saviane, S. Cassisi, M. Rejkuba, B. Barbuy, R. M. Rich, and E. Bica, 2003, Astron. Astrophys. **399**, 931.
Zurek, W. H., 1985, Astrophys. J. **289**, 603.